A Modular Approach to Model Predictive Control linking Classical and Predictive Control Concepts

Roland Leslie John Bolton

A thesis submitted to the Faculty of Engineering, University of the Witwatersrand, Johannesburg, in fulfilment of the requirements for the degree of Doctor of Philosophy.

Johannesburg, October 1997

Declaration

I declare that this thesis is my own, unaided work, except where otherwise acknowledged. It is being submitted for the degree of Doctor of Philosophy in the University of the Witwatersrand, Johannesburg. It has not been submitted before for any degree or examination in any other university.

Signed this 20th day of October 1997

Roland Leslie John Bolton.

Abstract

This thesis develops and investigates signal processing models that are useful both for interpreting and implementing certain types of Model Predictive Control. Two types of Model Predictive Control are investigated, namely, techniques based on Internal Model Control and Long Range Predictive Control.

The work on Internal Model Control is concerned with developing and testing an approach to implementing constrained Internal Model Control that caters for absolute and rate process input constraints. The proposed Internal Model Control configuration is also extended to include feedforward control. The resulting Internal Model Controller is unique in that both the feedback and feedforward controllers are serviced by the same constraint mechanism. Design equations and rules for ensuring integral action are presented.

The work on Long Range Predictive Control is concerned with developing a signal processing model for a Long Range Predictive Control algorithm called Multi-Step Predictive Control. The proposed model allows implementation of features such as integral action, dead-time compensation, absolute and rate process input constraints, a reference trajectory and constrained feedforward control. The proposed model is significant in that the interpretation of the signal processing and structure of the algorithm is now completely transparent. The proposed model facilitates the implementation of Long Range Predictive Control on standard control software development platforms, enabling rapid prototyping of Long Range Predictive Controllers.

The properties of Long Range Predictive Control are investigated using the proposed Multi-Step Control model. Equations linking Classical Control and Long Range Predictive Control are derived. Using these equations, it is possible to analyse prospective Multi-Step Predictive controllers using classical control concepts. A comparative study concludes that the Long Range Predictive Control algorithm has similar properties to an extended version of the Internal Model Control algorithm proposed in the literature, which has a special architecture for handling process input

constraints. This link confirms many reports in the control literature of successful applications of constrained Long Range Predictive Control.

Extensive testing of the proposed Model Predictive Control signal processing models, applied to laboratory equipment simulating a typical industrial heating process, provides evidence of practical implementations of the methods. The experimental results derived from the tests confirm many of the theoretical arguments presented in the thesis. A strong emphasis is placed on designing Long Range Predictive Controllers using the derived equations which link classical and predictive control. The experimental results compare favourably with the predicted behaviour based on classical control design.

Acknowledgements

The support and encouragement from my father is gratefully acknowledged.

I would also like to thank my supervisor, Prof I.M. MacLeod, for his contribution towards this thesis and for sharing with me his years of experience gained in feedback control.

Contents

List of Figures

List of Tables

List of Symbols

Internal Model Control

ζ	Damping factor in second order system
$d(t)$	Plant output disturbance
$F(s)$	Closed loop response filter
$F^{-1}(s)$	$1/F(s)$
$F_f(s)$	Feedforward response filter
$G(s)$	Transfer function of true plant dynamics
$\hat{G}(s)$	Transfer function of nominal plant model
$\hat{G}'(s)$	Controller's representation of the nominal plant model. All nonminimum phase zeros are omitted in this model
$(\hat{G}')^{-1}(s)$	$1/\hat{G}'(s)$
$G_d(s)$	Transfer function of true disturbance dynamics
$\hat{G}_d(s)$	Transfer function of nominal disturbance model
$K'(s)$	Intended filter, such that the IMC filter is $Q(s) = F(s)(\hat{G}')^{-1}(s)K'(s)$
$K(s)$	Transfer function of filter used in the inverted IMC filter
$l_m(\omega)$	Approximation error at frequency ω rad/sec
$n(t)$	Sensor noise

q_o	High frequency gain of the biproper transfer function $F(s)(\hat{G}')^{-1}(s)$
$Q(s)$	IMC feedback filter
$Q_f(s)$	IMC feedforward filter
t_r	Rise time
t	Present time
$u(t)$	Plant actuator input
v	Noise variance
ω_b	Noise bandwidth in rad/sec
ω_n	Natural frequency in rad/sec
ω_Q	Bandwidth of IMC filter Q in rad/sec
$y(t)$	Plant output
$y^*(t)$	Plant output set-point

Multi-Step Predictive Control

λ	Used in cost function of MSC algorithm
β	Used in cost function of MSC algorithm
Δ	Delta operator, where $\Delta = 1 - q^{-1}$
$\Delta U_{\min}$	Constraint setting for minimum rate change of plant input signal
$\Delta U_{\max}$	Constraint setting for maximum rate change of plant input signal
τ	Rise time of reference trajectory
a_{con}	Matrix describing the inequality constraints of the optimal control problem
b_{con}	Matrix describing the inequality constraints of the optimal control problem

C	Matrix used in expression defining the cost function (quadratic form)
CP	Control horizon length
D_1	Input signal to disturbance at the plants input
D_2	Input signal to disturbance at the plants output
E	Column vector of projected errors, assuming projected over the prediction horizon are equal to the present measured error
G	Model describing dynamics of plant model
G_D	Model describing dynamics of disturbance model
$\hat{G}$	Predictor plant model
$\hat{G}_D$	Feedforward predictor model
$\tilde{G}$	Template describing the plant model uncertainty
HP	Prediction horizon length
IMC	Internal Model Control
K_{FF}	Equivalent transfer function of the detuning filter of the feedforward controller module
K_{MSC}	Controller gain matrix. Closed form solution to the optimal control problem
$K_{<x>}$	Conversion matrix (used in modular framework)
$K_L(z)$	Transfer function of the equivalent classical controller
$\tilde{L}$	Template describing the loop transmission uncertainty
$L(z)$	Transfer function of the loop transmission
LRPC	Long Range Predictive Control
MIMO	Multi-input multi-output
MPC	Model Predictive Control

MSC	Multi-Step Predictive Control
P	Matrix used in expression defining the cost function (quadratic form)
q	Shift operator where $q\,x(t) = x(t+1)$
Q	Matrix used in predictor equation (feedback)
Q_D	Matrix used in feedforward predictor equation
$R_{\mathrm{RFB}}(z)$	Filter for providing rate feedback inside the MSC modular framework, where $R_{\mathrm{RFB}}(z) \approx \Delta = 1 - z^{-1}$ at low frequencies
R	Matrix used in predictor equation (feedback)
R_D	Matrix used in feedforward predictor equation
s	Laplace transform variable
SISO	Single-input single-output
$T_D(q^{-1})$	Internal model of disturbance (used in predictor equation)
T_{sp}	Sampling period of MSC controller
T	Sampling period of digital controller
$\tilde{T}$	Template describing the closed loop transfer function uncertainty
$T(z)$	Transfer function of the closed loop response
$u(t)$	Input to plant
$u_D(t)$	Disturbance input signal
$u'(t)$	Input to compensated predictor model
U_o	Column vector which is the solution to the optimal control problem
U_{past}	Column vector of past inputs to predictor model
U_{pred}	Column vector of projected inputs to predictor model

$U_{\min}$	Constraint setting for minimum of plant input signal
$U_{\max}$	Constraint setting for maximum of plant input signal
$\hat{U}_D$	Column vector of projected disturbance inputs
$U_{D\mathrm{past}}$	Col ınn vector of past inputs to feedforward predictor model
W	Matrix used in predictor equation (feedback)
W_D	Matrix used in feedforward predictor equation
$y(t)$	Output of plant
$\hat{y}(t)$	Predicted output of plant
$\hat{Y}_1$	Column vector of projected plant outputs, assuming projected plant inputs are unchanged
$\hat{Y}_e$	Column vector of projected errors, where $\hat{Y}_e = Y_{\mathrm{ref}} - \hat{Y}_1 - E$
Y_{ref}	Column vector of projected set-points
$\hat{Y}_{\mathrm{past}}$	Column vector of past outputs of predictor model
$\hat{Y}_{D\mathrm{past}}$	Column vector of past outputs of feedforward predictor model
$\hat{Y}$	Column vector of projected predictor model outputs
$\hat{Y}_D$	Column vector of projected feedforward predictor model outputs
ZOH	Zero Order Hold

Chapter 1

Introduction

1.1 Background

Interest in model-based control algorithms was spurred on by rapid development of digital computer technology in the 1970s (Smith 1972). The availability of advanced computer technology for process control applications prompted researches to find improved methods for designing and implementing process control systems. It was recognised that the classical control approach to the problem of designing and implementing process control systems was expensive and did not always meet the demands of industry.

The achievements of classical control methods as applied in industries such as the aerospace industry are well known. However, these methods of control have not been as successful in the process industries. The aerospace industry can afford to spend extensive effort on model identification and the design of each controller because the cost of design is usually spread over many units. However, the process industries cannot justify this effort because each control problem tends to be unique. Design specifications also vary a lot. Industrial processes are highly multivariable, long transport delays are a common characteristic and the physics of the process are usually not well understood. Also, process control systems are usually subject to stringent operating constraint requirements. These factors make the design of the controller difficult using classical control methods.

In a survey (Garcia, Prett & Morari 1989), it was pointed out that the operating points of a plant that satisfy the overall economic goals of the process will lie at the intersection of constraints (Arkun 1978. Prett & Gillette 1979). The constraint issue is usually ignored during the design phase of the classical controller and treated in an *ad hoc* manner in the implementation phase. This approach leads to significant performance compromises. To address these problems, a family of control methods, known as Model Predictive Control (MPC) has evolved.

Model Predictive Control (MPC) refers to a hierarchy of control algorithms that make explicit use of a dynamic model for the purpose of implementing feedback control. MPC algorithms are separated into groups which are identified according to the method of control algorithm formulation. Two distinct groups of MPC are identified, the Internal Model Control (IMC) and the Long Range Predictive Control (LRPC) algorithms.

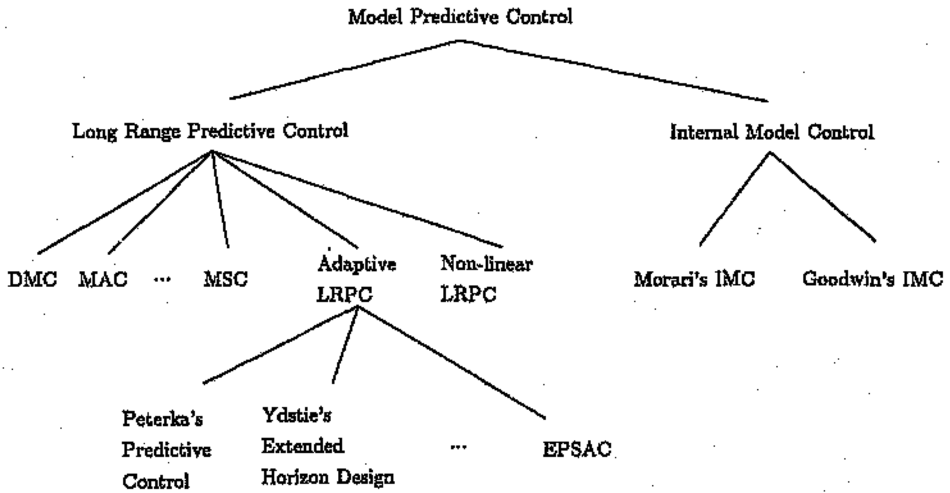

Figure 1.1: Hierarchy of Model Predictive Control Algorithms

Although the concept of MPC dates back to before the 1960s (Newton 1952), the process industry's interest in MPC developed mainly from a set of papers which appeared in the late 1970s. In 1978 Richalet (Richalet, Rault, Testud & Papon 1978) proposed a control algorithm called Model Predictive Heuristic Control, whose software implementation is called IDCOM (Identification and Command). The method was continuously and successfully applied to a dozen large scale industrial processes for more than a year before the method was published. At the same time, engineers (Cutler & Ramaker 1979, Prett & Gillette 1979) at Shell were working on a similar algorithm known as Dynamic Matrix Control (DMC) and in 1979 a successful application of DMC applied to a catalytic cracker was reported. The IDCOM and DMC algorithms were developed independently of each other. The algorithms relied on an explicit dynamic model of the plant to calculate moves of manipulated variables that minimise future projections of errors in the controlled variables. Hence the name "Model Predictive Control". Since these early publications, several MPC algorithms have emerged. The important Long Range Predictive Control Algorithms are the DMC algorithm (Cutler & Ramaker 1979, Prett & Gillette 1979, Cutler 1983), the QDMC algorithm (Garcia et al. 1989), the IDCOM algorithm (Richalet et al. 1978) and the MAC algorithm (Rouhani & Mehra 1982). Adaptive LRPC algorithms have also been reported: Clarke's GPC algorithm (Clarke, Mohtadi & Tuffs 1987*a*, Clarke, Mohtadi & Tuffs 1987*b*, Clarke & Mohtadi 1989), Peterka's Predictive Control (Peterka 1984), Ydstie's Extended Horizon Design (Ydstie, Kershenbaum & Sargent Nov 1985, Ydstie & Liu 1984), the EPSAC algorithm (VanCauwenberghe & DeKeyser June 1985) and the MUSMAR algorithm (Greco, Menga, Mosca & Zappa 1984). The Internal Model Control algorithm was advocated by Garcia and Morari (Garcia & Morari 1982). Goodwin (Seron, Goodwin & Graebe 1995, Goodwin, Graebe & Levine 1993) presented a variation of the IMC model and proposed an improved method for handling actuator saturation.

The LRPC algorithms reported in the literature are all based on a receding horizon control approach (Athans & Falb 1966), which refers to a policy whereby the control action for each sampling period is calculated by minimising the projected error in the controlled variable over a finite prediction horizon. At each sampling period the horizon appears to recede, as the control criterion is shifted one step ahead in time. This approach to implementing feedback control differs from the optimal control approach which usually derives a fixed controller from an infinite horizon cost criterion.

The LRPC algorithms calculate the control action for each step by solving a constrained optimisation problem which calculates the optimal set of projected control actions to minimise the projected error between the desired future plant outputs and the predicted future plant outputs. The solution is subject to operating constraints derived from the process constraints imposed on the system. This optimisation problem makes use of a dynamic model of the plant to project the plant's future outputs. This model will be referred to as the Predictor Model. The model representations differ between algorithms. The model can be represented either by a truncated impulse response model, a step response model, a state space model or a transfer function model.

The important features of LRPC algorithms are,

- inherent compensation for interaction,

- inherent dead time compensation,
- inherent integral action,
- high performance control with few, easy to select tuning parameters,
- it is easily tuned for robustness,
- it handles process constraints.

1.2 Contribution of this thesis

Current research on model based control seems to be moving towards incorporating non-linear models into MPC techniques (Brengel & Seider 1989, Hernandez & Arkun 1990, Patwardhan, Rawlings & Edgar 1990). The use of neural networks (Bhat & McAvoy 1990, Parisini & Zoppoli 1994), which offer potential for modelling non-linear processes, has been reported in applications of nonlinear MPC (Lee & Park 1992). However, recent research by Goodwin (Seron et al. 1995, Goodwin et al. 1993) seems to suggest that the work on MPC using linear system models is still incomplete. Goodwin showed that a special architecture is required if actuator saturation constraints are to be handled correctly. Goodwin's results and the block diagram modelling approach used to identify and solve the problem have prompted a similar investigation, carried out in this thesis, into other methods of MPC.

The aim of this thesis is to investigate MPC control and to develop signal processing models for improving the understanding and interpretation of MPC algorithms. Although the work is limited to the single-input-output case, it builds a foundation on which the multivariable algorithms may be developed and analysed.

Initial stages of this thesis continue the work of Goodwin on constrained IMC. The work includes the following contributions,

- A modified version of Goodwin's IMC model is proposed that extends the controller to the strictly proper case (Bolton & MacLeod 1997*m*).
- An extension to Goodwin's IMC model is presented that extends the controller's constraint handling ability to absolute as well as rate actuator constraints (Bolton & MacLeod 1997*c*).
- A new approach to designing and implementing feedforward control using an IMC configuration is presented (Bolton & MacLeod 1997*a*). Three important contributions are made,

- An architecture is proposed that incorporates feedforward control into the proposed IMC configuration. The architecture is significant in that it enables the same constraint handling mechanism to service both the feedback and feedforward controllers.
- A new design equation is proposed for designing the feedforward control filter. This is significant as it is a function of the feedback and feedforward controller response filters.
- Rules for ensuring integral action when using the proposed feedforward framework are presented.

Part II of the thesis is concerned with developing and investigating an LRPC algorithm called Multi-Step Predictive Control (MSC) (Bolton 1994, Bolton & MacLeod 1997*e*). A signal flow diagram of the MSC algorithm is developed using discrete building blocks. Investigations based on this model confirm that LRPC algorithms, such as the MSC algorithm, are consistent with Goodwin's constraint handling architecture. This is a significant finding. It confirms many reports of successful applications of constrained LRPC.

The contributions made in Part II of the thesis are,

- A predictor equation is defined which is a useful building block for developing LRPC algorithms (Bolton & MacLeod 1997*k*).
- A modular model of the MSC algorithm is proposed (Bolton & MacLeod 1997*i*). This model is useful for interpreting the signal processing and structure of the algorithm. The model has all the features of typical LRPC algorithms, including a reference trajectory (Bolton & MacLeod 1997*l*).
- Investigations based on the proposed MSC modular framework confirm that LRPC algorithms, such as the MSC algorithm, are consistent with Goodwin's constraint handling architecture (Bolton & MacLeod 1997*f*).
- Based on the link between the MSC algorithm and Goodwin's IMC model a new constraint handling mechanism is proposed which handles absolute and rate process input constraints (Bolton & MacLeod 1997*b*). The new method does away with the need for the quadratic program.
- Based on the proposed signal flow diagram of the MSC algorithm, transfer functions for the loop transmission and closed loop response are derived (Bolton & MacLeod 1997*g*). These equations, which are useful for analysing

the dynamic performance of a prospective LRPC controller, represent important links between classical and predictive control theories.

- A robust control design method is proposed for designing robust MSC controllers (Bolton & MacLeod 1997h).
- A feedforward control module is presented which extends the proposed MSC modular model to include feedforward control (Bolton & MacLeod 1997d, Bolton & MacLeod 1997j). The proposed model is similar to the feedforward IMC model presented in Part I. A mechanism for de-tuning the feedforward controller is included in the design. Both the feedforward and feedback controllers are serviced by the same constraint handling mechanism. Although the concept of feedforward control is not new to LRPC, the proposed framework is useful for interpreting the interaction between LRPC's feedback and feedforward control mechanisms.

Part III of the thesis is concerned with practical testing of the proposed IMC and MSC controllers. Experiments are carried out on Feedback Instrument's PT326 laboratory-scale process trainer. The experimental results confirm many issues put forward in Parts I and II. The contributions made in Part III of the thesis are,

- Experimental results emphasising the need for constraint mechanisms are presented.
  - Example1: Performance degradation resulting from integral windup.
  - Example2: Incorrect constraint handling approach. A common method for handling constraints is to place a constraint mechanism at the output of the controller, in an attempt to ensure no constraint violations. This method is shown to promote integral windup, which significantly degrades the controllers performance.
- Experimental results based on Morari's IMC actuator constraint handling architecture confirms Goodwin's suspicions that the method is incorrect. The experimental results show evidence of integral windup.
- Experimental results, demonstrating the absolute and rate actuator constraint mechanisms of the proposed IMC controller, are presented. No evidence of integral windup is observed. These results confirm that the proposed IMC framework for implementing absolute and rate actuator constraints is correct.
- Experimental results are presented, derived from experiments which demonstrate the proposed MSC modular framework presented in Figure 11.1. The

following issues are investigated.

- The absolute process input constraint handling mechanism.
- The interaction of the MSC algorithm's absolute and rate process input constraint handling mechanism.
- The MSC controller controlling a process that has a non-linear actuator.
- The MSC algorithm's reference trajectory mechanism.
- The effect the selection of the control horizon length has on the MSC controller's performance.

The results derived from these experiments are an important contribution as they provide practical results on which the algorithm may be assessed.

- Experiments are carried out to compare the robustness and transient performance of PID, IMC and MSC controllers. The following contributions are made in this section,

  - Equations are derived in the thesis which link classical and predictive control theory. These equations are used in a frequency domain design of a robust MSC controller. The measured performance of the MSC controller is a close match with the predicted control performance. These results are important contributions, because they confirm that the derived equations linking classical and predictive control theories are valid.
  - The experimental results confirm that although the model based controllers are designed using a fixed plant model, it is possible to obtain significant robustness with the MPC controller for changing plant conditions.
  - Experiments that compare the set-point and disturbance rejection transient responses of PID, IMC and MSC controllers confirm reports in the control literature that MPC controllers can out-perform PID controllers. Evidence of dead-time compensation can also be observed.

1.3 Overview of the thesis

Part I: Internal Model Control Extensions

Chapter 2: Strictly proper IMC with active process input constraints

Strictly proper controllers are essential for ensuring that actuator activity is insensitive to high frequency noise. This chapter shows how to design a strictly proper IMC controller with active input constraints. Simulation results emphasise the benefits of using a strictly proper controller for a system with severe high frequency sensor noise and emphasise the ability of the controller to handle input constraints.

Chapter 3: Absolute and Rate constraint mechanism

Actuator saturation may degrade the performance of a feedback control system and in some cases cause premature aging of the actuator. A method for handling actuator saturation is to include a constraint mechanism into the feedback controller. This chapter presents a new constraint mechanism which allows for active rate and absolute process inputs constraints. A simulation study of the proposed feedback controller with the new constraint mechanism is carried out. The simulation results emphasise the ability of the controller to handle input constraints.

Chapter 4: Improved feedforward control framework for IMC control

It is important to ensure that the inclusion of feedforward control into a system does not lead to actuator saturation. This chapter presents a new feedforward IMC framework with a constraint mechanism that supports both feedforward and feedback control. Simulation results emphasise the benefits of the proposed framework and show that improved disturbance rejection is possible with the inclusion of the feedforward controller and that the constraint mechanism supports both feedforward and feedback controllers.

Part II: Multi-Step Predictive Control

Chapter 5: The Predictor Equation

A predictor equation for Multi-Step Predictive Control is presented in this chapter. This equation is derived from a dynamic model of the process. It provides a foundation for the development of a modular approach to predictive control. Issues such as integral action are discussed in the chapter and a method for including integral action into the predictor equation is presented.

Chapter 6: The Reference Trajectory

The reference trajectory in a long range predictive control algorithm is a useful mechanism for describing the control criterion. The trajectory is usually generated using a recursive equation derived from a first order discrete time model. This chapter translates this recursive equation into a block diagram model. This model is a useful building block and is used (separate chapter) in the derivation of a complete modular model of the Multi-Step Predictive Control (MSC) algorithm.

Chapter 7: New Building Block for Predictive Control - First Order Filter

A building block for long range predictive control that performs the equivalent filtering action as a first order transfer function is presented in this chapter. A demonstration of the proposed filter shows that it is possible to regulate the filtering action by changing the time constant of the filter. This filter module is used in the feedforward module of the Multi-Step Predictive Control (MSC) algorithm.

Chapter 8: MSC Control - The Basic Algorithm

The advantages of using Long Range Predictive Control (LRPC) techniques are discussed and a LRPC algorithm called Multi-Step Predictive Contr l (MSC) is presented in this chapter. The technical details of MSC, such as the prediction horizons, the predictor equation, integral action, cost function, and reference trajectory are discussed. The material presented in this chapter builds a foundation for future work in which a modular model of MSC control is investigated.

Chapter 9: Modular Approach to Predictive Control

A modular framework for Multi-Step Predictive Control (MSC) is presented. This framework is formed by linking discrete building blocks together to form a dynamic model of the MSC algorithm. The significance of the proposed framework is its ability to be imported directly into dynamic simulators such as Simulink. This chapter builds a foundation for future work in which the dynamics of the unconstrained MSC controller are investigated using linear system analysis tools.

Chapter 10: Investigation into structure of Predictive Control

Goodwin has shown that a special architecture is required when implementing constraint mechanisms inside a feedback controller. This chapter investigates the constraint mechanism of Long Range Predictive Control (LRPC) and compares this with Goodwin's approach. The investigation is carried out using the modular framework of Multi-Step Predictive Control. The results show that LRPC's constraint architecture is similar to Goodwin's IMC method. This key result is a possible explanation as to why LRPC's constraint handling performance has been observed to be superior to other techniques.

Chapter 11: Proposed Constraint Mechanisms for MSC Control

A new constraint mechanism for Multi-Step Predictive Control is proposed which places constraints on the rate and absolute process input signals. An investigation into the architecture of the MSC algorithm shows that it is possible to transfer the rate and absolute constraints from the quadratic program to a separate module. This finding represents a significant advance because the quadratic program which calculates the projected optimal control actions is reduced to a closed form solution.

Significantly fewer computations are required using the proposed algorithm. The results of a simulation study demonstrating the proposed algorithm show the ability of the controller to handle rate and absolute process input constraints.

Chapter 12: Links between Classical Control and Predictive Control Theory

Links between classical and predictive control are investigated in this chapter. The transfer functions of the Loop Transmission and Closed Loop Response are derived by analysing the signal processing of the unconstrained Multi-Step Predictive Control modular framework. The equations derived in this chapter are important analytical tools for investigating the frequency domain characteristics of the Long Range Predictive Controller. A demonstration of the equations is presented where the equations are used to analyse typical predictive control problems.

Chapter 13: Robust MSC Control Design Method

A robust frequency response design method for Multi-Step Predictive Control (MSC) is presented. This design method relies on analytical tools that translate a given predictive controller into its equivalent classical controller. The robust design is then carried out using standard classical control analysis. Uncertainty is included in the design method by describing key frequency responses using plant uncertainty templates. Frequency response templates for the loop transmission, closed loop response and typical disturbance responses are generated. A flow chart of the design method as well as methods for tuning the MSC controller are presented. An example of a typical robust LRPC design is presented which demonstrates the potential of the design method.

Chapter 14: MSC Control with Feedforward Control

A modular framework for Multi-Step Predictive Control (MSC) with feedforward control is presented in this chapter. A signal flow diagram of the proposed feedforward controller is presented which provides insight into the interaction between the feedback and feedforward control mechanisms of Long Range Predictive Control. An important feature of the proposed model is the ability of the predictive controller's constraint mechanism to service both feedback and feedforward control. This feature is important as it prevents constraint violations from occurring when feedforward control is added into the system. A simulation study of the proposed MSC algorithm applied to a typical process control dynamics problem is presented. The simulation results show that the inclusion of the feedforward controller into the MSC algorithm provides improved disturbance rejection for disturbance responses which are accurately modelled and predictable.

Part III: Assessment of IMC and MSC Control

Chapter 15: Implementation

The hardware used to demonstrate the control algorithms is presented in this chapter. The essential hardware consists of Feedback Instrument's PT326 process trainer and dSpace's DS1102 digital signal processing card which has all the signal processing features required to implement advanced control algorithms. The dynamics of the PT326 are ideal for assessing advanced control algorithms. The unit has significant dead time and a mechanism for varying the dynamic characteristics of the process. Two generic models of the process are identified. The first is a low order model with a transport delay. This model is ideal for PID type controllers. The second is a high order model with a transport delay. This model is ideal for the proposed IMC and MSC controllers.

Chapter 16: Demonstration of IMC control

This chapter assesses IMC control's process input constraint handling mechanisms. Several experiments are carried out on Feedback Instrument's PT326 process trainer with the objective of demonstrating,

- the performance degradation resulting from integral windup caused by actuator saturation,
- incorrect methods of handling process input constraints,
- Morari's IMC constraint handling model,
- the proposed IMC controller (Chapter 3).

The results of the experiments confirm that Morari's IMC configuration for handling actuator saturation is incorrect. Morari's method shows evidence of controller windup when responding to a set-point step change. The proposed IMC model presented in Chapter 3 performs well. The results show no evidence of integral windup and no evidence of overshoot when responding to a set-point step change.

Chapter 17: Demonstration of MSC control

Practical tests of Multi-Step Predictive Control applied to Feedback Instrument's PT326 process trainer is presented in this chapter. These demonstrations investigate varies key features of the algorithm and provide a foundation, based on measured plant responses, on which the MSC algorithm is assessed. The features which are investigated are summarised as follows.

- Demonstration of MSC's absolute and rate constraint mechanisms.

- Demonstration of the MSC algorithm controlling a process which has a non-linear actuator, such as a pneumatic valve.
- Demonstration of MSC's reference trajectory feature.
- Investigation of what effect varying control horizon lengths have on the controller's performance.

The results of these demonstrations confirm that MSC control is a high performance control technique well suited to controlling industrial processes that require dead time compensation, process input constraints and integral action from the controller.

The demonstration of the algorithm's reference trajectory feature confirms that the reference trajectory adds an extra degree of freedom to the design and implementation of the controller, which enhances the quality of control.

Chapter 18: Comparison of PID, IMC and MSC control

This chapter compares PID, IMC and MSC control by carrying out experiments which investigate the robustness and transient performance of the controllers. The chapter is separated into two sections.

The first section investigates the robustness of the controllers. This is done by designing robust PID, IMC and MSC controllers that conform to design specifications. Issues such as plant uncertainty, constraints on controller bandwidth due to sensor noise and constraints on the transient response of the feedback system are considered in the design. These controllers are demonstrated on Feedback Instrument's PT326 process trainer. The process dynamics are changed by varying the throttle blower angle between 20° and 50°. The transient response thumb print for each controller is recorded and graphed.

The second section investigates the transient performance of the controllers. Two types of transient responses are considered. A set-point transient response and a disturbance rejection transient response.

The results of the study confirm that MSC control is a high performance control algorithm which improves on the quality of control offered by PID control. These results are significant as they demonstrate the benefits of using advanced control. The chapter is concluded with a table which compares the PID, IMC and MSC control.

Part I

Internal Model Control Extensions

Chapter 2

Strictly Proper IMC with Plant Input Amplitude Constraints

Recent developments show that the original IMC framework presented by Morari (Morari & Zafiriou 1989) is incomplete. Morari states that if control is implemented in the IMC configuration as shown in Figure 2.1 , input constraints do not cause any problems. However, Goodwin (Goodwin et al. 1993) shows that this IMC con-

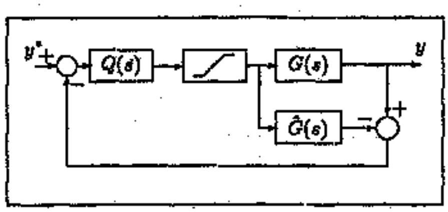

Figure 2.1: Conventional IMC control

figuration is still affected by constraint violations. Goodwin postulates that the plant model inherent in $Q(s)$ is not being driven by a constrained input. Using a unique feedback configuration Goodwin shows how to invert $Q(s)$, which enables a non-linear block to be incorporated into the inverted controller. In this way the plant and both plant models are driven by the same constrained input. Goodwin's method is identical to the configuration shown in Figure 2.2 when $K(s) = 1$. With $K(s)$ set to unity, the controller is not strictly proper. This is because the transfer function $F^{-1}(s)\hat{G}'(s)$ is biproper, which is a necessary requirement for the inversion of $Q(s)$.

This chapter extends Goodwin's IMC configuration to the strictly proper case and shows how this extension can reduce the effect of sensor noise at the plant input.

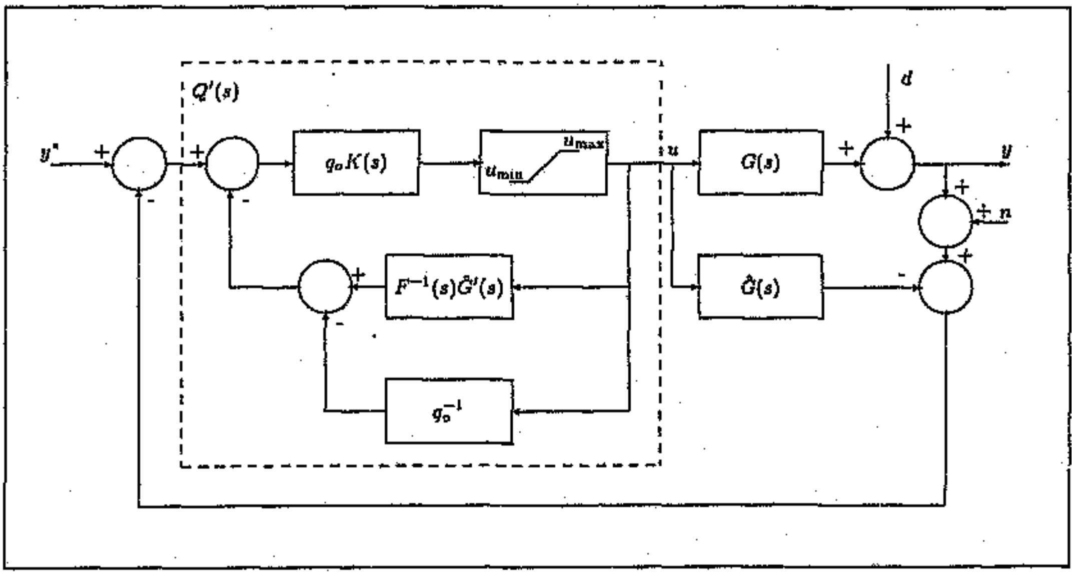

Figure 2.2: Signal flow diagram of simulation

This is an important improvement, because many kinds of actuator are adversely affected by noisy signals.

The chapter is organised as follows. Section 2.1 gives reasons why practical controllers should be strictly proper. A filter that ensures a strictly proper IMC controller is proposed in Section 2.2. Practical issues to consider when implementing the filter are presented in Section 2.3. The chapter is concluded with a simulation study.

2.1 Sensor noise

If the sensor output signal contains significant high-frequency noise and the controller's bandwidth is sufficiently large to pass these to the actuator signal, then premature failure of the actuator may result. A way of coping with this problem is to design the feedback loop such that the bandwidth is minimised and to decrease the controller gain as fast as possible for frequencies greater than the loop bandwidth (Horowitz 1963). This requires a strictly proper controller.

2.2 Proposed filter

The design of the filter $Q(s)$, based on Goodwin's method relies on the specification of $F(s)$, $\hat{G}'(s)$ and q_o. $\hat{G}'(s)$ is the IMC filter's plant model, which is initially assumed to have no NMP zeros and no transport delay. $F(s)$ is the specification of the closed loop response transfer function, which must have the same number of poles as $\hat{G}'(s)$ has zeros. This ensures that $F(s)(\hat{G}')^{-1}(s)$ is biproper i.e., has the same number of poles and zeros. The parameter q_o is the high frequency gain of the transfer function $F(s)(\hat{G}')^{-1}(s)$, defined as

$$q_o = \lim_{\omega\to\infty}[F(\jmath\omega)(\hat{G}')^{-1}(\jmath\omega)] \tag{2.1}$$

In Goodwin's interpretation of the IMC controller the filter Q is a biproper transfer function defined as,

$$Q(s) = F(s)(\hat{G}')^{-1}(s) \tag{2.2}$$

Suppose that an additional transfer function is connected in series with this transfer function, such that

$$Q'(s) = F(s)(\hat{G}')^{-1}(s)K'(s) \tag{2.3}$$

where $K'(s)$ is a low pass filter such that $Q'(s)$ is a good approximation of $Q(s)$ in the important frequency range. This condition can be stated in mathematical terms by defining,

$$l_m(\omega) = \left.\frac{|Q(s) - Q'(s)|}{|Q(s)|}\right|_{s=j\omega} \tag{2.4}$$

where $l_m(\omega)$ is the approximation error at frequency ω rad/sec. A possible criterion for the selection of $K'(s)$ is

$$l_m(\omega) \ll 1 \quad \text{for} \quad \omega < \omega_Q \tag{2.5}$$

where ω_Q is the bandwidth of the IMC filter $Q(s)$.

The filter $K'(s)$ can be incorporated into the IMC filter using the Equation derived in Appendix A.1

$$K(s) = \frac{F(s)(\hat{G}')^{-1}(s)K'(s)}{q_o - K'(s)[q_o - F(s)(\hat{G}')^{-1}(s)]} \tag{2.6}$$

which maps the transfer function of $K'(s)$ to $K(s)$. The inverse filter is shown in Figure 2.2, where the inclusion of the filter $K(s)$ ensures a strictly proper controller.

2.3 Issues in implementing filter

2.3.1 Stability of $K(s)$

It is important to ensure that $K(s)$ is stable. If not, any unstable mode present in $K(s)$ could be excited by noise and grow without bound. Equation 2.6 can be rewritten as (Appendix A.2),

$$K(s) = \frac{\frac{Q'(s)}{q_o[1-K'(s)]}}{1+\frac{Q'(s)}{q_o[1-K'(s)]}} \tag{2.7}$$

which can easily be tested for stability by checking the gain and phase gains of the transfer function,

$$\frac{Q'(s)}{q_o[1-K'(s)]} \tag{2.8}$$

Equation 2.8 can be rewritten as,

$$\left[\frac{K'(s)}{1-K'(s)}\right]\left[\frac{Q(s)}{q_o}\right] \tag{2.9}$$

Case studies have shown that the higher the bandwidth of $K'(s)$ in relation to $Q(s)$, the more poles and zeros are cancelled in the realisation of $K(s)$. Also, if the bandwidth of $K'(s)$ is sufficiently low, the transfer function $K(s)$ may have poles in the right hand plane.

Therefore a good criterion for the design of $K(s)$ is to select the bandwidth of $K'(s)$ small enough to reduce the actuator activity to an acceptable level, but also large enough such that no poles of $K(s)$ are in the RHP.

Equation 2.7 is derived in Appendix A.2. A Root Locus method for selecting a $K'(s)$ which results in a stable $K(s)$ is presented in Appendix A.2.

2.4 Simulated example

A simulation study is carried out to investigate the benefits of the proposed filter and also to emphasise the constraint handling ability of the controller. The signal flow diagram of the simulation is shown in Figure 2.2.

As the aim of the study is not to investigate the ability of the controller to handle model uncertainty, it is assumed that there is no modelling error. A plant model,

$$G(s) = \hat{G}(s) = \frac{e^{-8s}}{s^2+0.6s+1} \tag{2.10}$$

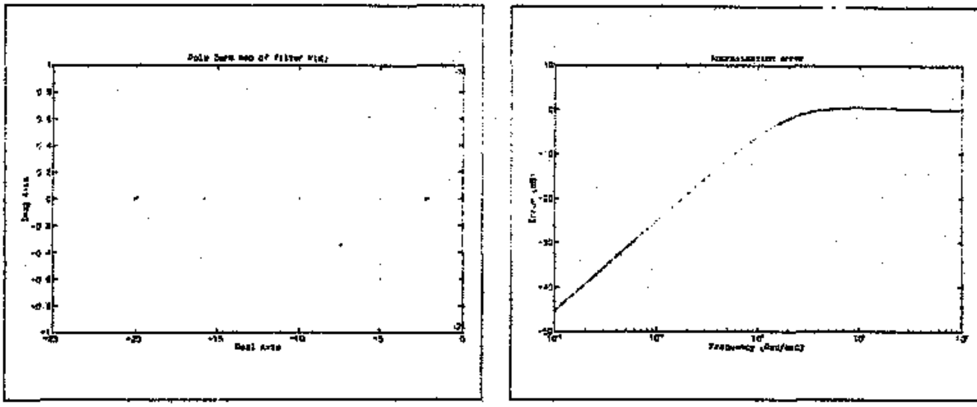

Figure 2.3: Pole zero map of filter and approximation error ($l_m(\omega)$)

is selected that has long dead time and small damping factor, common to certain types of industrial plants.

A suitable disturbance, occurring at the plant output, is specified that causes the actuator to saturate when the controller attempts to null the offset error caused by the disturbance. The disturbance at the plant output is defined as,

$$d(t) = \begin{cases} 0 & \text{if } t <= 100 \text{ sec} \\ -0.2 & \text{if } 100 < t <= 200 \text{ sec} \\ 0.5 & \text{if } t > 200 \text{ sec} \end{cases} \tag{2.11}$$

A sensor noise signal is specified that has a bandwidth significantly larger than the controller's bandwidth. The amplitude of the noise is selected large enough to cause oscillations in the plant input signal if precautions are not taken to ensure that the controller's gain is attenuated outside the operating bandwidth. The sensor noise signal, $n(t)$, has the following settings:

Noise Bandwidth	$= \omega_b = 628$ rad/sec
Noise amplitude distribution	$= v = 0.2$ units

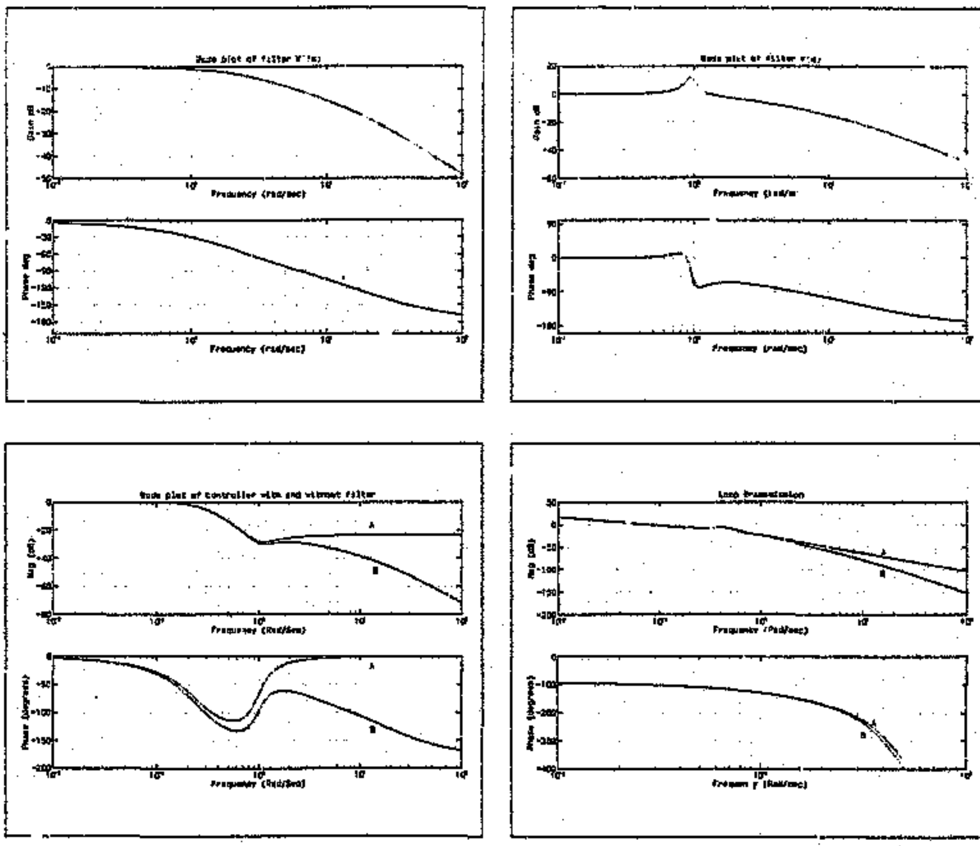

Figure 2.4: Bode Plots of specifications without filter (A) and with filter (B)

2.4.1 Controller design

A suitable model of the plant, inherent in the IMC filter $Q(s)$, is based on the nominal plant model defined in Equation 2.10 and may be approximated by,

$$\hat{G}'(s) = \frac{1}{s^2 + 0.6s + 1} \tag{2.12}$$

The IMC controller is tuned by specifying a suitable closed loop response filter, $F(s)$, that conforms to time domain specifications. For this design typical time domain specifications are,

$$t_r \approx 7 \text{ sec} \tag{2.13}$$

$$\zeta = 0.7 \tag{2.14}$$

Using the heuristic equation (Franklin, Powell & Emami-Naeini 1986),

$$\omega_n \approx 1.8/t_r \tag{2.15}$$

which selects the natural frequency for a second order prototype transfer function, an appropriate closed loop response filter is,

$$F(s) = \frac{0.0661}{s^2 + 0.36s + 0.0661} \tag{2.16}$$

Using Equation 2.1, the parameter q_o is calculated to be,

$$q_o = 0.0661 \tag{2.17}$$

The plant input constraint are taken to be,

$$u_{\min} = 0 \tag{2.18}$$

$$u_{\max} = 1.1 \tag{2.19}$$

2.4.2 Filter design

Based on the Bode plot of

$$\hat{Q}(s) = F(s)(\hat{G}')^{-1}(s)$$

an appropriate filter is

$$K'(s) = \frac{40}{s^2 + 22s + 40} \tag{2.20}$$

A Bode plot of $Q'(s)/q_o[1 - K'(s)]$ confirms that $K(s)$ is stable.

Using Equation 2.6, a minimal realisation of $K(s)$ is

$$K(s) = \frac{40s^2 + 24s + 40}{s^4 + 22.36s^3 + 47.99s^2 + 25.45s + 40} \tag{2.21}$$

The poles and zeros of the filter $K(s)$ and the error between $Q(s)$ and $Q'(s)$ are shown in Figure 2.3. The error plot shows that $Q'(s)$ is a good approximation of $Q(s)$ for low frequencies.

Two separate systems are simulated, the first omitting the filter $K(s)$ and the second including $K(s)$. The Bode plots of the IMC controllers and the loop transmissions are shown in Figure 2.4.

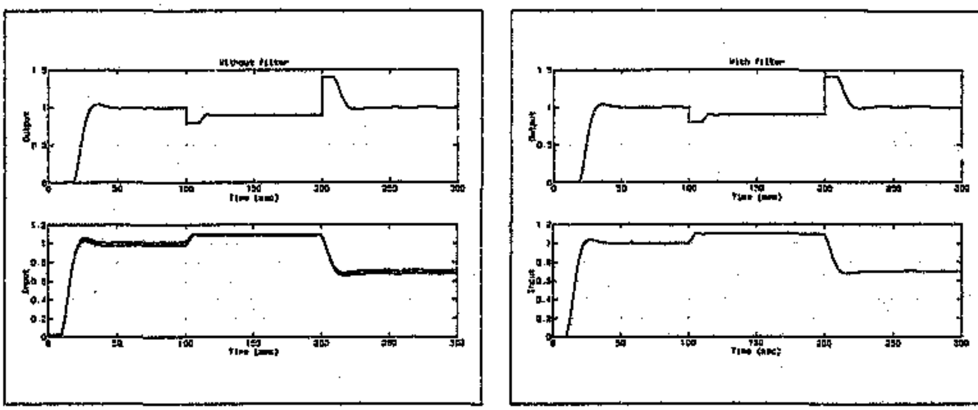

Figure 2.5: Simulation results

2.5 Simulation results

The simulation results are shown in Figure 2.5. The effect of sensor noise on the plant input is clearly reduced when the filter $K(s)$ is included in the system. No change of plant output is observed, as expected. Also, the controller's ability to handle input constraints can be clearly seen. When the controller responds to the disturbance at $t = [100, 200]$ seconds, the actuator signal increases until it reaches the maximum plant input constraint setting. When the disturbance changes at $t = 200$ seconds, the controller responds without any evidence of integral windup, which would occur if the actuator saturation were not handled correctly.

2.6 Summary

An additional filter has been introduced into the IMC controller proposed by Goodwin. The inclusion of this filter ensures a strictly proper controller, which is essential for ensuring that actuator activity is insensitive to high frequency noise.

A simulation study is carried out which emphasises both the benefits of using the strictly proper IMC controller to reduce the sensitivity of the actuator signal to sensor noise and the controller's ability to handle active input amplitude constraints.

Chapter 3

Absolute and Rate Constraint Mechanism

An important issue when implementing feedback control is to ensure that the feedback controller does not drive the actuator into saturation. If the actuator does saturate then the performance of the feedback system may be significantly degraded. Recent developments by Goodwin (Goodwin et al. 1993) shows that it is important to pay special attention to the way the feedback controller handles plant constraints. Goodwin proposes a new framework, based on the Internal Model Control (IMC) framework presented by Morari (Morari & Zafiriou 1989). Goodwin postulates that

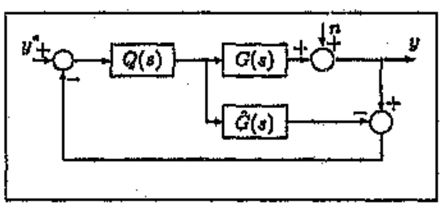

Figure 3.1: IMC framework

there are three separate plant models in the feedback system: the true plant dynamics, $G(s)$, an estimate of the plant dynamics, $\hat{G}(s)$ and the third model $\hat{G}'(s)$, which is the IMC filter's ($Q(s)$) representation of the nominal plant model. Goodwin shows that in order to successfully incorporate a constraint mechanism into a feedback controller, all three models must be driven by the same constrained plant input signal. Using a unique feedback configuration Goodwin shows how to invert the filter $Q(s)$, enabling a non-linear block to be incorporated into the inverted filter. In this way three plant models are driven by the same constrained input.

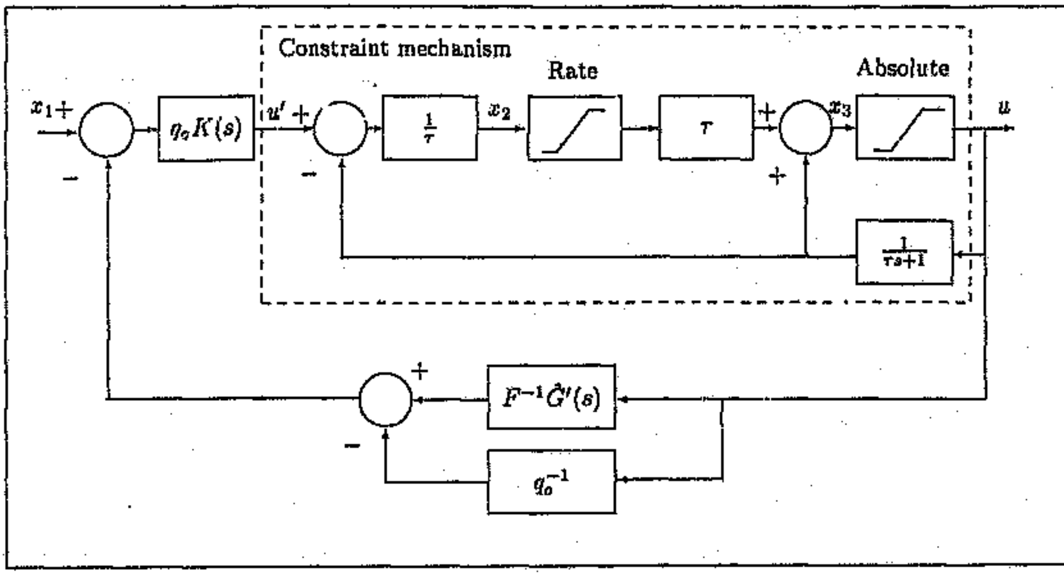

Figure 3.2: IMC controller ($Q'(s)$) with absolute and rate constraints

A strictly proper version of Goodwin's IMC control is presented in Chapter 2. This chapter extends the work done in Chapter 2 by introducing a new constraint mechanism that makes provision for rate constraints as well as an absolute plant input constraints. This is an important contribution, because often the physical plant is limited by non-linearities such as rate and absolute saturation constraints. The ability to include these constraints into the controller leads to improved control performance because the uncertainty caused by the saturation constraints is now removed from the feedback control system.

The chapter is organised as follows. Section 3.1 discusses the need for the inclusion of active constraints into the feedback controller. This is followed by Section 3.2, which presents the proposed feedback controller. A simulation study is presented in Section 3.5 that emphasises the constraint handling ability of the proposed feedback controller. The simulation results are presented in Section 3.6 and a summary is presented in Section 3.7.

3.1 Need for active constraints

Actuators are capable of delivering only a finite amount of power to a load. It is possible to drive the actuator into saturation by demanding more power from it than it can deliver, often resulting in windup and occasionally, damage to the actuator. However, in order to maximise plant efficiency, processes must be driven close to their plant output limits (Garcia et al. 1989).

One of the advantages of feedback control is its ability to reduce the response time of a system. The disadvantage of this is that it results in a more aggressive control action which can, if careful attention is not paid to the design of the controller, drive the actuator into saturation resulting in significant performance reduction. This problem is often the case when linear feedback controllers are used. In order to avoid driving the plant into saturation, the controller has to be detuned. This is a passive constraint handling mechanism. Also, once the controller has been designed and installed it is not a trivial procedure to adjust the control to suit different constraints.

For these reasons, there is a genuine need for a controller which has the ability to handle saturation constraints in a more direct or active manner.

3.2 Proposed IMC controller

The design of the IMC filter $Q(s)$, based on Goodwin's method relies on the specification of $F(s)$, $\hat{G}'(s)$ and q_o. $\hat{G}'(s)$ is the controller's plant model, which is assumed to have no NMP zeros and no transport delay. $F(s)$ is the specification of the closed loop response transfer function, which has the same number of poles as $\hat{G}'(s)$ has zeros. This ensures that $F(s)(\hat{G}')^{-1}(s)$ is biproper. The parameter q_o is the high frequency gain of the transfer function $F(s)(\hat{G}')^{-1}(s)$, defined as

$$q_o = \lim_{\omega \to \infty} [F(j\omega)(\hat{G}')^{-1}(j\omega)] \tag{3.1}$$

The IMC filter based on Goodwin's interpretation has the biproper transfer function,

$$Q(s) = F(s)(\hat{G}')^{-1}(s) \tag{3.2}$$

which is extended to the strictly proper case in Chapter 2. The extension is based on the inclusion of a filter $K(s)$ which has the transfer function,

$$K(s) = \frac{F(s)(\hat{G}')^{-1}(s)K'(s)}{q_o - K'(s)[q_o - F(s)(\hat{G}')^{-1}(s)]} \tag{3.3}$$

where $K'(s)$ is a low pass filter. The transfer function of the strictly proper IMC filter is,

$$Q'(s) = F(s)(\hat{G}')^{-1}(s)K'(s) \tag{3.4}$$

A block diagram of the proposed IMC controller is shown in Figure 3.2. The enhanced constraint mechanism, which is derived in Section 3.3, caters for absolute and rate plant input constraints and anti-windup of the controller's output.

3.3 Derivation of plant input constraint mechanism

The constraint mechanism, shown in Figure 3.2, contains absolute and rate plant input amplitude constraints. If the time constant (τ) of the first order transfer function in the constraint mechanism is selected small enough then,

$$u' \approx u \tag{3.5}$$

when no constraint violations occur.

The transfer function $\frac{x_2(s)}{u'(s)}$ is defined as,

$$\begin{aligned} \frac{x_2(s)}{u'(s)} &= \frac{1}{\tau}\left[1 - \frac{1}{\tau s + 1}\right] \\ &= \frac{s}{\tau s + 1} \end{aligned}$$

The Bode plot of the transfer function of $\frac{x_2(s)}{u'(s)}$ is shown in Figure 3.3. It can be

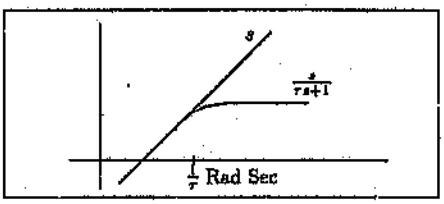

Figure 3.3: Magnitude Bode plot of $\frac{x_2(s)}{u'(s)}$

seen that when

$$w < \frac{1}{\tau} \quad \text{rad/sec} \tag{3.6}$$

then,

$$\frac{x_2(s)}{u'(s)} \approx s \tag{3.7}$$

The transfer function $\frac{x_3(s)}{u'(s)}$ is defined as,

$$\begin{aligned}\frac{x_3(s)}{u'(s)} &= \left[1 - \frac{1}{\tau s + 1}\right] + \frac{1}{\tau s + 1} \\ &= 1\end{aligned}$$

Therefore, the saturation elements defined in the constraint mechanism shown in Figure 3.2 clearly constrain the amplitude of the rate and absolute plant input signals.

3.4 Issues in designing controller

3.4.1 Selection of $K(s)$

Issues in designing the filter $K(s)$ are presented in Chapter 2. In short, a good criterion for the design of $K(s)$ is to select the bandwidth of $K'(s)$ small enough to reduce the actuator activity to an acceptable level, but also large enough such that no poles of $K(s)$ are in the RHP.

3.4.2 Selection of τ

The transfer function $\frac{x_2(s)}{u'(s)}$ is a good approximation of a differentiator in the important frequency range if τ is sufficiently small. One possible criterion for the selection of τ is

$$\frac{1}{\tau} > \text{bandwidth}[K'(s)] \tag{3.8}$$

3.4.3 Selection of constraints

Constraint settings should be selected based on knowledge of the constraints present in the physical plant. Over estimation of plant constraints leads to robust control, as true plant constraints are always met. However, this is at the expense of system performance.

3.5 Simulated example

A simulation study is carried out to demonstrate the constraint handling ability of the proposed IMC controller. The signal flow diagram of the simulation is shown in Figure 3.2.

As the aim of the study is not to investigate the ability of the controller to handle model uncertainty, it is assumed that there is no modelling error. A plant model,

$$G(s) = \hat{G}(s) = \frac{e^{-8s}}{s^2 + 0.6s + 1} \tag{3.9}$$

is selected that has long dead time and small damping factor, common to certain types of industrial plants.

A suitable disturbance, occurring at the plant output, is specified that causes the actuator to saturate when the controller attempts to null the offset error caused by the disturbance. The disturbance at the plant output is defined as,

$$d(t) = \begin{cases} 0 & \text{if } t <= 100 \text{ sec} \\ -0.2 & \text{if } 100 < t <= 200 \text{ sec} \\ 0.5 & \text{if } t > 200 \text{ sec} \end{cases} \tag{3.10}$$

Sensor noise, $n(t)$, has the following settings:

Noise Bandwidth $= w_b = 3$ rad/sec
Noise variance $= v = 5.07\text{e-}5$ units

3.5.1 Controller design

A suitable model of the plant, inherent in the IMC filter $Q(s)$, is based on the nominal plant model defined in Equation 3.9 and may be approximated by,

$$\hat{G}'(s) = \frac{1}{s^2 + 0.6s + 1} \tag{3.11}$$

The IMC controller is tuned by specifying a suitable closed loop response filter, $F(s)$, that conforms to time domain specifications. For this design typical time domain specifications are,

$$t_r \approx 7 \text{ sec} \tag{3.12}$$

$$\zeta = 0.7 \tag{3.13}$$

Table 3.1: Constraint settings

Simulation No.	u_{min}	u_{max}	$\left[\frac{du}{dt}\right]_{min}$	$\left[\frac{du}{dt}\right]_{max}$
1	0	1.1	-10	10
2	0	1.1	-3	3
3	0	1.1	-1	1
4	0	1.1	-0.8	0.8
5	0	1.1	-0.6	0.6
6	0	1.1	-0.4	0.4
7	0	1.1	-0.2	0.2
8	0	1.1	-0.1	0.1
9	0	1.1	-0.09	0.09
10	0	1.1	-0.08	0.08
11	0	1.1	-0.07	0.07
12	0	1.1	-0.06	0.06
13	0	1.1	-0.05	0.05
14	0	1.1	-0.04	0.04
15	0	1.1	-0.03	0.03
16	0	1.1	-0.02	0.02
17	0	1.1	-0.015	0.015
18	0	1.1	-0.01	0.05

Using the heuristic equation (Franklin et al. 1986),

$$\omega_n \approx 1.8/t_r \tag{3.14}$$

which selects the natural frequency for a second order prototype transfer function, an appropriate closed loop response filter is,

$$F(s) = \frac{0.0661}{s^2 + 0.36s + 0.0661} \tag{3.15}$$

Using Equation 3.1, the parameter q_o is calculated to be,

$$q_o = 0.0661 \tag{3.16}$$

A range of controllers with different rate constraint settings are simulated. The constraint settings for the controllers are shown in Table 3.1.

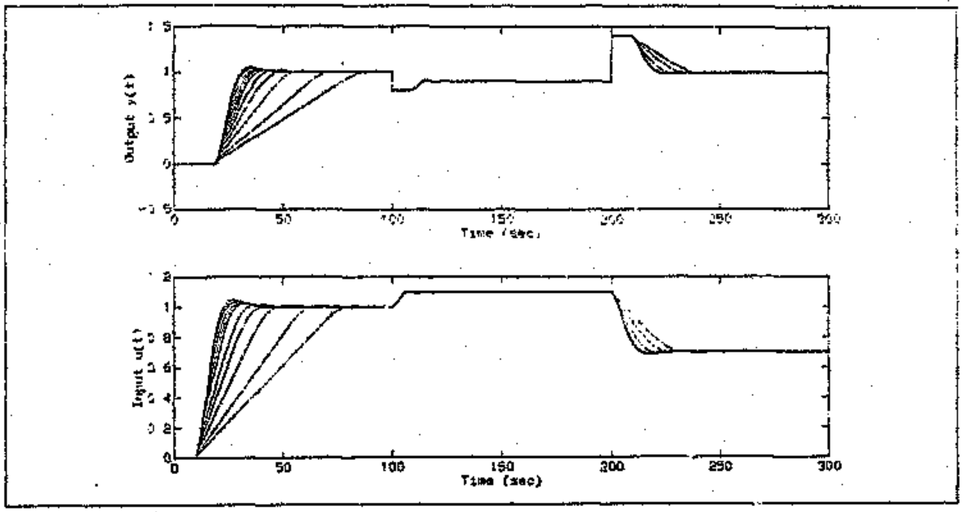

Figure 3.4: Simulation results

3.5.2 Filter design

Based on the Bode plot of

$$Q(s) = F(s)(\hat{G}')^{-1}(s)$$

an appropriate low pass filter for extending the biproper IMC controller ($Q(s)$) to the strictly proper controller ($Q'(s)$) is,

$$K'(s) = \frac{40}{s^2 + 22s + 40} \tag{3.17}$$

Using Equation 3.3, the transfer function of the filter $K(s)$ is,

$$K(s) = \frac{40s^2 + 24s + 40}{s^4 + 22.36s^3 + 47.99s^2 + 25.45s + 40} \tag{3.18}$$

3.6 Simulation results

The simulation results for Simulations 1 to 17 are shown in Figure 3.4. This plot clearly shows the controller's ability to handle absolute and rate constraints. When the controller responds to the disturbance at $t = [100, 200]$ seconds, the actuator signal increases until it reaches the maximum plant input constraint setting. When the disturbance changes at $t = 200$ seconds, the controller responds without any evidence of integral windup, which would occur if the actuator saturation were not handled correctly. The performance of the controller's rate constraint mechanism is visible in the range $t < 100$ seconds. No set-point overshoot caused by integral

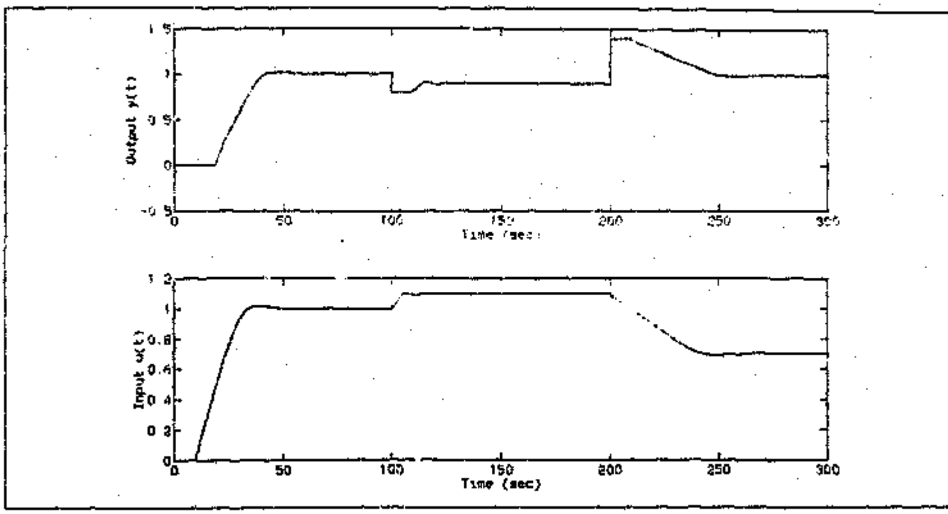

Figure 3.5: Simulation results (Different rate constraint bounds)

windup is evident, which confirms that the rate constraint mechanism is operating correctly.

The simulation result for Simulation 18 is shown in Figure 3.5. This simulation demonstrates the controller's ability to handle different rate constraint bounds (ie. different max. and min. rate constraint bounds), which is impossible to achieve using purely linear control. This type of control is useful, e.g. when actuators such as pneumatic valves are used which have different opening and closing characteristics. This information can be included in the design by specifying the IMC controller's rate constraint bounds accordingly.

3.7 Summary

A new constraint mechanism is presented that includes rate and absolute plant input constraints into the feedback controller. This is an important contribution because often the physical plant is limited by non-linearities such as rate and absolute saturation constraints. The ability to include these constraints into the controller leads to improved control performance because the uncertainty caused by the saturation constraints is now removed from the feedback control system.

A simulation study is carried out which emphasises the benefits of using the constraint mechanism.

Chapter 4

Improved Feedforward Control Framework for IMC Control

The objective of feedback control is to reduce uncertainty and reject disturbances that affect the output of the plant. In most process control problems a feedback controller with integral action is sufficient for providing the necessary robustness to ensure good control. However, if known disturbances are measurable and predictable then it is often a good idea to include a feedforward controller into the control system. This scheme leads to improved disturbance rejection because the control actions for rejecting the disturbance are initiated before the effect of the disturbance is observed at the plant output.

Recent developments in IMC control presented by Goodwin (Seron et al. 1995, Goodwin et al. 1993) shows that special attention must be paid to the architecture of a feedback controller when a constraint mechanism for process input constraints is included in the controller. Goodwin shows that there are three separate plant models present in the feedback system and that a special framework is required to ensure all three plant models have the same input signal. A strictly proper version of Goodwin's Internal Model Controller (IMC) with modifications to the constraint mechanism to include active absolute and rate constraints on the process input is presented in Chapter 3. This chapter extends the framework presented in Chapter 3 to include feedforward control. While the concept of feedforward control is not new to IMC control (Morari & Zafiriou 1989), the framework presented in this chapter proposes a new approach to the implementation of feedforward control. The feedforward controller is now integrated into the feedback controller and takes advantage of the feedback controller's constraint mechanism. This is an important improvement because feedforward control can now be implemented without the possibility of actuator saturation.

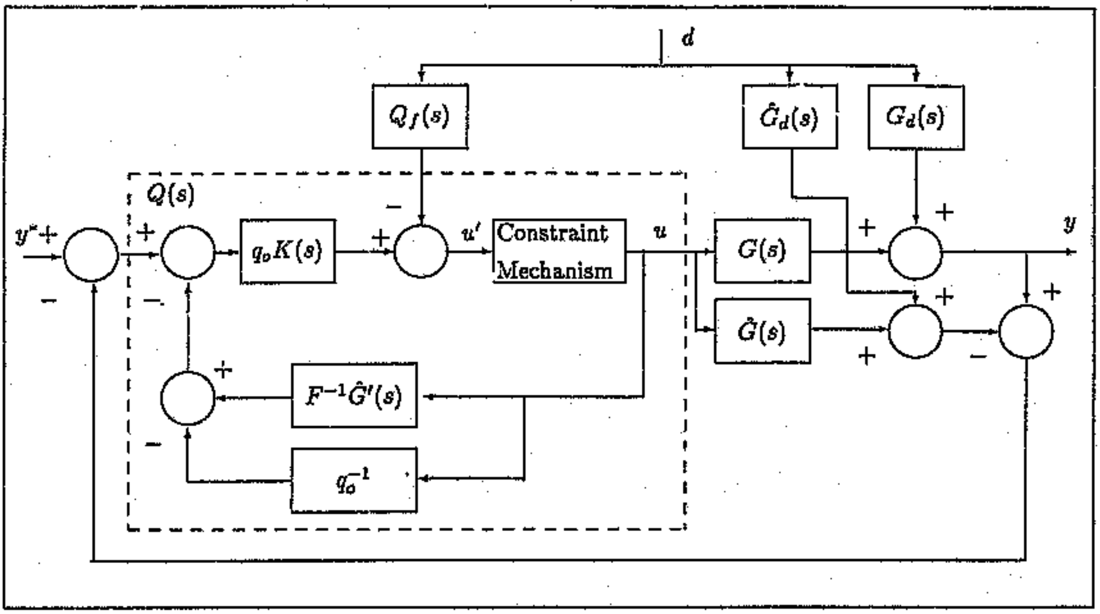

Figure 4.1: Proposed IMC Framework for Feedforward Control

The chapter is organised as follows. Section 4.1 gives reasons motivating the need for the proposed feedforward framework. Section 4.2 presents the feedforward controller and discusses the architecture of the proposed IMC framework. Section 4.3 discusses issues relevant to the design of the feedforward controller. A simulation study is presented in Section 4.4 which demonstrates the proposed feedforward framework. The simulation results are presented in Section 4.5. A summary of the chapter is presented in Section 4.6.

4.1 Improved method of feedforward control design

Recent developments (Goodwin et al. 1993) show that a special framework is required when process constraints are included in the controller. If a feedforward controller is included in the system then it is important that the feedforward controller does not cause constraint violations. It is therefore important how the feedforward controller is integrated into the feedback loop. The method proposed in this chapter is to include the output signal of the feedforward controller into the IMC filter, as shown in Figure 4.1. This method ensures that the process input signal does not violate the process input constraints defined in the constraint mechanism.

4.2 Proposed feedforward IMC framework

The proposed feedforward IMC framework is presented in Figure 4.1.

4.2.1 Architecture

The architecture of the IMC filter ($Q(s)$) is based on Goodwins IMC method (Goodwin et al. 1993). An additional filter $K(s)$ is included in the controller. This filter ensures that the feedback controller is strictly proper (Chapter 2). The constraint mechanism, defined in Chapter 3, places constraints on the rate and absolute process input. G_d and $\hat{G}_d$ are the real and estimated disturbance models. G and $\hat{G}$ are the real and estimated plant models. F is the closed loop response filter and q_o is defined as,

$$q_o = \lim_{\omega \to \infty} [F(\jmath\omega)(\hat{G}')^{-1}(\jmath\omega)] \tag{4.1}$$

$Q_f(s)$ is the feedforward IMC filter.

4.2.2 Transfer function of feedforward disturbance response

The transfer function of the disturbance response is,

$$\frac{y(s)}{d(s)} = \frac{G_d(1 - Q\hat{G}) - G(\frac{Q_F}{L_Q+1} - Q\hat{G}_d)}{1 + Q(G - \hat{G})} \tag{4.2}$$

where,

$$Q(s) = F(s)\left(\hat{G}'(s)\right)^{-1} \tag{4.3}$$

and $L_Q(s)$, which is the loop gain of the IMC module (Q) defined in Figure 4.1 is,

$$L_Q(s) = q_o F^{-1}(s)\,\hat{G}'(s)\,K(s) - K(s) \tag{4.4}$$

Refer to Appendix A.3 for the derivation of Equations 4.2 and 4.4.

4.3 Issues in designing the feedforward controller

The following issues are important for ensuring a robust feedforward design.

4.3.1 Selection of disturbance model

The success of the feedforward controller depends heavily on the accuracy of the estimated disturbance model ($\hat{G}_d$). It is important that the model $\hat{G}_d$ be accurate over the bandwidth of the feedforward controller.

4.3.2 Feedforward controller design

The design equation for the feedforward controller, $Q_f(s)$, is presented in Equation 4.5. The controller is designed using response filters. $F_f(s)$ is the filter defining the disturbance rejection response and $F(s)$ is the closed loop response filter. q_o is defined in Equation 4.1.

$$Q_f(s) = q_o F_f(s) F^{-1}(s) \tag{4.5}$$

Refer to Appendix A.3 for the derivation of this equation.

4.3.3 Integral action

When feedforward control is included in a system and there is uncertainty in the gain of the disturbance model, then constant offsets may appear at the plant output. A method of nulling constant offsets at the plant output is to include integral action into the controller.

In order to ensure integral action, the following equations must hold at DC ($s = j\omega$ where $\omega = 0$ rad/ c).

$$Q(s)\,\hat{G}(s) = 1 \tag{4.6}$$

$$Q(s)\,\hat{G}'(s) = 1 \tag{4.7}$$

$$F_f(s) = \hat{G}_d(s) \tag{4.8}$$

where,

$$Q(s) = F(s)\,(\hat{G}'(s))^{-1} \tag{4.9}$$

Refer to Appendix A.3 for the derivation of these equations.

4.4 Simulated example

A simulation study is carried out to demonstrate the proposed feedforward controller. The signal flow diag ·m of the simulation is shown in Figure 4.1. As the aim of the study is not to investigate the ability of the controller to handle mr del uncertainty, it is assumed that there is no modelling error.

A plant model is selected that has long dead time and small damping factor, common to certain types of industrial plants. A disturbance model is selected that has a short dead time relative to the plant model.

$$G(s) = \hat{G}(s) = \frac{e^{-5s}}{s^2 + 0.6s + 1} \tag{4.10}$$

$$G_d(s) = \hat{G}_d(s) = \frac{e^{-3s}}{3s + 1} \tag{4.11}$$

A suitable disturbance, occurring at the plant output, is specified that causes the actuator to saturate when the controller attempts to null the offset error caused by the disturbance. The disturbance at the plant output is defined as,

$$d(t) = \begin{cases} 0 & \text{if } t <= 100 \text{ sec} \\ -0.2 & \text{if } 100 < t <= 200 \text{ sec} \\ 0.5 & \text{if } t > 200 \text{ sec} \end{cases} \tag{4.12}$$

The sensor noise signal, $n(t)$, has the following settings:

Noise Bandwidth	$= \omega_b = 3$ rad/sec
Noise amplitude distribution	$= v \; = 5.07\text{e-}5$ units

4.4.1 Feedback controller design

A suitable model of the plant, inherent in the IMC filter $Q(s)$, is based on the nominal plant model defined in Equation 4.10 and may be approximated by,

$$\hat{G}'(s) = \frac{1}{s^2 + 0.6s + 1} \tag{4.13}$$

The IMC controller is tuned by specifying a suitable closed loop response filter, $F(s)$, that conforms to time domain specifications. For this design typical time domain specifications are,

$$t_r \approx 7 \text{ sec} \tag{4.14}$$

$$\zeta = 0.7 \tag{4.15}$$

Using the heuristic equation (Franklin et al. 1986),

$$\omega_n \approx 1.8/t_r \tag{4.16}$$

which selects the natural frequency for a second order prototype transfer function, an appropriate closed loop response filter is,

$$F(s) = \frac{0.0661}{s^2 + 0.36s + 0.0661} \tag{4.17}$$

Using Equation 4.1, the parameter q_o is calculated to be,

$$q_o = 0.0661 \tag{4.18}$$

The plant input constraints are taken to be,

$$u_{\min} = 0 \tag{4.19}$$

$$u_{\max} = 1.1 \tag{4.20}$$

$$\left[\frac{du}{dt}\right]_{\min} = -0.03 \tag{4.21}$$

$$\left[\frac{du}{dt}\right]_{\max} = 0.03 \tag{4.22}$$

4.4.2 Filter design

Based on the Bode plot of

$$Q(s) = F(s)(\hat{G}'(s))^{-1} \tag{4.23}$$

an appropriate low pass filter for extending the biproper IMC controller to the strictly proper controller is

$$K'(s) = \frac{40}{s^2 + 22s + 40} \tag{4.24}$$

Equation 4.25 translates the filter $K'(s)$ into the actual filter implemented in the IMC filter, $K(s)$. Refer to Chapter 2 for the derivation of Equation 4.25.

$$K(s) = \frac{F(s)(\hat{G}')^{-1}(s)K'(s)}{q_o - K'(s)[q_o - F(s)(\hat{G}')^{-1}(s)]} \tag{4.25}$$

Using Equation 4.25, the transfer function of the filter is

$$K(s) = \frac{40s^2 + 24s + 40}{s^4 + 22.36s^3 + 47.99s^2 + 25.45s + 40} \tag{4.26}$$

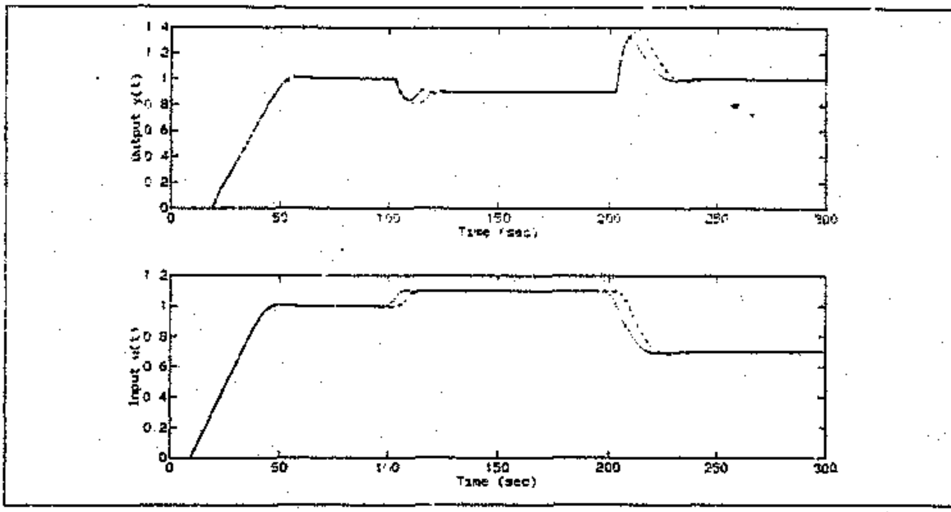

Figure 4.2: Simulation results (Solid = Feedforward, Dashed = Feedback only)

4.4.3 Feedforward controller design

It is important that the feedforward IMC filter ($Q_f(s)$) is strictly proper. This ensures that the feedforward controller is insensitive to high frequency noise. To ensure that $Q_f(s)$ is strictly proper, the order of the transfer function of $F_f(s)$ must be greater than the order of $F(s)$.

A typical time domain specification for the feedforward response filter is,

$$t_r \approx 6 \text{ sec} \tag{4.27}$$

$$\zeta = 0.7 \tag{4.28}$$

Using the heuristic equation (Franklin et al. 1986),

$$\omega_n \approx 1.8/t_r \tag{4.29}$$

an appropriate transfer function for the response filter is,

$$F_f(s) = \frac{0.09}{0.01s^3 + 1.0042s^2 + 0.4209s + 0.09} \tag{4.30}$$

Using Equation 4.5, the feedforward IMC filter is,

$$Q_f(s) = \frac{0.09s^2 + 0.0324s + 0.005951}{0.01s^3 + 1.0042s^2 + 0.04209s + 0.09} \tag{4.31}$$

4.5 Simulation results

The simulation results are shown in Figure 4.2. The response of the IMC feedback controller (dashed line) is superimposed onto the response of proposed IMC feedback and feedforward controller (solid line).

The following conclusions are drawn from the results.

- The feedback controller, unlike the feedforward controller, can only initiate control actions to reject a disturbance when the effect of the disturbance is observed at the plant output. The inclusion of the feedforward controller into the control scheme improves the disturbance rejection properties of the feedback system.
- No constraint violations occur when the proposed feedforward controller is included in the system. Observe that the constraint specifications at $t = 100$ and $t = 200$ seconds are not compromised when the proposed IMC controller responds to a step change in the disturbance signal.
- The controller has integral action. Observe that in the range $t = [100, 200]$ seconds the integral component of the controller increases until the plant input signal equals the maximum absolute plant input constraint.
- There is no evidence of integral windup, which can occur when the controller attempts to drive the output against a constraint. Observe that at $t = 200$ seconds, the controller responds to the disturbance without a delay, which would not be possible if integral windup were present in the controller.

4.6 Summary

A new framework for implementing feedforward IMC control is presented. The benefits of the proposed IMC framework is that the feedforward controller is integrated into the feedback controller in such a way that the constraint mechanism supports both feedback and feedforward control.

An equation for designing the feedforward controller is presented. This equation relies on the specification of response filters for the closed loop and feedforward disturbance rejection properties of the system.

A simulation study is carried out which emphasises the benefits of the proposed feedforward control framework. The study shows that improved disturbance rejection is possible with the inclusion of the feedforward controller and that the constraint mechanism supports both the feedforward and feedback controllers.

Part II

Multi-Step Predictive Control

Chapter 5

The Predictor Equation

Model Predictive Control (MPC) refers to a family of controllers in which direct use of a plant model is made for the purpose of feedback control. Well known algorithms such as DMC, GPC, IDCOM and MAC (Cutler & Ramaker 1979, Garcia et al. 1989, Ricker 1985, Clarke et al. 1987*a*, Richalet et al. 1978) are reported in the literature. Although these algorithms differ in their formulation, the resulting control policies are similar. The algorithms are all based on a receding horizon control approach as explained in Section 1.1. A fundamental calculation for all the algorithms is that of forecasting future plant outputs over a finite prediction horizon.

A new building block useful for developing Long Range Predictive Control (LRPC) algorithms is presented in this chapter, called the Predictor Equation. This equation, defined in Equation 5.1, is a matrix equation that projects the future predicted plant outputs ($\hat{Y}$) over a prediction horizon, given the future control inputs (U_{pred}) projected over the control horizon.

$$\hat{Y} = Q\,\hat{Y}_{\text{past}} + R\,U_{\text{past}} + W\,U_{\text{pred}} \tag{5.1}$$

This equation provides a foundation for future work, in which a LRPC algorithm called Multi-Step Predictive Control (MSC) is developed in Chapter 8.

The chapter is organised as follows. Section 5.1 presents the predictor model. Section 5.2 presents the compensated predictor model. The issue of integral action is addressed in Section 5.3. The prediction horizons are explained in Section 5.4. The Predictor Equation is presented in Section 5.5 and the calculation of the Predictor Equation's Q.R and W constants is presented in Section 5.6.

5.1 The predictor model

The predictor equation is based on the dynamic model of the plant, which is referred to as the predictor model. The predictor model, using an ARX model structure (Goodwin & Sin 1984), is defined as,

$$A(q^{-1})\,\hat{y}(t) = B(q^{-1})\,u(t) \tag{5.2}$$

where q is the shift operator and

$$B(q^{-1}) = 0 + b_1q^{-1} + b_2q^{-2} + ... + b_{\mathrm{nb}}q^{-\mathrm{nb}} \tag{5.3}$$

$$A(q^{-1}) = 1 + a_1q^{-1} + a_2q^{-2} + ... + a_{\mathrm{na}}q^{-\mathrm{na}} \tag{5.4}$$

5.2 Compensated predictor model

It is possible for a controller to cancel a particular disturbance by including the model of the disturbance into the controller. It is proposed that the predictor model should be modified to include a model of the disturbance, $T_D(q^{-1})$, and that this model should be called the compensated predictor model.

The ARX model, defined in Equation 5.2, is rewritten as,

$$\hat{y}(t) = \left[\frac{B(q^{-1})}{A(q^{-1})}T_D(q^{-1})\right]\ \frac{u(t)}{T_D(q^{-1})} \tag{5.5}$$

The compensated predictor model is defined as,

$$\frac{B'(q^{-1})}{A'(q^{-1})} = \frac{B(q^{-1})}{A(q^{-1})}T_D(q^{-1}) \tag{5.6}$$

where

$$B'(q^{-1}) = 0 + b'_1q^{-1} + b'_2q^{-2} + ... + b'_{\mathrm{nb'}}q^{-\mathrm{nb'}} \tag{5.7}$$

$$A'(q^{-1}) = 1 + a'_1q^{-1} + a'_2q^{-2} + ... + a'_{\mathrm{na'}}q^{-\mathrm{na'}} \tag{5.8}$$

The input to the compensated predictor model is,

$$u'(t) = \frac{u(t)}{T_D(q^{-1})} \tag{5.9}$$

5.3 Integral action

Integral action, which is required to null constant offset disturbances, is incorporated into the controller by assigning,

$$T_D(q^{-1}) = \frac{1}{1-q^{-1}} = \frac{1}{\Delta} \tag{5.10}$$

The input to the compensated predictor model,

$$u'(t) = \frac{u(t)}{T_D(q^{-1})} = \Delta u(t) \tag{5.11}$$

is interpreted as an incremental input.

5.4 The prediction horizons

The objective of a predictive controller is to find, at each step, the optimal set of projected control inputs which when applied to the predictor model drives the projected outputs to the set-point.

The set of future predicted plant outputs are projected over a prediction horizon, HP steps into the future $(\hat{y}(t+1)...\hat{y}(t+\mathrm{HP}))$. The set of future control actions are projected over the control horizon, CP steps into the future $(u'(t)...u'(t+\mathrm{CP}-1))$, where $\mathrm{CP} \leq \mathrm{HP}$.

If $\mathrm{CP} < \mathrm{HP}$ then it is assumed that the future control inputs $u'(t+\mathrm{CP})...u'(t+\mathrm{HP}-1)$ are zero and are therefore excluded from the algorithm.

5.5 Predictor Equation

The predictor equation is defined as,

$$\hat{Y} = Q\,\hat{Y}_{\mathrm{past}} + R\,U_{\mathrm{past}} + W\,U_{\mathrm{pred}} \tag{5.12}$$

where,

$$\hat{Y} = \begin{bmatrix} \hat{y}(t+1) \\ \hat{y}(t+2) \\ \vdots \\ \hat{y}(t+\mathrm{HP}) \end{bmatrix} \tag{5.13}$$

$$\hat{Y}_{\mathrm{past}} = \begin{bmatrix} \hat{y}(t) \\ \hat{y}(t-1) \\ \vdots \\ \hat{y}(t-(\mathrm{na}'-1)) \end{bmatrix} \tag{5.14}$$

$$U_{\text{past}} = \begin{bmatrix} u'(t-1) \\ u'(t-2) \\ \vdots \\ u'(t-(\text{nb}'-1)) \end{bmatrix} \tag{5.15}$$

$$U_{\text{pred}} = \begin{bmatrix} u'(t+\text{CP}-1) \\ u'(t+\text{CP}-2) \\ \vdots \\ u'(t) \end{bmatrix} \tag{5.16}$$

5.6 Calculation of Q, R and W matrices

The j step ahead predictor can be expressed using the equation (Appendix B),

$$\hat{y}(t+j) = q_j \hat{Y}_{\text{past}} \; + \; x_j \begin{bmatrix} U_{\text{pred}} \\ \Gamma_{\text{past}} \end{bmatrix} \tag{5.17}$$

where the constants q_j and x_j are solved using the equations,

$$q_j = (q_{j-1}S_3)q_1 + q_{j-1}S_1 \tag{5.18}$$

$$x_j = (q_{j-1}S_3)x_1 + x_{j-1}S_2 \tag{5.19}$$

$$S_1 = \begin{bmatrix} 0 \; ... \; 0 \\ I_1 \;\; \vdots \\ \quad\;\; 0 \end{bmatrix} S_2 = \begin{bmatrix} 0 \; ... \; 0 \\ I_2 \;\; \vdots \\ \quad\;\; 0 \end{bmatrix} \tag{5.20}$$

$$S_3 = [1 \;\; 0 \;\; ... \;\; 0]^T \tag{5.21}$$

$$q_1 = [-a'_1 \;\; -a'_2 \; ... \; -a'_{\text{na}'}] \tag{5.22}$$

$$x_1 = [0 \;\; ... \;\; 0 \;\; b'_1 \;\; b'_2 \;\; ... \;\; b_{\text{nb}'}] \tag{5.23}$$

I_1 is an identity matrix with dimensions (na$'-1$) x (na$'-1$). I_2 is an identity matrix with dimensions (CP+nb$'-1$) x (CP+nb$'-1$).

Matrices Q and X are defined based on the row vectors q_j and x_j,

$$Q = \begin{bmatrix} q_1 \\ q_2 \\ \vdots \\ q_{\text{HP}} \end{bmatrix} \qquad X = \begin{bmatrix} x_1 \\ x_2 \\ \vdots \\ x_{\text{HP}} \end{bmatrix} \tag{5.24}$$

Matrices W and R are sub-matrices of X, such that,

$$\begin{aligned} X \begin{bmatrix} U_{\text{pred}} \\ U_{\text{past}} \end{bmatrix} &= [W \; R] \begin{bmatrix} U_{\text{pred}} \\ U_{\text{past}} \end{bmatrix} \\ &= WU_{\text{pred}} + RU_{\text{past}} \end{aligned} \tag{5.25}$$

5.7 Summary

A new building block, called the Predictor Equation, useful for developing Long Range Predictive Control algorithms is presented. This equation provides a foundation for the development of a modular approach to predictive control. The issue of integral action is discussed and a method of including integral action into the predictor equation is presented.

Chapter 6

The Reference Trajectory

Long Range Predictive Control (LRPC) algorithms such as IDCOM (Richalet et al. 1978), GPC (Clarke et al. 1987*a*) and MAC (Rouhani & Mehra 1982) make use of a reference trajectory which describes the desired future controlled variable over the prediction horizon. It provides the controller's optimisation routine with a projection of reference set-points that the plant's projected output is expected to track. The trajectory is generated according to some criterion (e.g. no overshoot, fixed time response). The method of generating the trajectory is usually in the form of a recursive routine based on a first order discrete time model. The inclusion of this feature into the algorithm has important practical benefits. It provides an on-line method for tuning the controller.

This chapter presents a module which calculates the reference trajectory, given the measured plant output ($y_o(t)$) and the set-point value ($y^*(t)$). This module is necessary for future work in which a modular model of a LRPC algorithm called Multi-Step Predictive Control (MSC) is derived in Chapter 9.

The chapter is organised as follows. Section 6.1 presents the recursive algorithm used by most LRPC algorithms to generate a reference trajectory. Section 6.2 presents an equation that calculates the j-step ahead reference set-point. Section 6.3 presents the equivalent block diagram model of the recursive routine used to generate the reference trajectory. A summary is presented in Section 6.4.

6.1 Discrete time model of reference trajectory

The proposed reference trajectory model presented in this chapter is derived from the first order transfer function model,

$$R(s) = \frac{1}{\tau_{\text{ref}} s \ + \ 1} \tag{6.1}$$

A discrete time model of Equation 6.1 is,

$$y_{\text{ref}}(t+1) = \beta \ y_{\text{ref}}(t) \ + \ [1-\beta] \ y^*(t) \tag{6.2}$$

where,

$$\beta = e^{-T_{sp}/\tau_{\text{ref}}} \tag{6.3}$$

If,

$$a = 1 - \beta \tag{6.4}$$

then Equation 6.2 becomes,

$$y_{\text{ref}}(t+1) = \beta \ y_{\text{ref}}(t) \ + \ a \ y^*(t) \tag{6.5}$$

Refer to Appendix B.2 for the derivation of the Equation 6.5.

6.2 j-step ahead reference

It can be shown that the j-step ahead reference $y_{\text{ref}}(t+j)$ is,

$$y_{\text{ref}}(t+j) = \beta^j \ y_o(t) + [1-\beta^j] \ y^* \tag{6.6}$$

where $y_o(t)$ is the measured plant output at time t seconds and y^* is the reference set-point.

Refer to Appendix B.2 for the derivation of Equation 6.6.

6.3 Block diagram model

The block diagram model shown in Figure 6.1 generates the reference trajectory, Y_{ref}.

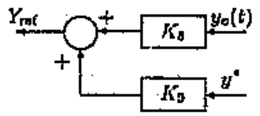

Figure 6.1: Block Diagram Model

The model is based on the following equation,

$$\begin{aligned} Y_{ref} &= \begin{bmatrix} y_{ref}(t+1) \\ y_{ref}(t+2) \\ \vdots \\ y_{ref}(t+\mathrm{HP}) \end{bmatrix} \\ &= \begin{bmatrix} \beta \\ \beta^2 \\ \vdots \\ \beta^{\mathrm{HP}} \end{bmatrix} y_o(t) + \begin{bmatrix} 1-\beta \\ 1-\beta^2 \\ \vdots \\ 1-\beta^{\mathrm{HP}} \end{bmatrix} y^* \\ &= K_8\, y_o(t) \;+\; K_9\, y^* \end{aligned} \tag{6.7}$$

The matrices K_8 and K_9 are called conversion matrices. This model is a building block in the derivation of a complete modular model of a LRPC algorithm called Multi-Step Predictive Control (MSC), presented in Chapter 9.

6.4 Summary

The reference trajectory of a LRPC algorithm is usually generated using a recursive equation. A block diagram model is presented that performs the identical calculation as the recursive equation. This model is significant because it generates the trajectory in a single calculation. It is a useful building block for the development of a complete modular model of a LRPC algorithm called Multi-Step Predictive Control (MSC).

Chapter 7

New Building Block for Predictive Control - First Order Filter

A block diagram model that calculates the reference trajectory, in a single calculation, is presented in Chapter 6. This chapter presents a similar building block which is used in Multi-Step Predictive Control's feedforward control module, presented in Chapter 14. The module presented in this chapter provides the equivalent filtering action as a first order transfer function. Consider the Long Range Predictive Control (LRPC) filter shown in Figure 7.1.

Figure 7.1: LRPC filter

$$X = \begin{bmatrix} x(t+1) \\ x(t+2) \\ \vdots \\ x(t+\mathrm{HP}) \end{bmatrix} Y = \begin{bmatrix} y(t+1) \\ y(t+2) \\ \vdots \\ y(t+\mathrm{HP}) \end{bmatrix}. \tag{7.1}$$

The input to the filter is a trajectory projected over the prediction horizon. The purpose of the filter module is to filter the trajectory X, based on a first order transfer function, to produce an output trajectory Y.

The chapter is organised as follows. Section 7.1 presents the discrete time model of the filter. Section 7.2 presents the equivalent LRPC filter which is demonstrated in Section 7.3. A summary is presented in Section 7.4.

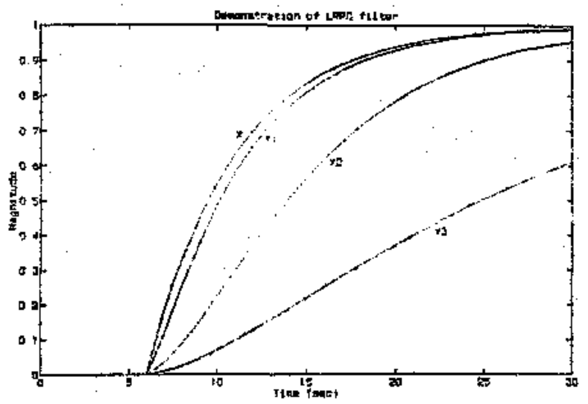

Figure 7.2: Demonstration of filtering action of LRPC filter

7.1 Discrete time model

The continuous time transfer function of the proposed filter is,

$$T(s) = \frac{1}{\tau\, s + 1} \tag{7.2}$$

The discrete time transfer function of the filter, with a zero order hold on the input is,

$$\begin{aligned} T(z) &= (1 - z^{-1})\, Z\left[\frac{T(s)}{s}\right] \\ &= \frac{1-\beta}{z-\beta} \end{aligned} \tag{7.3}$$

where $\beta = e^{-T_{sp}/\tau}$, T_{sp} is the sampling period and τ is the time constant of the filter.

Equation 7.3 is re-written,

$$T(z) = \frac{[1-\beta]\, z^{-1}}{1 - \beta\, z^{-1}} \tag{7.4}$$

and neglecting the delay,

$$T'(z) = \frac{1-\beta}{1-\beta\, z^{-1}} \tag{7.5}$$

The transfer function (Equation 7.5) is written in discrete time using a time-shift operator,

$$[1 - \beta\, q^{-1}]\, y(t) = [1-\beta]\, x(t) \tag{7.6}$$

and expanding,

$$y(t) = \beta\, y(t-1) + a\, x(t) \tag{7.7}$$

where,

$$a = 1 - \beta \tag{7.8}$$

7.2 Equivalent LRPC filter

The equivalent LRPC filter is defined as,

$$Y = K_{14} X \tag{7.9}$$

where,

$$K_{14} = K_{14A} + a K_{14B} \tag{7.10}$$

The matrices K_{14A} and K_{14B} are,

$$K_{14A} = \begin{bmatrix} \beta & 0 & \dots & 0 \\ \beta^2 & 0 & \dots & 0 \\ \beta^3 & 0 & \dots & 0 \\ \beta^4 & 0 & \dots & 0 \\ \vdots & & & \\ \beta^{\mathrm{HP}} & 0 & \dots & 0 \end{bmatrix} \tag{7.11}$$

and

$$K_{14B} = \begin{bmatrix} 1 & 0 & 0 & 0 & \dots & 0 \\ \beta & 1 & 0 & 0 & \dots & 0 \\ \beta^2 & \beta & 1 & 0 & \dots & 0 \\ \beta^3 & \beta^2 & \beta & 1 & \dots & 0 \\ \vdots & & & & & \\ \beta^{\mathrm{HP}-1} & \beta^{\mathrm{HP}-2} & \beta^{\mathrm{HP}-3} & \beta^{\mathrm{HP}-4} & \dots & 1 \end{bmatrix} \tag{7.12}$$

Refer to Appendix B.4 for the derivation of the LRPC filter.

In the limit as the time constant (τ) of the filter is reduced to zero, so $\beta \to 0$ and all elements in $K_{14A} \to 0$, $K_{14B} \to I$ (I is the identity matrix) and $a \to 1$.

The key result here is,

$$\lim_{\tau \to 0} K_{14} \to I \tag{7.13}$$

Therefore as τ is reduced, the effect of the filtering action is reduced and in the limit as $\tau \to 0$ the output Y is identical to X and no filtering action is present.

7.3 Demonstration

The graph shown in Figure 7.2 is a demonstration of the filtering action of the proposed LRPC filter.

The input to the filter is the step response of the transfer function,

$$P(s) = \frac{e^{-5s}}{5s+1} \tag{7.14}$$

with a sampling period of $T_{sp} = 1$ second and horizon of HP $= 30$ steps.

Where: X $=$ Horizon to be filtered. (Input to filter)
Y1 $=$ Horizon after filtering action, with $\tau = 1$ second.
Y2 $=$ Horizon after filtering action, with $\tau = 5$ seconds.
Y3 $=$ Horizon after filtering action, with $\tau = 20$ seconds.

The results shown in Figure 7.2 verify Equation 7.13. The filtering action is regulated by the time constant τ.

Note: There is no delay between the output of the filter and the input. As $\tau \to 0$, then $Y \to X$.

7.4 Summary

A new building block for Long Range Predictive Control is presented. The module presented performs the equivalent filtering action as a first order transfer function. A demonstration of the proposed filter shows that it is possible to regulate the filtering action by changing the time constant of the filter. The significance of the model is that it consist of only one matrix and can, if necessary, be de-tuned to reduce the filtering action by decreasing the filter's time constant.

Chapter 8

MSC Control - The Basic Algorithm

Advances in computer technology have opened the way to new methods of control which have had a significant impact on the process control industry. The conventional approach to feedback design relies on classical frequency domain techniques, which provide design tools capable of ensuring stable and robust control systems. However, there are disadvantages to using these control techniques when applied to process control problems; namely, that the design procedure for multi-input-output systems is often difficult and expensive. Process control engineers, particularly in the chemical industry, have therefore investigated other methodologies.

One such advanced control methodology is Model Predictive Control (MPC), which takes full advantage of the benefits that modern digital computers offer. Long range predictive control (LRPC) which is a subset of MPC, is based on a receding horizon control policy (Athans & Falb 1966). A pre-calculated model of the process, called the Predictor Model, is used to project the future performance of the process over a prediction horizon. The LRPC algorithm calculates, at each control step, the optimum set of future control actions projected over a control horizon which produce the best projected plant performance. This forms the basis of the optimal control problem for LRPC algorithms.

A significant feature of LRPC is it ability to incorporate process dynamics into the design of the predictive controller making it possible for the controller to maintain an awareness of dead-time and other unusual dynamic behaviour. Also, the LRPC architecture leads to a high order controller with few tuning parameters. In addition to this characteristic, the LRPC architecture is important in that it guarantees a stable feedback system as long as the plant and predictor models are stable (Garcia et al. 1989). LRPC algorithms usually include integral action which is necessary for nulling constant offset disturbances that appear at the plant output. Another important feature of LRPC is its ability to include process constraints into the design of the controller. The optimal control problem. which is solved at each control step, is usually formulated as a quadratic program with process constraints in the form of inequality constraints.

LRPC algorithms such as IDCOM, MAC, DMC and GPC (Richalet et al. 1978, Rouhani & Mehra 1982, Cutler & Ramaker 1979, Clarke et al. 1987*a*) are presented in the literature. This chapter presents the Multi-Step Predictive Control (MSC) algorithm. Although this chapter concentrates on the single-input-output MSC algorithm, it is possible to extend the algorithm presented in this chapter to the multi input-output case. Refer to (Bolton & MacLeod 1995) for details of a simulation study of MSC control applied to a multi-variable control problem.

The chapter is organised as follows. An overview of the MSC algorithm is presented in Section 8.1. The predictor equation, which calculates the projected plant output trajectory, is presented in Section 8.3. An explanation of the prediction horizons is given in Section 8.2. The optimal control problem's objective function (cost function) is presented in Section 8.4. The cost function expressed in quadratic form is presented in Section 8.5. The recursive equation for calculating the reference trajectory is presented in Section 8.6. Two separate versions of the MSC algorithm are presented. The unconstrained MSC controller in Section 8.7 and the constrained MSC controller in Section 8.8. A summary is presented in Section 8.9.

8.1 Overview of the MSC algorithm

The MSC algorithm is a LRPC technique that makes use of a predictor model in the form of a linear, discrete time transfer function. The predictor model, using an ARX model struc e (Goodwin & Sin 1984), is defined as,

$$A(q^{-1})\,\hat{y}(t) \;=\; B(q^{-1})\,u(t) \tag{8.1}$$

where q is the shift operator and

$$B(q^{-1}) = 0 + b_1 q^{-1} + b_2 q^{-2} + \ldots + b_{\mathrm{nb}} q^{-\mathrm{nb}} \tag{8.2}$$

$$A(q^{-1}) = 1 + a_1 q^{-1} + a_2 q^{-2} + \ldots + a_{\mathrm{na}} q^{-\mathrm{na}} \tag{8.3}$$

This model is used to build a predictor equation (Chapter 5) which projects the future outputs of the plant over the prediction horizon.

Figure 8.1 presents an overview of the signal flow diagram of the MSC algorithm.

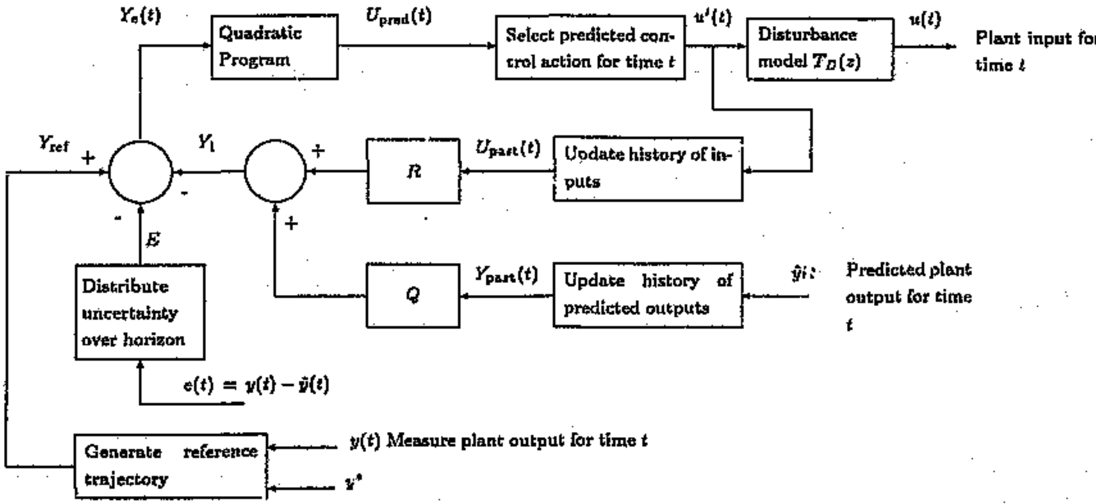

Figure 8.1: Signal flow diagram of MSC predictive control

Features of typical LRPC algorithms such as dead time compensation, integral action and the ability to include process constraints are key features of the MSC algorithm.

The MSC algorithm makes use of an optimisation routine for solving the optimal control problem. This optimal control problem, which is solved for each control step, takes the form of a quadratic program with inequality constraints. If no process constraints are included in the feedback control design, then a closed form solution to the optimal control problem exists. In this case the optimisation routine is replaced with a controller gain matrix, which is the solution to the optimal control problem.

The MSC algorithm makes use of a reference trajectory which describes the desired future controlled variable over the prediction horizon. It provides the controller's optimisation routine with a projection of reference set-points that the plant's projected output is expected to track.

8.2 The prediction horizons

The objective of a predictive controller is to find, at each step, the optimal set of projected control inputs which when applied to the predictor model drives the projected outputs to the set-point.

The set of future predicted plant outputs are projected over a prediction horizon, HP steps into the future ($\hat{y}(t+1)...\hat{y}(t+\mathrm{HP})$). The set of future control actions are projected over the control horizon, CP steps into the future ($u'(t)...u'(t+\mathrm{CP}-1)$), where CP $\leq$ HP.

If CP $<$ HP, then it is assumed that the future control inputs $u'(t+\mathrm{CP})...u'(t+\mathrm{HP}-1)$ are zero and are therefore excluded from the algorithm.

8.3 The predictor equation

The predictor equation (Chapter 5) is defined as,

$$\hat{Y} = Q\,\hat{Y}_{\mathrm{past}} + R\,U_{\mathrm{past}} + W\,U_{\mathrm{pred}} \tag{8.4}$$

where,

$$\hat{Y} = \begin{bmatrix} \hat{y}(t+1) \\ \hat{y}(t+2) \\ \vdots \\ \hat{y}(t+\mathrm{HP}) \end{bmatrix} \tag{8.5}$$

$$\hat{Y}_{\mathrm{past}} = \begin{bmatrix} \hat{y}(t) \\ \hat{y}(t-1) \\ \vdots \\ \hat{y}(t-(\mathrm{na}'-1)) \end{bmatrix} \tag{8.6}$$

$$U_{\mathrm{past}} = \begin{bmatrix} u'(t-1) \\ u'(t-2) \\ \vdots \\ u'(t-(\mathrm{nb}'-1)) \end{bmatrix} \tag{8.7}$$

$$U_{\mathrm{pred}} = \begin{bmatrix} u'(t+\mathrm{CP}-1) \\ u'(t+\mathrm{CP}-2) \\ \vdots \\ u'(t) \end{bmatrix} \tag{8.8}$$

This matrix equation projects the future predicted plant outputs ($\hat{Y}$) over a prediction horizon based on the projected future control inputs (U_{pred}) over the control horizon.

Integral action, which is required to null constant offset disturbances, is incorporated into the controller by assigning

$$T_D(q^{-1}) = \frac{1}{1-q^{-1}} = \frac{1}{\Delta} \tag{8.9}$$

Where $T_D(q^{-1})$ is the internal disturbance model defined in Chapter 5.

8.4 The cost function

The optimal control problem, solved at each control step, finds the set of future control actions (U_{pred}) that minimise the mismatch between the reference (Y_{ref}) and projected output ($\hat{Y}$) trajectories.

The objective function used in the optimal control problem is defined in Equation 8.10.

$$\begin{aligned} \text{Cost} \;=\; & \sum_{k=1}^{\text{HP}} \Big[\lambda(k)^2 [Y_{\text{ref}}(t+k) \;-\; \hat{Y}(t+k)]^2 \\ & \quad + \beta(k)^2\, u'(t+k-1)^2\Big] \end{aligned} \tag{8.10}$$

Equation 8.10 gives a quantitative measure of the error between the predictive output trajectory and the reference trajectory. The second term in Equation 8.10 gives a quantitative measure of the control effort required to track the reference trajectory. The parameters λ and β are used to tune the controller. Usually λ is set to unity. β is an important tuning parameter and is used to tune the controller for robustness. Increasing β reduces the incremental change ($u'(t)$). This is a method of regulating the bandwidth of the controller.

8.5 The cost function in quadratic form

The cost function presented in Equation 8.10 is expressed in quadratic form (Kunzi & Wilhelm 1962) in Equation 8.11.

$$\begin{aligned} \text{Cost} \;=\; & (U_{\text{pred}})^T P\, U_{\text{pred}} \;+\; C\, U_{\text{pred}} \\ & +(\gamma Y_e)^T(\gamma Y_e) \end{aligned} \tag{8.11}$$

The last term of Equation 8.11 is not a function of U_{pred} and is considered to be a constant. This term is removed from the cost function. A new cost function is defined in Equation 8.12,

$$\text{Cost}' = (U_{\text{pred}})^T P\, U_{\text{pred}} \;+\; C\, U_{\text{pred}} \tag{8.12}$$

where,

$$P = (\gamma W)^T(\gamma W) + \beta^T\beta \tag{8.13}$$

$$C = -2(\gamma W)^T(\gamma Y_e) \tag{8.14}$$

$$\gamma = \mathrm{diag}[\lambda(1), \lambda(2), ..., \lambda(\mathrm{HP})] \tag{8.15}$$

$$\beta = \mathrm{diag}[\beta(1), \beta(2), ..., \beta(\mathrm{CP})] \tag{8.16}$$

$$Y_e = Y_{\mathrm{ref}} - \hat{Y}_1 - E \tag{8.17}$$

$$\hat{Y}_1 = Q\,Y_{\mathrm{past}} + R\,U_{\mathrm{past}} \tag{8.18}$$

$$E = K_7\,(y(t) - \hat{y}(t)) \tag{8.19}$$

K_7 is a column vector with HP elements. Each element in K_7 is set to 1.

8.6 The reference trajectory

The model for generating the reference trajectory is based on a first order transfer function,

$$R(s) = \frac{1}{\tau_{\mathrm{ref}} s \; + \; 1} \tag{8.20}$$

A discrete time model is derived from Equation 8.20. The recursive equation,

$$y_{\mathrm{ref}}(t+1) = \beta \; y_{\mathrm{ref}}(t) \; + \; [1-\beta] \; y^*(t) \tag{8.21}$$

where,

$$\beta = e^{-T_{sp}/\tau_{\mathrm{ref}}} \tag{8.22}$$

makes use of this discrete time model to generate the reference trajectory. T_{sp} is the sampling period of the controller and τ_{ref} is the time constant of the reference trajectory model.

Let $a = 1 - \beta$, then

$$y_{\mathrm{ref}}(t+1) = \beta \; y_{\mathrm{ref}}(t) \; + \; a \; y^*(t) \tag{8.23}$$

8.7 MSC control - unconstrained case

The solution to the unconstrained, convex quadratic program (Kunzi & Wilhelm 1962) resulting from the optimal control problem is,

$$\begin{aligned} U_o &= -\frac{1}{2}(P^{-1})C \\ &= -\frac{1}{2}(P^{-1})[-2(\gamma W)^T(\gamma Y_e)] \\ &= P^{-1}[(\gamma W)^T\gamma]Y_e \end{aligned} \tag{8.24}$$

where U_o is the vector of optimal control actions that minimise the cost function. The optimal predictive controller gain matrix is defined as,

$$K_{\mathrm{msc}} = P^{-1}[(\gamma W)^T \gamma] \tag{8.25}$$

8.8 MSC control - constrained case

The solution to the constrained, convex quadratic program (Kunzi & Wilhelm 1962) resulting from the optimal control problem is,

$$U_o = \min\{ \quad (U_{\mathrm{pred}})^T P U_{\mathrm{pred}} + C U_{\mathrm{pred}} \qquad | \; a_{\mathrm{con}} U_{\mathrm{pred}} \leq b_{\mathrm{con}} \quad \} \tag{8.26}$$

The process constraints are expressed as inequality constraints,

$$a_{\mathrm{con}} U_{\mathrm{pred}} \leq b_{\mathrm{con}} \tag{8.27}$$

Unfortunately, no known closed form solution to the constrained quadratic program shown in Equation 8.26 exists. The solution to the program relies on numerical methods (Kunzi & Wilhelm 1962).

8.9 Summary

This chapter presents the Multi-Step Predictive Control (MSC) algorithm. Although the chapter concentrates on the single-input-output MSC algorithm, it is possible to extend the algorithm presented in this chapter to the multi-input-output case. This chapter builds a foundation for future work in which a modular model of MSC control is developed.

The technical details of the MSC algorithm are presented in this chapter. Issues such as the prediction horizons, the predictor equation, integral action, cost function, and reference trajectory are discussed. The optimisation routine for solving the predictive controllers optimal control problem is of the form of a quadratic program with inequality constraints. Investigations show that when no process constraints are included in the controller then a closed form solution is obtainable. In this case the optimisation routine is replaced with a matrix, called the controller gain matrix.

Chapter 9

Modular Approach to Predictive Control

Long Range Predictive Control (LRPC) algorithms (Clarke et al. 1987*a*, Cutler & Ramaker 1979, Richalet et al. 1978) are usually implemented in the form of a computer program. This computer program is difficult to interpret and gives little insight into the structure and signal processing of the algorithm.

A modular framework of a LRPC algorithm, called Multi-Step Predictive Control (MSC), is presented in this chapter. This framework has the advantage over the conventional approach in that the structure and signal processing of the algorithm can now be interpreted more easily. An added benefit of the modular approach is the ability to test and implement the algorithm on standard control software development platforms.

The chapter is organised as follows. The proposed modular framework for the MSC algorithm is presented in Section 9.1. Section 9.2 discusses the initialisation procedure for setting-up the model. A summary is presented in Section 9.3.

9.1 Proposed modular framework for MSC control

The Multi-Step Predictive Control algorithm, presented in Chapter 8, makes use of a predictor model in the form of a linear, discrete time transfer function. This model is used to build a predictor equation (Chapter 5) which projects the future outputs of the plant over the prediction horizon. Features of typical LRPC algorithms such as dead time compensation, integral action and the ability to include process constraints into the controller are key features of the MSC algorithm. The signal flow

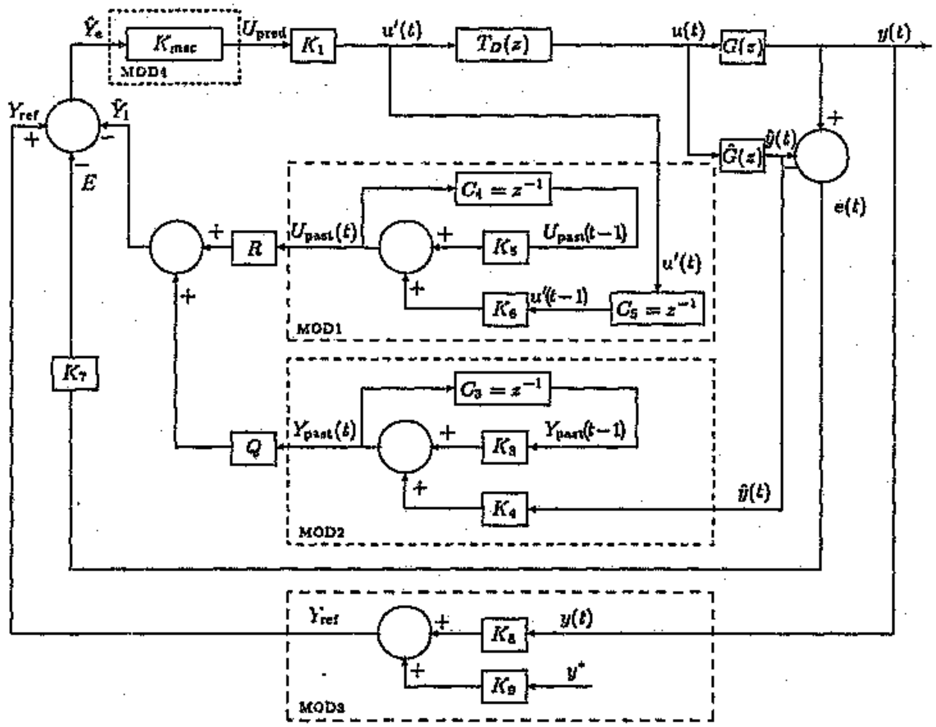

Figure 9.1: Signal flow diagram of Modular Framework

diagram of the MSC algorithm is shown in Figure 8.1.

The MSC algorithm makes use of an optimisation routine for solving the optimal control problem. This optimal control problem, which is solved for each control step, takes the form of a quadratic program with inequality constraints. If no process constraints are included in the feedback control design, then a closed form solution to the optimal control problem exists. In this case the optimisation routine is replaced with a controller gain matrix (K_{MSC}), which is the solution to the optimal control problem.

The MSC algorithm makes use of a reference trajectory which describes the desired future controlled variables over the prediction horizon. It provides the controller's optimisation routine with a projection of reference set-points that the plant's projected output is expected to track.

The proposed modular framework for the MSC algorithm is presented in Figure 9.1.

This signal processing model is a direct translation of the signal flow diagram of the MSC algorithm presented in Figure 8.1. The important modules shown in Figure 9.1 are listed in Table 9.1.

Table 9.1: Table of module codes and interpretation

Module	Input	Output	Interpretation
MOD1	$u'(t)$	$U_{\text{past}}(t)$	Update history of past inputs
MOD2	$\hat{y}(t)$	$Y_{\text{past}}(t)$	Update history of past predicted outputs
MOD3	$y(t)$, y^*	$Y_{\text{ref}}(t)$	Generate reference trajectory
MOD4	$\hat{Y}_e(t)$	$U_{\text{pred}}(t)$	Quadratic program

The interfacing of the varies sections of the algorithm are done using conversion matrices (K_x). These matrices convert the output of a section to a variable that is suitable in structure for the input to the following section.

9.1.1 MOD1

Module MOD1 calculates the history vector of past inputs, $U_{\text{past}}(t)$. The matrix K_5 is an (nb$'$-1) x (nb$'$-1) matrix defined as,

$$K_5 = \begin{bmatrix} 0 \dots 0 & \\ I & \vdots \\ & 0 \end{bmatrix} \tag{9.1}$$

where I is an identity matrix.

The matrix K_6 is an (nb$'$-1) x 1 matrix defined as,

$$K_6 = \begin{bmatrix} 1 \\ 0 \\ \vdots \\ 0 \end{bmatrix} \tag{9.2}$$

The output of module MOD1 is,

$$K_5\, U_{\text{past}}(t-1) + K_6\, q^{-1}\, u'(t) = \begin{bmatrix} 0 \dots 0 & \\ I & \vdots \\ & 0 \end{bmatrix} \begin{bmatrix} u'(t-2) \\ u'(t-3) \\ \vdots \\ u'(t-(\text{nb}'-1)-1) \end{bmatrix}$$

$$
\begin{aligned}
& + \begin{bmatrix} 1 \\ 0 \\ \vdots \\ 0 \end{bmatrix} u'(t-1) \\
&= \begin{bmatrix} 0 \\ u'(t-2) \\ u'(t-3) \\ \vdots \\ u'(t-(\mathrm{nb}'-1)) \end{bmatrix} + \begin{bmatrix} u'(t-1) \\ 0 \\ 0 \\ \vdots \\ 0 \end{bmatrix} \\
&= \begin{bmatrix} u'(t-1) \\ u'(t-2) \\ u'(t-3) \\ \vdots \\ u'(t-(\mathrm{nb}'-1)) \end{bmatrix} \\
&= U_{\mathrm{past}}(t)
\end{aligned}
$$

9.1.2 MOD2

Module MOD2 calculates the history vector of past outputs, $Y_{\mathrm{past}}(t)$, of the predictor model as shown in Equation 8.6. The matrix K_3 is an na$'$ x na$'$ matrix defined as,

$$
K_3 = \begin{bmatrix} 0 \dots 0 \\ I \quad \vdots \\ \quad\; 0 \end{bmatrix} \tag{9.3}
$$

where I is an identity matrix.

The matrix K_4 is an na$'$ x 1 matrix defined as,

$$
K_4 = \begin{bmatrix} 1 \\ 0 \\ \vdots \\ 0 \end{bmatrix} \tag{9.4}
$$

The output of module MOD2 is,

$$
K_3 Y_{\mathrm{past}}(t-1) + K_4 \hat{y}(t) = \begin{bmatrix} 0 \dots 0 \\ I \quad \vdots \\ \quad\; 0 \end{bmatrix} \begin{bmatrix} \hat{y}(t-1) \\ \hat{y}(t-2) \\ \vdots \\ \hat{y}(t-(\mathrm{na}'-1)-1) \end{bmatrix}
$$

$$+\begin{bmatrix}1\\0\\\vdots\\0\end{bmatrix}\hat{y}(t)$$

$$\begin{aligned}
&= \begin{bmatrix}0\\\hat{y}(t-1)\\\hat{y}(t-2)\\\vdots\\\hat{y}(t-(\mathrm{na}'-1))\end{bmatrix}+\begin{bmatrix}\hat{y}(t)\\0\\0\\\vdots\\0\end{bmatrix}\\
&= \begin{bmatrix}\hat{y}(t)\\\hat{y}(t-1)\\\hat{y}(t-2)\\\vdots\\\hat{y}(t-(\mathrm{na}'-1))\end{bmatrix}\\
&= Y_{\mathrm{past}}(t)
\end{aligned}$$

9.1.3 MOD3

Module MOD3 calculates the reference trajectory, Y_{ref}. This module is presented in Chapter 6. The matrix K_8 is an HP x 1 matrix defined as,

$$K_8 = \begin{bmatrix}\beta\\\beta^2\\\vdots\\\beta^{\mathrm{HP}}\end{bmatrix} \tag{9.5}$$

and matrix K_9 is an HP x 1 matrix defined as,

$$K_9 = \begin{bmatrix}1-\beta\\1-\beta^2\\\vdots\\1-\beta^{\mathrm{HP}}\end{bmatrix} \tag{9.6}$$

The output of module MOD3 is,

$$K_8\,y(t)+K_9\,y^* = \begin{bmatrix}\beta\\\beta^2\\\vdots\\\beta^{\mathrm{HP}}\end{bmatrix}y(t)+\begin{bmatrix}1-\beta\\1-\beta^2\\\vdots\\1-\beta^{\mathrm{HP}}\end{bmatrix}y^*$$

$$
\begin{aligned}
&= \begin{bmatrix} y_{\mathrm{ref}}(t+1) \\ y_{\mathrm{ref}}(t+2) \\ \vdots \\ y_{\mathrm{ref}}(t+\mathrm{HP}) \end{bmatrix} \\
&:= Y_{\mathrm{ref}}
\end{aligned}
$$

9.1.4 MOD4

The MSC algorithm calculates, at each control step, the set of optimum future control actions (U_{pred}) projected over the control horizon that minimise the error between the projected plant outputs and the refere... trajectory. This forms the basis of the optimal control problem, which is solved by modu... MOD4. This module is a quadratic program with inequality constraints or simp... controller gain matrix, if no constraint are included in the controller.

The transfer function of the module, assuming no constraints, is

$$U_{\mathrm{pred}} = K_{\mathrm{msc}} \hat{Y}_e \tag{9.7}$$

9.2 Initialisation of model parameters

The matrices Q, R and W are the matrices of the predictor equation (Chapter 5),

$$\hat{Y} = Q \hat{Y}_{\mathrm{past}} + R U_{\mathrm{past}} + W U_{\mathrm{pred}} \tag{9.8}$$

This equation is derived based on the predictor model, the internal disturbance model ($T_D(z)$), the prediction horizons (HP and CP) and the sampling period (T_{sp}) of the controller.

The matrix K_{msc} is the optimal controller gain matrix for the unconstrained MSC controller as explained in Chapter 8.

The conversion matrix K_1 is a matrix of dimension 1 x CP, where only the first element is set to 1,

$$K_1 = [1\ 0\ ...\ 0] \tag{9.9}$$

The conversion matrix K_7 is a matrix of dimension HP x 1, where each element is equal to 1,

$$K_7 = \begin{bmatrix} 1 \\ \vdots \\ 1 \end{bmatrix} \tag{9.10}$$

Table 9.2: Table of convergence matrices

	Dimension	Equation
K_1	1 x CP	9.9
K_3	na′ x na′	9.3
K_4	na′ x 1	9.4
K_5	(nb′ − 1) x (nb′ − 1)	9.1
K_6	(nb′ − 1) x 1	9.2
K_7	HP x 1	9.10
K_8	HP x 1	9.5
K_9	HP x 1	9.6

A summary of the convergence matrices is given in Table 9.2.

The disturbance model $T_D(z)$, defined in Equation 8.9, is included in the forward path of the controller.

$G(s)$ and $\hat{G}(z)$ are the real and estimated plant models respectively.

9.3 Summary

A modular framework for the Multi-Step Predictive Control algorithm is presented in this chapter. The framework is the result of linking building blocks together to form a dynamic model of the algorithm.

The proposed modular framework has the advantage over the conventional approach in that the structure and signal processing of the algorithm can now be interpreted more easily. An added benefit of the modular approach is the ability to test and implement the algorithm on standard control software development platforms.

Chapter 10

Investigation into Structure of Predictive Control

Nonlinearities, such as actuator saturation can cause ringing or integral windup of the plant input signal. Morari (Morari & Zafiriou 1989) identified this problem and proposed the inclusion of an additional saturation element into the Internal Model Control (IMC) framework to compensate for the saturation of the actuator. Goodwin (Goodwin et al. 1993) extends this work and shows that there are three separate models of the plant present in the IMC framework. Goodwin postulates that if all three plant models are driven by the output of a good representation of the saturation constraint then the effect of the non-linearity is significantly reduced.

This chapter shows that the framework of Long Range Predictive Control (LRPC) is similar to Goodwin's framework of IMC control. This key result is a possible explanation as to why LRPC's constraint handling performance is observed to be superior to other techniques.

The chapter is organised as follows. An overview of actuator saturation is presented in Section 10.1. The IMC Control approach to handling constraints is presented in Section 10.2. Section 10.3 presents the constraint handling mechanism of LRPC and compares it with Goodwin's IMC method. A summary is presented in Section 10.4.

10.1 Actuator saturation

Actuators are capable of operating only over a finite range. It is possible to drive the actuator into saturation by demanding more from the actuator than it can deliver. This causes problems. If a linear controller as shown in Figure 10.1 is used in a feedback control scheme, then the controller (C) has no knowledge of the saturation constraint and ringing or integral windup of the plant input may occur. A possible cure for this problem is to de-tune the controller which decreases the amplitude of the controller's output signal. This reduces the ringing in the plant input, but has the undesirable effect of reducing the bandwidth of the controller which may result in poorer disturbance rejection properties.

For these reasons there is a need for a non-linear controller which includes active constraints on its outputs.

10.2 IMC approach to constraint handling

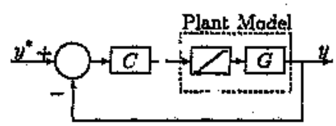

Figure 10.1: Signal flow diagram of feedback control using classical controller

Figure 10.1 is a signal flow diagram of a feedback scheme where C is the classical controller and G is the plant model. Morari (Morari & Zafiriou 1989) shows that the scheme shown in Figure 10.1 can be expressed equally well using the IMC representation shown in Figure 10.2. Q is the IMC filter and $\hat{G}$ is the estimated plant model.

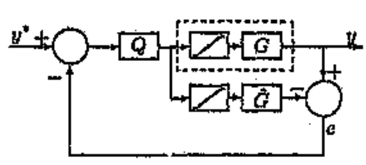

Figure 10.2: Morari's IMC model

Morari identified the problem caused by actuator saturation and proposed the introduction of a saturation constraint which is to precede the $\hat{G}$ element. This constraint is to ensure that the input signals to the models G and $\hat{G}$ are equal.

Goodwin extends Morari's work by presenting a new formulation of the IMC filter, Q. Goodwin shows that there are three models of the plant present in the feedback system. G is a model of the real plant, $\hat{G}$ is an estimate of the plant model and $\hat{G}'$ is an estimate of the plant model with all NMP zeros removed from the transfer function. In order to combat the problem caused by actuator saturation Goodwin points out that all plant models must be driven by the same constrained variable. This is made possible by including the constraint into Q as shown in Figure 10.3.

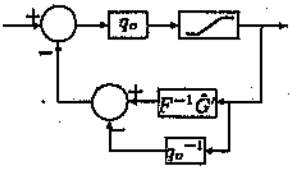

Figure 10.3: Goodwin's interpretation of Q

10.3 LRPC'S approach to handling constraints

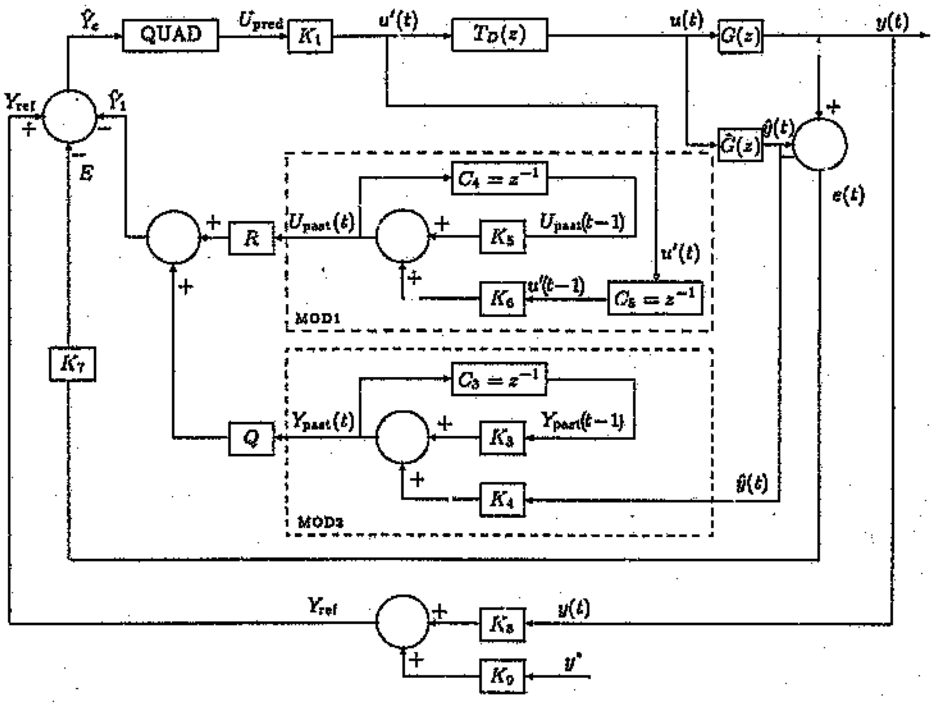

Figure 10.4: Signal flow diagram of Modular Framework

A modular framework for predictive control is developed in Chapter 9. This framework is presented in Figure 10.4.

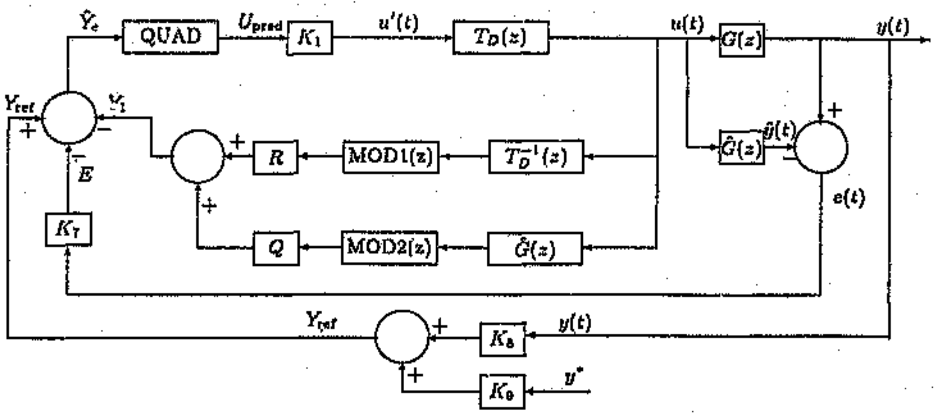

Figure 10.5: Simplified signal flow diagram of modular framework

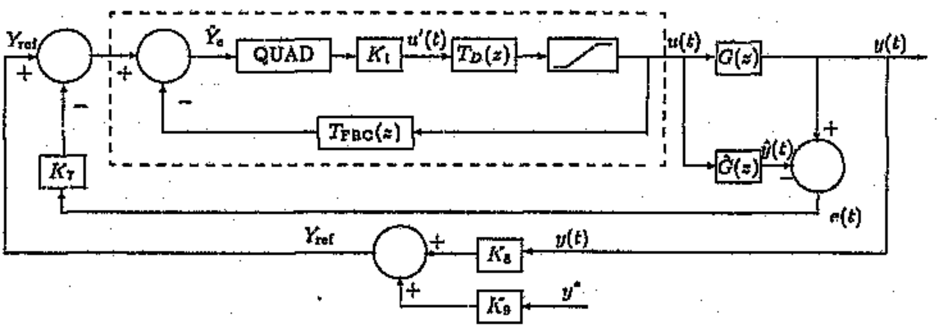

Figure 10.6: Simplified signal flow diagram of modular framework

Through block diagram manipulation the model shown in Figure 10.4 is reduced to the model shown in Figure 10.5 which is reduced further to the model shown in Figure 10.6 by defining,

$$\begin{aligned} T_{FBC}(z) &= R\,\mathrm{MOD}_1(z)\,T_D{}^{-1}(z) \\ &\quad + Q\,\mathrm{MOD}_2(z)\,\hat{G}(z) \end{aligned} \tag{10.1}$$

Constraints are incorporated into the predictive control algorithm by formulating a quadratic program with inequality constraints (Chapter 8). This quadratic program is represented by element QUAD. The saturation constraint in Figure 10.6 is merely a reminder that the constrained variable in element QUAD is the output variable of the controller, $u(t)$.

The dashed block shown in Figure 10.6 has a similar structure to the IMC filter (Q) presented by Goodwin.

The key result, shown in Figure 10.6, is that all the feedback elements inside the controller ($T_{\mathrm{FBC}}(z)$ and $\hat{G}(z)$) are driven by the output of the saturation constraint. The constraint is therefore absorbed into the controller.

10.4 Summary

This chapter investigates links between Long Range Predictive Control and Goodwin's Internal Model Control. Goodwin shows that a special architecture is required when implementing constraint mechanisms inside a feedback controller. Investigation into LRPC's constraint mechanism, using the modular framework of Multi-Step Predictive Control, shows that LRPC's constraint mechanism is similar to Goodwin's IMC. This key result is a possible explanation as to why LRPC's constraint handling performance is observed to be superior to other techniques.

Chapter 11

Proposed Constraint Mechanisms for MSC Control

The majority of Long Range Predictive Controller (LRPC) (Cutler & Ramaker 1979, Garcia et al. 1989, Clarke et al. 1987*a*, Richalet et al. 1978) are formulated as optimal control problems, whose objective is to minimise, at each control step, a cost function which gives a quantitative measure of the mismatch between a desired and predicted future plant output trajectory. The solution to this optimal control problem is defined as a quadratic program with inequality constraints which describe process constraints. This quadratic program must be solved at each control step.

The ability of predictive controllers to handle process constraints is well known. However, the computational burden caused by the quadratic program is great.

This chapter proposes a new method for handling certain process constraints, namely the rate and absolute constraints on controller output. The new method removes the constraints from the quadratic program and introduces a new constraint mechanism for dealing with the constraints. The advantage of using the new constraint mechanism is that the computational load is greatly reduced when compared to the quadratic program approach. The new algorithm is demonstrated by simulation.

The chapter is organised as follows. A detailed description of the proposed constraint mechanism is presented in Section 11.1. Features of the new algorithm are presented in Section 11.2. A simulation study demonstrating the proposed constraint mechanism is presented in Section 11.3 and the simulation results are presented in Section 11.4. A summary is presented in Section 11.5.

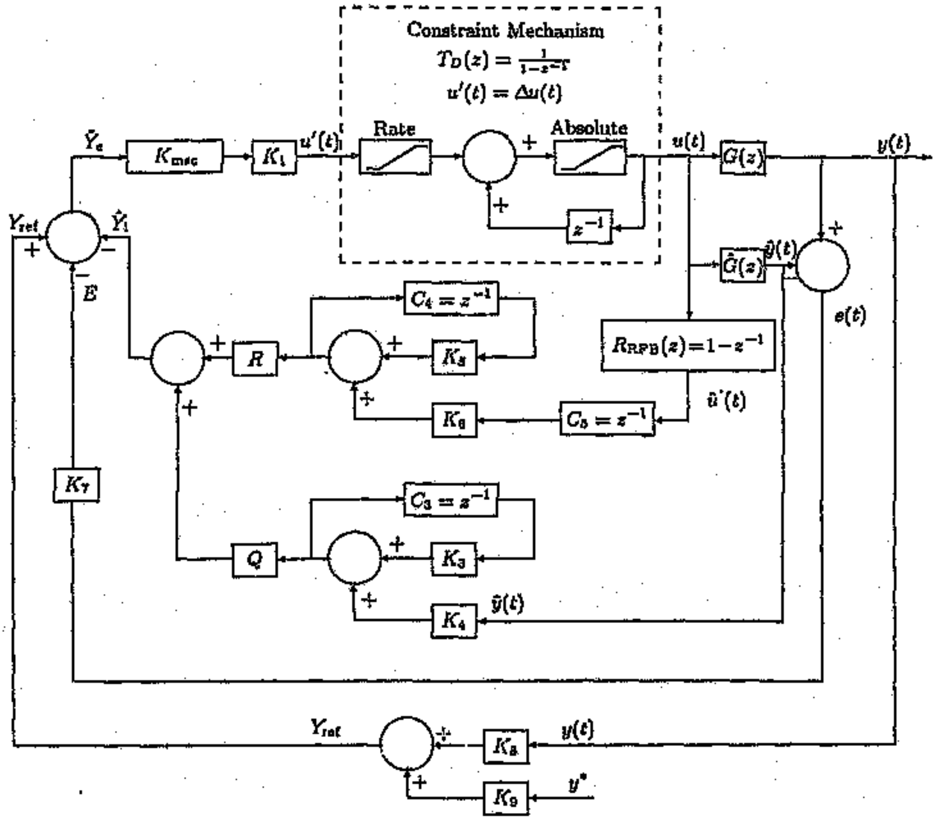

Figure 11.1: Signal flow diagram of the MSC Algorithm

11.1 New constraint mechanism

Predictive Control's traditional approach to constraint handling is to include process constraints in the quadratic program (Garcia et al. 1989) which is formulated in such a way that all projected plant inputs are constrained. However, it is felt that for certain types of constraints, such as plant input constraints, only the initial projected inputs are likely to attempt to violate the constraint bounds. The reason is that if a disturbance occurs then the projected control actions required to null the disturbance will change most rapidly during the early stages of the transient and then settle down to a steady state value during the remaining portion of the projection. Also, because the optimal control problem is solved for each control step, only the first projected control action is of vital significance. It is therefore proposed that only the first projected plant input requires the constraint mechanism.

A linear framework for Multi-Step Predictive Control (MSC) is formulated in Chapter 9. This framework is presented in Figure 9.1. Integral action is included in the controller by defining the internal disturbance model as,

$$T_D(z) = \frac{1}{1 - z^{-1}} \tag{11.1}$$

Then,

$$u'(t) = \Delta u(t)$$

where

$$\Delta = 1 - q^{-1}$$

The parameter $\Delta u(t)$ is interpreted as the incremental change of $u(t)$.

The proposed constraint mechanism is presented in Figure 11.1. If the saturation constraint elements are ignored then the transfer function of the constraint mechanism block is $T_D(z)$. A method of illuminating integral windup of the controller's output is to absorb the absolute constraint into the integrator, as shown in Figure 11.1.

When the constraint mechanism is included in the feedback controller, then the transfer function of the constraint mechanism block is not always $T_D(z)$ as the output signal can be distorted by the saturation elements. It is therefore important that the internal feedback signal of the controller $u'(t)$ is re-calculated based on the output of the constraint mechanism. $\hat{u}'(t)$ is estimated using the proposed rate feedback filter, $R_{\mathrm{RFB}}(z)$, where,

$$R_{\mathrm{RFB}}(z) = 1 - z^{-1}$$

11.2 Features of the new algorithm

Goodwin (Goodwin et al. 1993) shows that there are 3 separate dynamic plant models present in a feedback control system. $G(z)$ is a model of the real plant, $\hat{G}(z)$ the estimated plant model and the third model is $\hat{G}'(z)$ which in this case is part of the feedback component inside the controller which calculates $\hat{Y}_1$.

An important observation concerning the structure of predictive control is pointed out in Chapter 10. The key result is that all dynamic elements inside the predictive controller are driven by the output of the constraint mechanism. This result implies that all plant models in the control system are driven by the same constrained plant input.

This is an important result because it shows that although the new constraint mechanism is no longer part of the quadratic program it is still inside the controller, driving all dynamic elements of the feedback system.

The important features of the algorithm are,

1. Fewer computations are required, when compared to the quadratic program approach to constraint handling.
2. The controller has integral action, necessary for nulling constant offset disturbances.
3. Ability to include rate and absolute plant input amplitude constraints into the controller.
4. The controller has an anti windup mechanism to prevent integral windup of the controller's output.
5. Use of a set-point reference trajectory.

11.3 Simulated example

A simulation study is carried to demonstrate the constraint handling ability of the proposed algorithm.

A plant model with a small damping factor and dead time is selected.

11.3.1 Plant model

$$G(s) = \frac{{\omega_n}^2 \, e^{-t_d s}}{s^2 + 2\zeta\omega_n s + {\omega_n}^2} \tag{11.2}$$

where,

$$\omega_n = 0.5 \text{ rad/sec} \tag{11.3}$$

$$\zeta = 0.4 \tag{11.4}$$

$$t_d = 2 \text{ sec} \tag{11.5}$$

11.3.2 Predictor model

As the simulation study is not investigating the ability of the controller to handle modelling uncertainty, it is assumed that there is no modelling error.

$$\hat{G}(s) = G(s) \tag{11.6}$$

11.3.3 Controller settings

Sampling period.

$T_{sp} = 1$ sec

Horizons.

Prediction Horizon	HP $= 20$
Control Horizon	CP $= 5$

Tuning parameters.

$\lambda = 1$

$\beta = 3$

Reference Trajectory.

$\tau = 2$ sec

11.3.4 Constraint settings

Table 11.1 gives details of the constraint settings for the simulations.

11.3.5 Disturbance at plant output

A suitable disturbance, occurring at the plant output, is specified that causes the actuator to saturate when the controller attempts to null the offset error caused by the disturbance. The disturbance at the plant output is defined as,

$$d(t) = \begin{cases} 0 & \text{if } t <= 100 \text{ sec} \\ -0.2 & \text{if } 100 < t <= 150 \text{ sec} \\ 0.5 & \text{if } t > 150 \text{ sec} \end{cases} \tag{11.7}$$

Table 11.1: Table of constraint settings

No.	Rate $[\Delta u]_{\min}$	Rate $[\Delta u]_{\max}$	Absolute $u_{\min}$	Absolute $u_{\max}$
1	-1	1	0	1.3
2	-0.1	0.1	0	1.3
3	-0.075	0.075	0	1.3
4	-0.06	0.06	0	1.3
5	-0.05	0.05	0	1.3
6	-0.04	0.04	0	1.3
7	-0.03	0.03	0	1.3
8	-0.02	0.02	0	1.3
9	-0.015	0.015	0	1.3
10	-0.01	0.06	0	1.3

11.3.6 Initialisation of model parameters

The matrices Q and R are the matrices of the predictor equation (Chapter 5),

$$\hat{Y} = Q\,\hat{Y}_{\mathrm{past}} + R\,U_{\mathbf{past}} + W\,U_{\mathbf{pred}} \tag{11.8}$$

This equation is derived based on the predictor model, the internal disturbance model ($T_D(z)$), the prediction horizons (HP and CP) and the sampling period (T_{sp}) of the controller.

The matrix K_{msc} is the optimal controller gain matrix for the unconstrained MSC controller as explained in Chapter 8.

The matrices K_1, K_3, K_4, K_5, K_6, K_7, K_8 and K_9 are called conversion matrices. Refer to Chapters 6 and 9 for the calculation of the matrices.

11.4 Simulation results

The simulation results for simulations 1 to 9 are presented in Figure 11.2. These plots clearly show the controller's ability to handle absolute and rate constraints. When the controller responds to the disturbance at $t = [100, 150]$ seconds, the actuator signal increases until it reaches the maximum plant input constraint setting. When the disturbance changes at $t = 150$ seconds, the controller responds without any

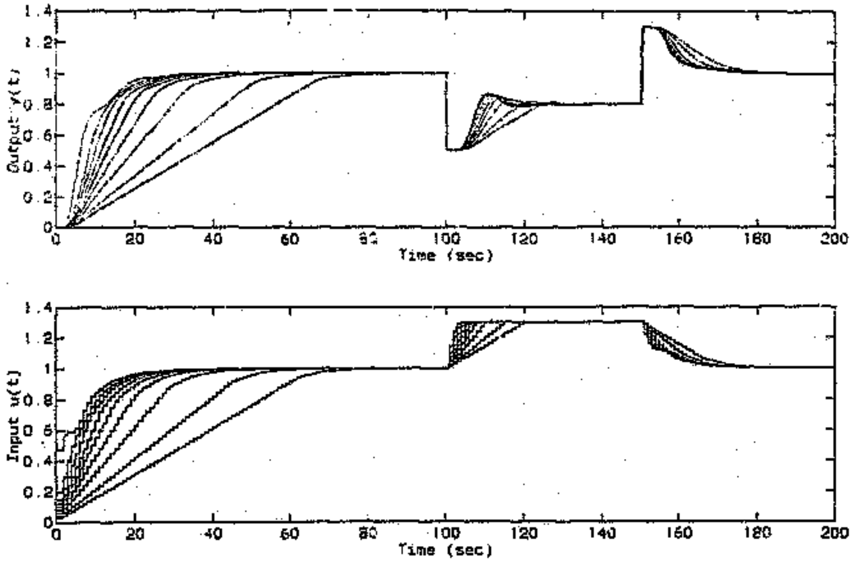

Figure 11.2: Simulation results (no. 1 to 9)

evidence of integral windup, which would occur if the actuator saturation were not handled correctly. The performance of the controller's rate constraint mechanism is visible in the range $t < 100$ seconds. No set-point overshoot caused by integral windup is evident, which confirms that the rate constraint mechanism is operating correctly.

The simulation result for simulation 10 is shown in Figure 11.3. This simulation demonstrates the controller's ability to handle different rate constraint bounds (i.e. different max. and min. rate constraint bounds), which is impossible to achieve using purely linear control.

11.5 Summary

This chapter introduces a new constraint mechanism for Multi-Step Predictive Control. The traditional approach to implementing process constraints in Long Range Predictive Control is to include the process constraints in a quadratic program. This chapter investigates the predictive control architecture using the modular framework developed for Multi-Step Predictive Control. The investigation suggests that it is sufficient to constrain only the initial projected control output to implement rate and absolute constraints in predictive control. An alternate method of including the process constraints in the predictive controller is presented. The proposed approach

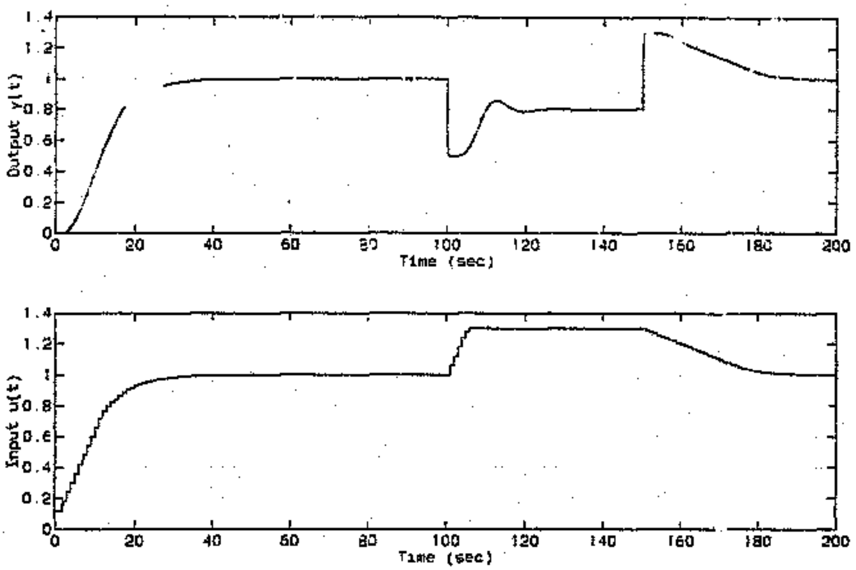

Figure 11.3: Simulation results (no. 10)

is to remove the rate and absolute process input constraints from the quadratic program and to introduce a new constraint mechanism for these constraints. The quadratic program is replaced with the unconstrained MSC controller gain matrix. Special attention is paid to issues such as integral action and anti-windup mechanisms.

A simulation study is carried out demonstrating the proposed constraint mechanism. The results show the controller's ability to handle absolute and rate constraints. The effects of the controllers integral action and anti-windup mechanism are also shown in the results.

The significance of the proposed algorithm lies in its ability to implement rate and absolute plant input constraints without having to solve a constrained quadratic program at each step, thus reducing the number of computations per step.

Chapter 12

Links between Classical and Predictive Control Theory

The achievements of classic and modern control theory applied to aerospace guidance problems are remarkable. However, the implementation of such techniques to industrial control has not been as successful. Industrial control poses difficulties due to the presence of process dead time and process constraints. For these reasons a new control concept known as Long Range Predictive Control (LRPC)(Richalet et al. 1978) was conceived in the 1970s primarily by the processing industry. This control method is well known for its constraint handling ability, inherent dead time compensation and ease of tuning for robustness. However, LRPC techniques (Richalet et al. 1978, Cutler & Ramaker 1979, Clarke et al. 1987*a*) lack the powerful analysis tools that classical-type controllers have at their disposal. The reason is that LRPC techniques have evolved from time domain specifications and are analysed using time domain concepts. Classical controllers are based on frequency domain specifications and their analysis tools are based primarily on frequency domain concepts.

A new LRPC algorithm called Multi-Step Predictive Control (MSC) is presented in this thesis. The modular framework of the MSC algorithm with integral action and anti-windup is shown in Figure 11.1. An important feature of this algorithm is its constraint mechanism (Chapter 11), which is an alternative to the usual approach of including the constraint in the quadratic program of the predictive controller.

This chapter forges links between classical control and predictive control theory. Equations for the loop transmission and closed loop transfer function are derived by analysing the modular framework of the unconstrained MSC algorithm. These equations, which are important tools for the analysis of the dynamics of the controller are demonstrated by analysing the dynamics of typical predictive control problems.

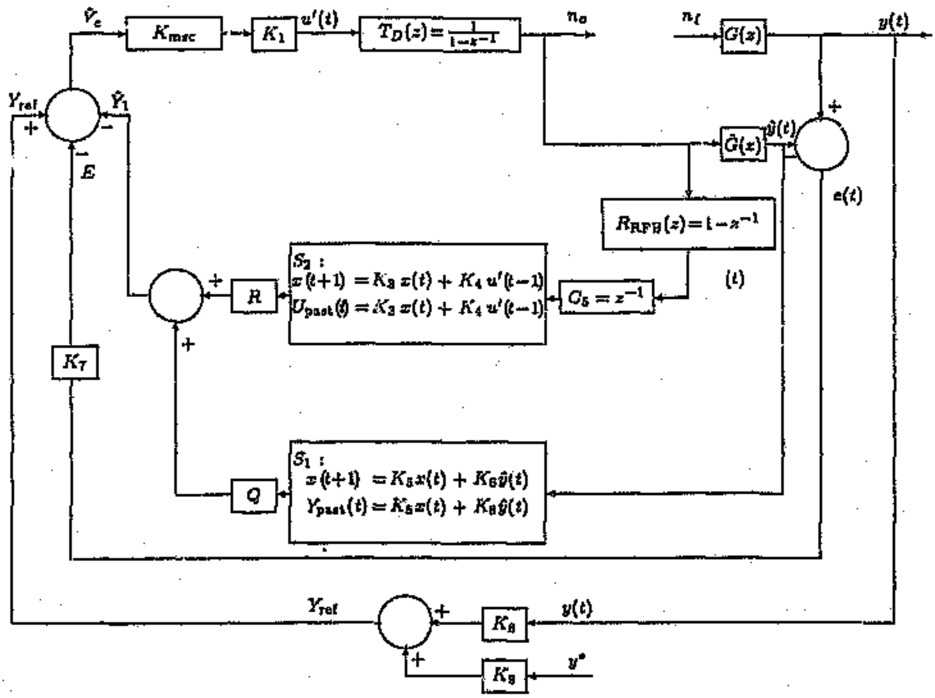

Figure 12.1: Signal flow diagram for calculation of loop transmission (L(z))

The chapter is organised as follows. Needs for links with classical control are discussed in Section 12.1. The procedure for the calculation of the loop transmission is presented in Section 12.2 and the procedure for calculating the closed loop transfer function is presented in Section 12.3. The usefulness of the equations derived in Sections 12.2 and 12.3 is demonstrated in Section 12.4, where typical predictive control problems are analysed. A summary is presented in Section 12.5.

12.1 Need for links with classical control

The concept of loop transmission is fundamental to all feedback control systems. This concept may be obscured by the way the control algorithm is formulated but is central to the true understanding of the dynamic behaviour of the feedback system.

Robustness properties of classical-type controllers can be analysed by plotting the loop transmission of the feedback control system. Important indicators such as gain

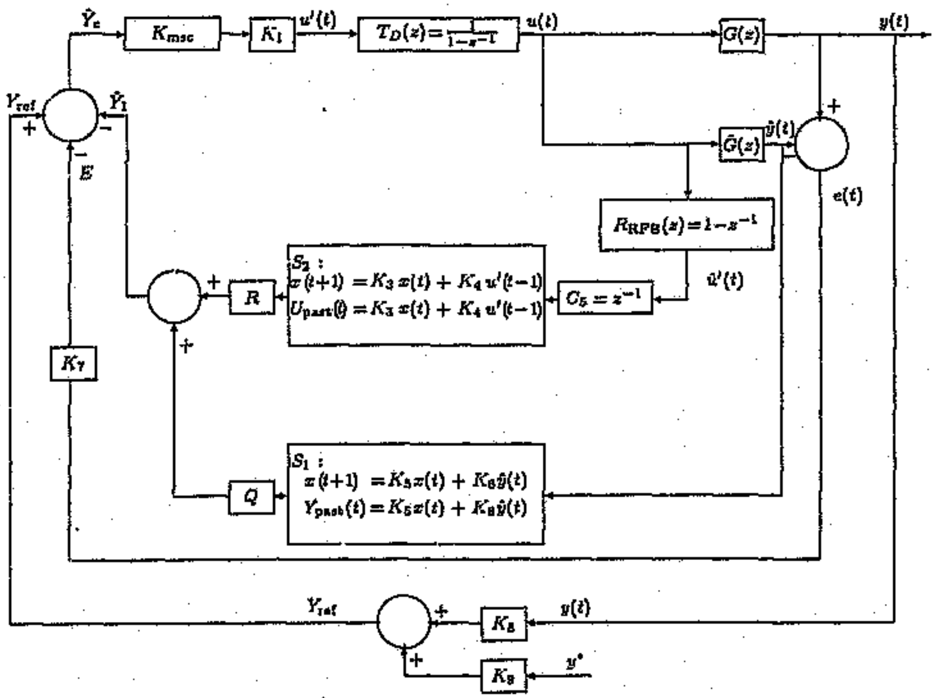

Figure 12.2: Signal flow diagram for calculation of closed loop transfer function (T(z))

and phase margins are useful for assessing the performance of the feedback system.

Predictive control has rules for selecting controller settings. Typical parameters of interest are the prediction horizon, control horizon and β which is used to tune the controller. These settings are based on time domain concepts. If the dynamics of the controller are expressed in a .requency domain notation then classical control analysis tools can be applied.

12.2 Derivation of the transfer function for the loop transmission

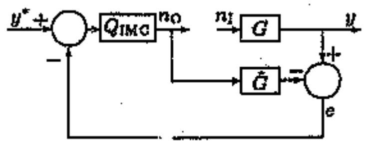

Figure 12.3: Scheme for calculation of L(z)

The loop transmission of a feedback control system can be measured experimentally by breaking the loop, injecting a test signal n_I into the feedback loop and measuring the return signal n_O. This signal processing scheme, using the Internal Model Control (IMC) signal flow diagram, is shown in Figure 12.3. The transfer function for the loop transmission is,

$$L(z) = -\frac{n_O(z)}{n_I(z)} \tag{12.1}$$

The signal flow diagram for the MSC algorithm is shown in Figure 11.1. Figure 12.1 is the model of the simplified MSC algorithm, with the constraint mechanism removed and the internal feedback element inside the controller reduced to state space models S_1 and S_2.

Based on the model presented in Figure 12.1, the equation of the loop transmission is,

$$L(z) = \frac{T_D K_1 K_{\text{MSC}}[K_7 - K_8]G}{1 - T_D K_1 K_{\text{MSC}}[K_7\hat{G} - QS_1\hat{G} - RS_2C_5R_{\text{RFB}}]} \tag{12.2}$$

Let $L(z) = K_L G$, where

$$K_L(z) = \frac{T_D K_1 K_{\text{MSC}}[K_7 - K_8]}{1 - T_D K_1 K_{\text{MSC}}[K_7\hat{G} - QS_1\hat{G} - RS_2C_5R_{\text{RFB}}]} \tag{12.3}$$

is the transfer function of the equivalent classical controller.

Refer to Appendix B.5 for the derivation of Equation 12.2.

12.3 Derivation of the closed loop transfer function

The closed loop transfer function is defined as,

$$T(z) = \frac{y(z)}{y^*(z)} \tag{12.4}$$

The closed loop transfer function is derived using the signal flow diagram shown in Figure 12.2.

$$T(z) = \frac{GT_D K_1 K_{\mathrm{MSC}} K_9}{1 - T_D K_1 K_{\mathrm{MSC}}[(K_8 - K_7)G + (K_7 - QS_1)\hat{G} - RS_2 C_5 R_{\mathrm{RFB}}]} \tag{12.5}$$

Refer to Appendix B.6 for the derivation of Equation 12.5.

12.4 Demonstration

The usefulness of Equations 12.2 and 12.5 are demonstrated by analysing a predictive control design.

Three different predictive controllers are proposed for a feedback design. The characteristics of each controller are investigated by analysing the loop transmission.

12.4.1 Nominal plant model

The nominal plant model is described using a second order transfer function with a small damping factor and significant dead time.

$$\hat{G}(s) = G(s) = \frac{{\omega_n}^2 \, e^{-t_d s}}{s^2 + 2\zeta\omega_n s + {\omega_n}^2} \tag{12.6}$$

where,

$$\omega_n = 0.5 \text{ rad/sec} \tag{12.7}$$

$$\zeta = 0.4 \tag{12.8}$$

$$t_d = 4 \text{ sec} \tag{12.9}$$

12.4.2 Controller settings

Sampling period.

$T_{sp} = 1$ sec

Horizons.

Prediction Horizon	HP = 20
Control Horizon	CP = 5

Reference Trajectory.

$\tau = 5$ sec

Table 12.1: Table of proposed controller tuning parameters

Controller No.	β	λ
1	1.5	1
2	3.0	1
3	5.0	1

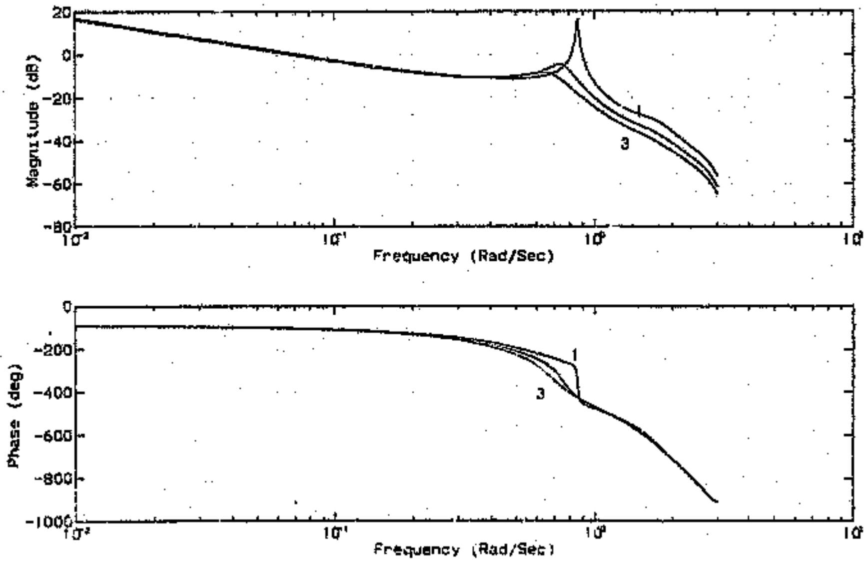

Figure 12.4: Bode Plot of Loop Transmission

12.4.3 Bode plots of loop transmission

The Bode plot of the loop transmission for each controller is shown in Figure 12.4. These plots are useful for analysing the robustness of the controllers. For example, it can be seen that at $\omega = 0.85$ rad/sec the loop gain for controller 1 is greater than 0 dB. This indicates that controller 1 is unsuitable, because if noise enters the feedback loop at this frequency it can cause the system to oscillate. Controller 2 is an improvement over controller 1 because the peak loop gain is below 0 dB. The best controller is controller 3 which does not have a significant peak loop gain.

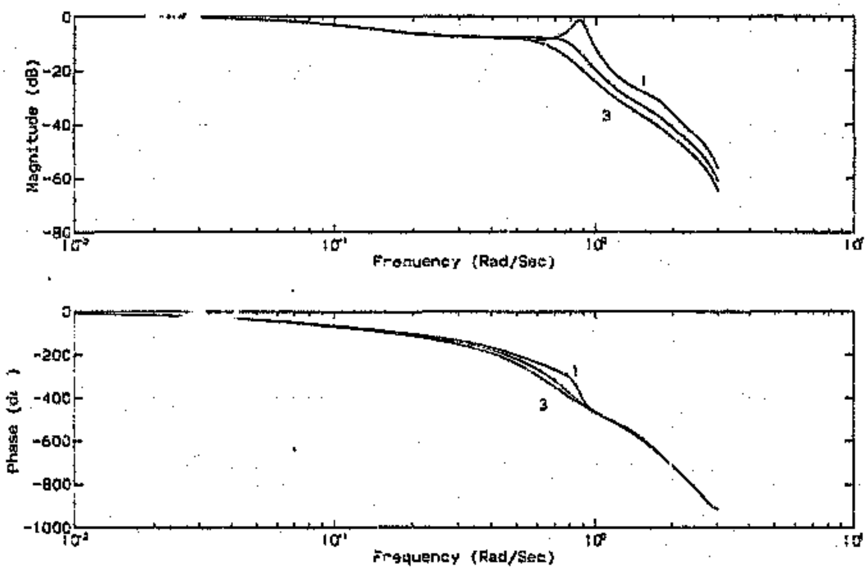

Figure 12.5: Bode Plot of Closed Loop Transfer Function

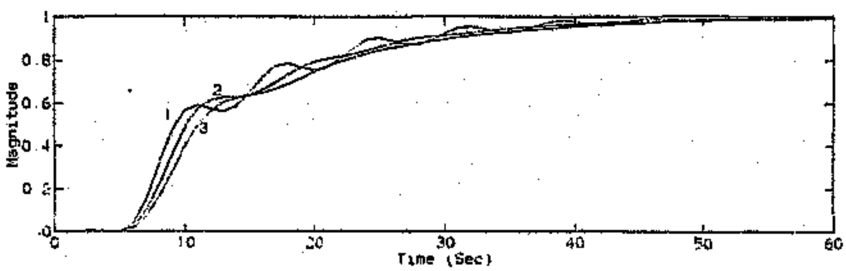

Figure 12.6: Closed Loop Step Response

12.4.4 Closed loop response

The Bode plot of the closed loop transfer function for each controller is shown in Figure 12.5. These plots are useful for analysing the closed loop response of the system. Controller 1 has an oscillatory responses due to the resonant peaks shown in Figure 12.5. These observations are seen in Figure 12.6 which is a graph of the step responses of the system using for controller.

12.5 Summary

This chapter forges links between classical and predictive control. Equations for the loop transmission and closed loop transfer functions are derived for the Multi-Step Predictive Control (MSC) algorithm. These equations are derived by investigating the signal processing model of the unconstrained MSC algorithm. A demonstration of the derived equations is presented by using these equations to analyse typical predictive control problems. The results of frequency response plots generated using these equations represent important links between classical and predictive control.

The equations derived in this chapter are significant as they represent quantitative analysis tools for investigating the frequency domain properties of the Long Range Predictive Controller. These equations provide a foundation for development of robust predictive control design methods.

Chapter 13

Robust MSC Control Design Method

A key consideration in any feedback design is that of attaining performance specifications in the presence of plant uncertainty and external disturbance inputs. Important Robust Control design methods such as the Quantitative Feedback Theory (QFT) (Horowitz 1979, Horowitz 1982, Horowitz & Sidi 1980) and the H-Infinity Theory (Chu 1985, Maciejowski 1989) are presented in the control literature. These control theories are extensions of classical control theory. They are concerned with the designing of a fixed controller that reduces the effects of plant uncertainty to an acceptable level resulting in a feedback system that meets design specifications.

This chapter presents a method for designing a robust Multi-Step Predictive Controller (MSC). Robust control design relies on frequency domain specifications of the controller. This presents problems, because the predictive controller is formulated as an optimal control problem derived from time domain specifications, which obscures the controller's frequency domain properties. This problem is addressed in Chapter 12, where an equation for the transfer function of the equivalent classical controller is derived. This equation represents important links between predictive and classical control theories and is put to use in the proposed robust control design method.

The chapter is organised as follows. The important issues regarding robust control design and the importance of frequency domain design techniques are discussed in Section 13.1. New analysis tools for predictive control, such as the equation for deriving the equivalent classical controller, are presented in Section 13.2. The MSC robust control design method is presented in Section 13.3. The tuning of the MSC controller is an important issue. Tuning guidelines are presented in Section 13.4.

The proposed design method is demonstrated by solving a typical process control design problem. The model of the process is predominantly second order with significant resonance and long dead time. The uncertainty of the process model is known and is modelled via parameter variations. The problem is to design a suitable predictive controller to meet design specifications. This design example is presented in Section 13.5. A summary is presented in Section 13.6.

13.1 Robust control design

A controller is robust if it maintains good control in the presence of plant variation and external disturbance inputs.

The frequency domain is the natural environment for designing feedback controllers because the plant's dynamics are conveniently described by its frequency response. Also, frequency response design methods provide good designs in the presence of plant model uncertainty.

The frequency response model of the plant is usually only accurate at low frequencies. This is an important consideration when designing controllers, because the controller's dynamics must be tailored in such a way that feedback is proportional to the amount of uncertainty. Also, the phase uncertainty places constraints on the bandwidth of the controller. Another important reason for frequency domain design is that often noise constraints placed on the design require that the feedback controller be band limited, where only the low frequencies of the feedback loop are required for control.

The initial phase of the design of a feedback controller is concerned with identifying the plant's dynamic model and estimating the uncertainty of this model. This information provides a foundation for the controller design phase and is necessary for a good control design.

The objective of the controller design phase is to design a controller that compensates for uncertainty in the plant dynamics. However, when designing the controller there are often conflicting requirements between the robustness and performance specifications of the feedback system. These issues, and others such as the noise rejection properties of the feedback system are visible in the frequency response of the loop transmission. Indicators such as the gain and phase margins of the feedback loop are useful measures of confidence for assessing the robustness of the controller. These issues motivate the need for frequency domain design techniques.

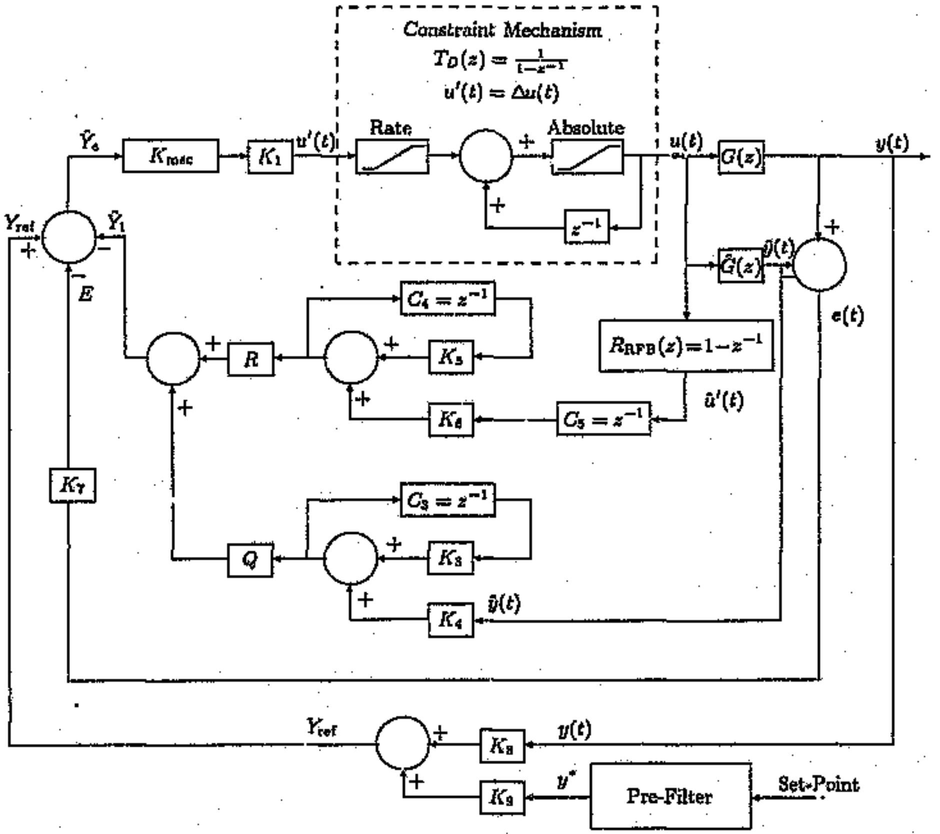

Figure 13.1: Signal flow diagram of the MSC Algorithm

If the closed loop dynamics of the system are too slow, then a pre-filter may be used to speed-up the set-point response of the system. This design approach leads to a two degree of freedom design. The feedback controller provides robustness, while the pre-filter improves on set-point tracking performance.

13.2 New analysis tools for predictive control

A LRPC algorithm known as Multi-Step Predictive Control (MSC) is presented in this thesis. The modular framework of the MSC algorithm is shown in Figure 13.1. An important feature of this algorithm is its constraint mechanism, which is an alternative to the usual approach of including the constraints in the quadratic program

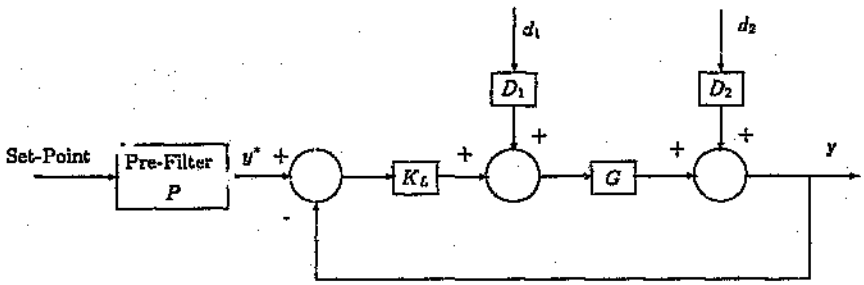

Figure 13.2: Signal flow diagram of equivalent feedback control system

of the predictive controller. The constraint mechanism places rate and absolute constraints on plant inputs. Features common to most predictive control algorithms such as integral action and set-po : reference trajectory are also included. For details of this model refer to Chapters 8, 9 and 11.

Analysis of the modular framework produced important links between classical and predictive control theories (Chapter 12). The transfer functions of the loop transmission, closed loop and equivalent classical controller were derived by analysing the signal processing of the unconstrained MSC modular framework.

The equation for the loop transfer function is presented in Equation 13.1 and the equivalent classical controller is presented in Equation 13.2.

$$L(z) = \frac{T_D K_1 K_{\mathrm{MSC}}[K_7 - K_8]G}{1 - T_D K_1 K_{\mathrm{MSC}}[K_7 \hat{G} - Q S_1 \hat{G} - R S_2 C_5 R_{\mathrm{RFB}}]} \tag{13.1}$$

Let $L(z) = K_L G$, where

$$K_L(z) = \frac{T_D K_1 K_{\mathrm{MSC}}[K_7 - K_8]}{1 - T_D K_1 K_{\mathrm{MSC}}[K_7 \hat{G} - Q S_1 \hat{G} - R S_2 C_5 R_{\mathrm{RFB}}]} \tag{13.2}$$

The closed loop transfer function is presented in Equation 13.3.

$$T(z) = \frac{G T_D K_1 K_{\mathrm{MSC}} K_9}{1 - T_D K_1 K_{\mathrm{MSC}}[(K_8 - K_7)G + (K_7 - Q S_1)\hat{G} - R S_2 C_5 R_{\mathrm{RFB}}]} \tag{13.3}$$

13.2.1 Equivalent feedback control system

The equivalent block diagram model of the MSC predictive control algorithm is shown in Figure 13.2. K_L is the equivalent classical controller. G is the plant model. D_1 and D_2 are disturbance models. P is a pre-filter which may be required if necessary.

13.3 MSC Robust Control

Reasons motivating the need for frequency domain design methods are discussed in Section 13.1. MSC Robust Control is a frequency response design method that makes use of results presented in Section 13.2 that links classical and predictive control. Normally closed loop stability of feedback systems which use predictive controllers is not an issue. This is because predictive controllers produce stable feedback systems provided that the plant model is stable (Garcia et al. 1989). However, what is an issue in robust control design is designing a feedback controller that meets design specifications, given the uncertainty in the plant dynamics. This issue is address by the MSC Robust Control design method which incorporates plant model uncertainty into the controller design. MSC Robust Control's method of representing uncertainty, initially presented by Horowitz (Horowitz 1963), relies on the use of templates which are useful for representing uncertainty in the frequency domain.

13.3.1 Design procedure

The equivalent classical controller, necessary for analysing the predictive controller in the frequency domain, is based on the model shown in Figure 13.1. The interpretation of this model is presented in Chapter 9. The following information is required to build this model.

- Sampling period (T_{sp})
- Predictor Model ($\hat{G}$)
- Prediction Horizon (HP)
- Control Horizon (CP)
- Tuning parameters in cost function (β and λ)

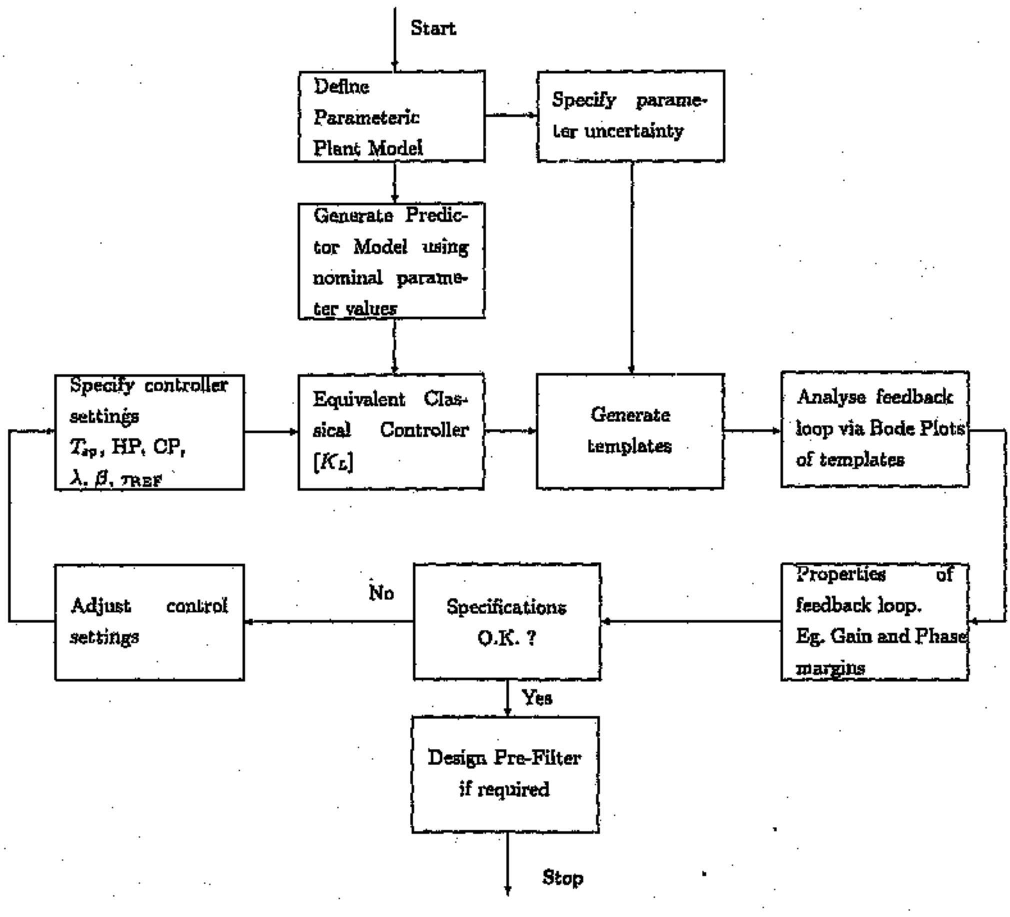

Figure 13.3: Flow chart for the design procedure of MSC Robust Control Design

- Reference trajectory time constant (τ_{ref})

A flow chart outlining the design procedure for designing an MSC Robust Controller is presented in Figure 13.3. The initial stage of the controller design is to select a suitable parametric model which describes the dominant dynamics of the plant and to specify the model's parameter variations. This model and its parameter variations are used to generate plant model uncertainty templates ($\tilde{G}$). Based on the $\tilde{G}$ templates and the transfer function of the equivalent classical controller (K_L), other templates are generated using the following equations,

- Loop transmission

$$\tilde{L} = K_L\, \tilde{G} \tag{13.4}$$

- Closed loop response

$$\tilde{T} = \frac{\tilde{L}}{1+\tilde{L}} \tag{13.5}$$

- Plant input disturbance response

$$\frac{y}{d_1} = \frac{\tilde{G}}{1+K_L\, \tilde{G}} \tag{13.6}$$

- Plant output disturbance response

$$\frac{y}{d_2} = \frac{1}{1+K_L\, \tilde{G}} \tag{13.7}$$

An important feature of the design method is its ability to specify uncertainty in the frequency response plots, which is vital for aiding the designer in assessing the robustness of the controller. Typical frequency response plots of the templates are shown in Appendix B.7. The designer can now make full use of classical control analysis methods.

13.4 Tuning the MSC controller

MSC controllers are high order contollers with few, easy to select tuning parameters. MSC predictive control (Chapter 8) relies on the cost function shown in Equation 13.8. The parameters λ and β tune the controller. Usually λ is set to unity, while β tunes the controller for robustness. Increasing β penalises the magnitudes of the u' projections, where u' is defined as the incremental change in the plant's input (assuming the controller has integral action).

Table 13.1: Graphs of final design iteration

Figure	Description
B.1	Frequency response of plant model bounds
B.2	Frequency response of equivalent classical controller
B.3	Frequency response of loop transmission
B.4	Frequency response of plant input disturbance rejection
B.5	Frequency response of plant output disturbance rejection
B.6	Frequency response of closed loop bounds
B.7	Frequency response of prefilter
B.8	Frequency response of prefilter plus closed loop
B.9	Plant output thumb print caused by a unit step change in the set-point
B.10	Plant output thumb print caused by a unit step change in the plant input disturbance (d_1)
B.11	Plant output thumb print caused by a unit step change in the plant output disturbance (d_2)

$$\begin{aligned} \text{Cost} \;=\; & \sum_{k=1}^{\text{HP}} \Big[\lambda(k)^2 \left[Y_{\text{ref}}(t+k) \;-\; \hat{Y}(t+k)\right]^2 \\ & \quad + \beta(k)^2 u'(t+k-1)^2\Big] \end{aligned} \tag{13.8}$$

The MSC algorithm also caters for a reference trajectory (Chapters 6 and 8), which provides the optimisation module with a projection of future set-points which the plant output is expected to track. The reference trajectory is calculated at each control step and is based on a first order transfer function model. The rise time (τ_{ref}) of the this transfer function is a useful on-line tuning parameter.

A subtle tuning parameter (assuming integral action) is the DC gain of the predictor model ($\hat{G}(z)$). If this gain is decreased then the controller bandwidth increases. Refer to Appendix B.8 for an explanation.

13.5 Example

A design study is presented to demonstrate the MSC Robust Control design method.

The plant model selected is typical of certain industrial processes. The plant dynamics are predominantly second order with significant resonance, variable gain and long dead time.

$$G(s) = K\left(\frac{{\omega_n}^2}{s^2 + 2\zeta\omega_n s + {\omega_n}^2}\right)e^{-t_d s} \tag{13.9}$$

Table 13.2: Plant model parameters

Parameter	Min	Max	Nominal
K	0.7	1.7	1
ω_n	0.45	0.55	0.5
ζ	0.35	0.45	0.4
t_d	3	5	4

The disturbance models are,

$$D_1(s) = D_2(s) = \frac{1}{5s+1} \tag{13.10}$$

The design iterations for the MSC Robust Control design are shown in Table 13.3. The final iteration had the following controller settings.

- Sampling period. $T_{sp} = 0.5$ sec.
- Prediction Horizon. HP = 20 steps.
- Control Horizon. CP = 6 steps.
- $\lambda = 1$ and $\beta = 15$
- $\tau_{ref} = 5$ sec.
- The predictor model is based on the nominal plant model and has unity DC gain.

Refer to Appendix B.7 for the frequency response and step response plots of the final design iteration. The design also included a pre-filter for speeding-up the systems response to set-point changes. The design of this filter is outside the scope of this chapter, but for completeness is included in the final design shown in Appendix B.7.

Table 13.3: Design iterations

#	β	τ_{ref}	Comment
1	3	10	Resonant peak. Noise problem.
2	6	10	Resonant peak reduced. Noise problem.
3	10	10	No significant resonant peak.
4	15	10	Better.
4	15	5	Best controller. Due to response shape for plant with pure delay

13.6 Summary

A robust frequency response design method for a Long Range Predictive Control algorithm called Multi-Step Predictive Control (MSC) is presented in this chapter. The MSC Robust Control design method makes use of equations that link classical and predictive control. Equations are presented that calculate the transfer functions for the loop transmission, closed loop response and equivalent classical controller. Uncertainty is included in the design method by describing key frequency responses using uncertainty templates. Equations for calculating frequency response templates for the loop transmission, closed loop response and typical disturbance responses are presented. These templates provide a measure of uncertainty and are essential for assessing the robustness of the control design.

A flow chart of the design method as well as methods for tuning the MSC controller are presented in the chapter. An example of a typical robust LRPC design is presented which demonstrates the potential of the design method.

Chapter 14

MSC Control with Feedforward Control

The objective of feedback control is to reduce uncertainty and reject disturbances that effect the output of the plant. In most process control problems a feedback controller with integral action is sufficient for providing the necessary robustness to ensure good control. However, if known disturbance are measurable and predictable then it is often a good idea to include a feedforward controller into the control system. This scheme leads to improved disturbance rejection because the control actions for rejecting the disturbance are initiated before the effect of the disturbance is measured at the plant output.

The Multi-Step Predictive Control (MSC) algorithm is presented in Chapter 8, which serves as a foundation for further development in which a modular framework of the MSC algorithm is developed in Chapters 9 and 11. This chapter extends this framework to include feedforward control. While the concept of feedforward control is not new to predictive control (Garcia et al. 1989, Garcia & Morshedi 1986), the framework presented in this chapter gives valuable insight into predictive control's feedback and feedforward mechanisms. The feedforward framework presented in this chapter is similar to the proposed IMC feedforward framework presented in Chapter 4. Both methods have similar structure and interpretation. Both methods make use of constraint mechanisms that service both the feedback and feedforward controllers.

The chapter is organised as follows. A brief overview of the modular framework for the MSC algorithm is presented in Section 14.1. The framework of the proposed feedforward module for the MSC algorithm is presented in Section 14.2. This is followed by a simulation study of a typical process control problem. This study,

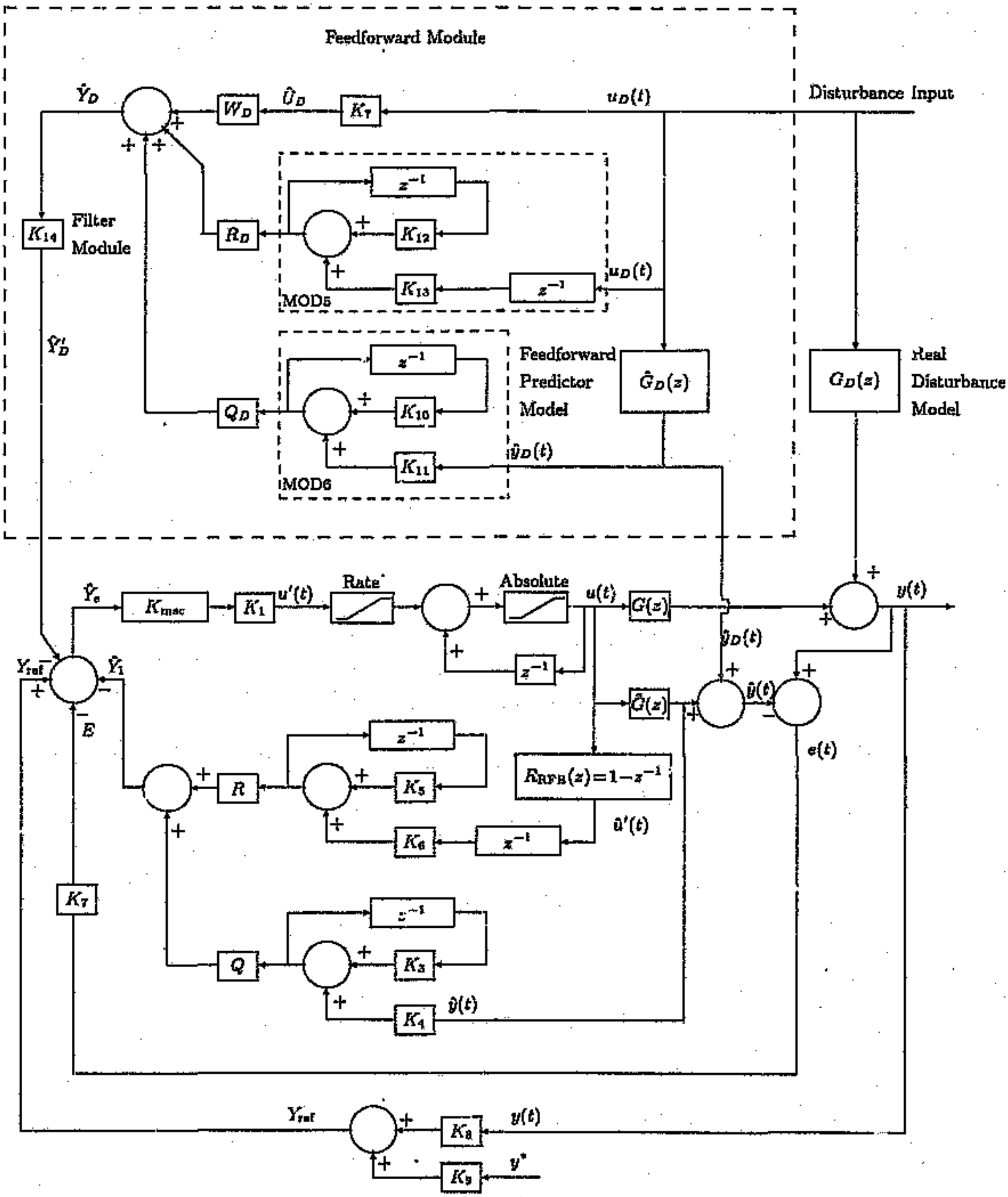

Figure 14.1: Signal flow diagram of the MSC Algorithm with Feedforward Control

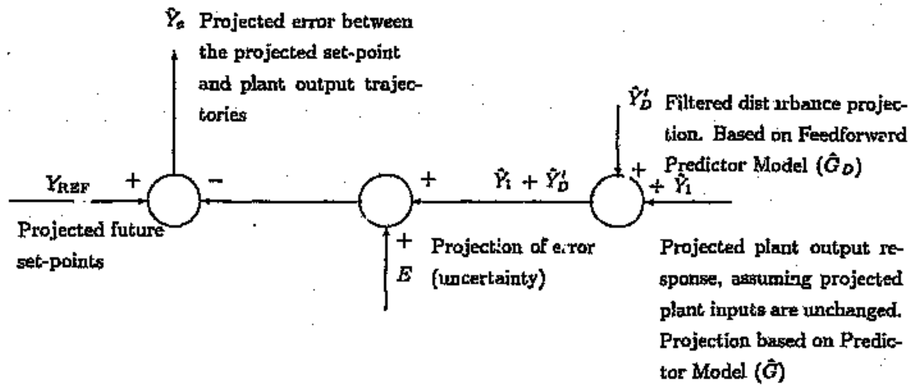

Figure 14.2: Signal flow diagram of input signals to optimisation routine

presented in Section 14.3, demonstrates the proposed feedforward module and shows that the inclusion of this module into the MSC algorithm improves the disturbance rejection properties of the controller. A summary is presented in Section 14.4.

14.1 Modular framework of the MSC algorithm

The modular framework of the MSC algorithm with the feedforward module included is presented in Figure 14.1. This framework is an extension of the framework presented in Chapter 9. The main features of the feedback module of the MSC algorithm are summarised as follows:

- The feedback controller includes a constraint mechanism for constraining the rate and absolute plant inputs. This constraint mechanism has important properties which are explained in Chapter 10.
- The feedback controller has integral action which is useful for nulling constant offset disturbances at the plants output.
- Included in the feedback controller is an anti-windup mechanism.
- Provision is made for a reference trajectory, which is a common feature of most predictive control algorithms (Clarke et al. 1987*a*, Richalet et al. 1978).

For an explanation of the MSC framework refer to Chapter 9.

14.2 Feedforward module for MSC algorithm

The feedforward module for the MSC algorithm is presented in Figure 14.1. This module relies on an accurate, predictable model of the disturbance. This model will be referred to as the Feedforward Predictor Model ($\hat{G}_D$).

14.2.1 . The predictor equation for the feedforward control module

The optimisation routine of a predictive control algorithm can be considered as the heart of the algorithm. If no constraints are included in this optimisation routine, then the solution to the optimal control problem has a closed form solution and can be expressed using a single matrix. This matrix is called the controller gain matrix, K_{MSC}, as shown in Figure 14.1.

The input to the K_{MSC} block, $\hat{Y}_e$, is the projection of the expected error between the projected plant outputs and the projected set-point reference trajectory. This input is the obvious entry point for the feedforward controller, because the projected disturbance can be calculated (Equation 14.1) and $\hat{Y}_e$ can be adjusted accordingly.

The concept of a predictor equation is presented in Chapter 5. This equation is useful for projecting the output of a model, which in this case is the Feedforward Predictor Model, $\hat{G}_D$. The feedforward predictor equation is shown in Equation 14.1. For the interpretation of this equation, refer to Chapter 5.

$$\hat{Y}_D = W_D \hat{U}_D + R_D U_{D\text{past}} + Q_D \hat{Y}_{D\text{past}} \tag{14.1}$$

Note: No internal compensation is used in the Feedforward Predictor Equ.tion. ($T_D = 1$)

The projection of the disturbance at the plant output is based on an assumption about the typ of disturbance.
Assumption: It is assumed that the projected disturbance input signals are constant over the prediction horizon and are equal to $u_D(t)$, the measured disturbance input signal at time t.

14.2.2 Interfacing of feedforward module

The interfacing of the feedforward controller to the feedback controller is done at two separate nodes. The output signals of the feedforward controller are $\hat{y}_D$ and $\hat{Y}'_D$, as shown in Figure 14.1. The signal $\hat{y}_D$ is the predicted disturbance appearing at the plant output and $\hat{Y}_D$ is a projection of the disturbance, HP steps into the future, at the plant output. Both signals are based on the measured disturbance input signal u_D. $\hat{Y}'_D$ is the filtered signal originating from $\hat{Y}_D$, where

$$\hat{Y}'_D = K_{14}\hat{Y}_D \tag{14.2}$$

K_{14} represents a predictive control building block of a first order filter (Chapter 7), $K_{\mathrm{FF}}(s)$, where

$$K_{\mathrm{FF}}(s) = \frac{1}{\tau_{\mathrm{FF}}s + 1} \tag{14.3}$$

The signal $\hat{y}_D$ is included into the feedback loop by adding $\hat{y}_D$ to the output of the Predictor Model ($\hat{G}$). The output of this summation is interpreted as the predicted plant output, $\hat{y}(t)$.

The signal $\hat{Y}'_D$ is included into the feedback loop by including $\hat{Y}'_D$ in the summation node as shown in Figure 14.1. Figure 14.2 gives a detail break-down of the signal components which yield $\hat{Y}_s$.

14.2.3 Conversion matrices in feedforward module

The interfacing of the varies sections of the algorithm are done using conversion matrices (K_x). These matrices convert the output of a section to a variable that is suitable in structure for the input of the following section. The feedforward control module has 6 conversion matrices. A summary of the conversion matrices for the feedforward MSC module is presented in Table 14.1.

K_7 is a column vector with HP elements, each equal to 1. K_{14} is a first order filter building block, defined in Chapter 7.

Table 14.1: Table of convergence matrices (feedforward module)

	Dimension	Equation
K_7	HP x 1	9.10
K_{10}	na x na	14.7
K_{11}	na x 1	14.8
K_{12}	$(\mathrm{nb}-1) \times (\mathrm{nb}-1)$	14.4
K_{13}	$(\mathrm{nb}-1) \times 1$	14.5
K_{14}	HP x HP	7.9

14.2.4 MOD5

Module MOD5 calculates the history vector of past inputs, $U_{D\mathrm{past}}(t)$. The matrix K_{12} is an (nb-1) x (nb-1) matrix defined as,

$$K_{12} = \begin{bmatrix} 0 \dots 0 \\ I \quad \vdots \\ \quad\; 0 \end{bmatrix} \tag{14.4}$$

where I is an identity matrix.

The matrix K_{13} is an (nb-1) x 1 matrix defined as,

$$K_{13} = \begin{bmatrix} 1 \\ 0 \\ \vdots \\ 0 \end{bmatrix} \tag{14.5}$$

The output of module MOD5 is,

$$K_{12}\,U_{D\mathrm{past}}(t-1) + K_{13}\,u_D(t-1) = \begin{bmatrix} 0 \dots 0 \\ I \quad \vdots \\ \quad\; 0 \end{bmatrix} \begin{bmatrix} u_D(t-2) \\ u_D(t-3) \\ \vdots \\ u_D(t-(\mathrm{nb}-1)-1) \end{bmatrix} + \begin{bmatrix} 1 \\ 0 \\ \vdots \\ 0 \end{bmatrix} u_D(t-1)$$

$$
\begin{aligned}
&= \begin{bmatrix} 0 \\ u_D(t-2) \\ u_D(t-3) \\ \vdots \\ u_D(t-(\text{nb}-1)) \end{bmatrix} + \begin{bmatrix} u_D(t-1) \\ 0 \\ 0 \\ \vdots \\ 0 \end{bmatrix} \\
&= \begin{bmatrix} u_D(t-1) \\ u_D(t-2) \\ u_D(t-3) \\ \vdots \\ u_D(t-(\text{nb}-1)) \end{bmatrix} \\
&= U_{D\text{past}}(t)
\end{aligned}
\tag{14.6}
$$

Where nb is the order of the numerator of the transfer function of the feedforward disturbance model.

14.2.5 MOD6

Module MOD6 calculates the history vector of past outputs. $\hat{Y}_{D\text{past}}(t)$. The matrix K_{10} is an na x na matrix defined as,

$$
K_{10} = \begin{bmatrix} 0 \ldots 0 \\ I \quad \vdots \\ \quad\; 0 \end{bmatrix} \tag{14.7}
$$

where I is an identity matrix.

The matrix K_{11} is an na x 1 matrix defined as,

$$
K_{11} = \begin{bmatrix} 1 \\ 0 \\ \vdots \\ 0 \end{bmatrix} \tag{14.8}
$$

The output of module MOD6 is,

$$
K_{10}\hat{Y}_{D\text{past}}(t-1) + K_{11}\hat{y}_D(t) = \begin{bmatrix} 0 \ldots 0 \\ I \quad \vdots \\ \quad\; 0 \end{bmatrix} \begin{bmatrix} \hat{y}_D(t-1) \\ \hat{y}_D(t-2) \\ \vdots \\ \hat{y}_D(t-(\text{na}-1)-1) \end{bmatrix}
$$

$$
\begin{aligned}
& + \begin{bmatrix} 1 \\ 0 \\ \vdots \\ 0 \end{bmatrix} \hat{y}_D(t) \\
= & \begin{bmatrix} 0 \\ \hat{y}_D(t-1) \\ \hat{y}_D(t-2) \\ \vdots \\ \hat{y}_D(t-(\mathrm{na}-1)) \end{bmatrix} + \begin{bmatrix} \hat{y}_D(t) \\ 0 \\ 0 \\ \vdots \\ 0 \end{bmatrix} \\
= & \begin{bmatrix} \hat{y}_D(t) \\ \hat{y}_D(t-1) \\ \hat{y}(t-2) \\ \vdots \\ \hat{y}_D(t-(\mathrm{na}-1)) \end{bmatrix} \\
= & \hat{Y}_{D\mathrm{past}}(t)
\end{aligned}
$$

Where na is the order of the denominator of the transfer function of the feedforward disturbance model.

14.2.6 Tuning the feedforward controller

A first order filter is included at the output of the feedforward controller, defined in block K_{14}. This filter is based on the continuous time transfer function shown in Equation 14.3. This filter is useful for de-tuning the feedforward controller. This is done by increasing the time constant of the filter, which will decrease the feedforward controllers response to the disturbance. The filtering action of K_{14} can be reduced by decreasing τ_{FF}. In the limit, as τ_{FF} is decreased, K_{14} approaches a unit matrix (Chapter 7).

14.2.7 Structure of proposed MSC algorithm

The proposed MSC framework presented in Figure 14.1 has a unique structure. The feedforward controller is not, unlike the traditional classical feedforward controller, separated from the feedback controller. The outputs of the feedforward module are used to adjust the feedback controller. The advantage of this is that feedforward control takes advantage of the constraint mechanism of the feedback controller.

The important benefits of the proposed feedforward mechanism is that no constraint violations occur as a result of the feedforward control. Also, the tuning of the feedforward controller relies on less parameters than the classical control approach to feedforward control design.

14.3 Example

A simulation study is carried out to demonstrate the proposed feedforward module.

14.3.1 Simulation models

A typical process plant model is selected. The model is based on a second order transfer function with significant resonance and long dead time. The plant model is shown in Equation 14.9.

$$G(s) = \frac{0.25}{s^2 + 0.4s + 0.25} e^{-3s} \tag{14.9}$$

The disturbance model is shown in Equation 14.10.

$$G_D(s) = \frac{1}{5s+1} e^{-5s} \tag{14.10}$$

The intension of this simulation study is to demonstrate the feedforward controller and not to show how the controller handles model uncertainty. For this reason it is assumed that there is no modelling uncertainty.

Predictor Model:

$$\hat{G} = G \tag{14.11}$$

Feedforward Predictor Model:

$$\hat{G}_D = G_D \tag{14.12}$$

14.3.2 Controller settings

The first step in tuning the MSC controller is to select a suitable sampling period for the controller. The next step is to select the prediction horizons. HP must be selected so that the projected response of the plant over the prediction horizon approaches a steady state condition. Usually CP is only a fraction of HP. Suitable values for λ and β are selected. These parameters are defined in the cost function (Chapter 8) and are useful for tuning the controller. Usually $\lambda = 1$ and β is selected large enough to ensure the robustness of the feedback controller. When the plant model has a long delay compared to the sampling period, then it is advisable, based on experience, not to use a reference trajectory in the feedback controller (use small τ_{ref}).

The feedforward controller is de-tuned, if necessary, using the parameter τ_{FF}. The larger τ_{FF}, the slower the feedforward controller reacts to the feedforward disturbance input.

The MSC controller settings are summarised as follows:

- Sampling Period $T_{\text{sp}} = 0.5$ sec
- Prediction Horizon HP=25
- Control Horizon CP=10
- Tuning parameters $\lambda = 1$ and $\beta = 12$
- Reference trajectory $\tau_{\text{ref}} = 1$ sec
- Feedforward Filter $\tau_{\text{FF}} = 5$ sec
- Constraint mechanism

$$\begin{aligned} u_{\min} &= 0 \\ u_{\max} &= 1.1 \\ \Delta u_{\min} &= -0.003 \\ \Delta u_{\max} &= 0.01 \end{aligned} \tag{14.13}$$

where $\Delta = 1 - q^{-1}$

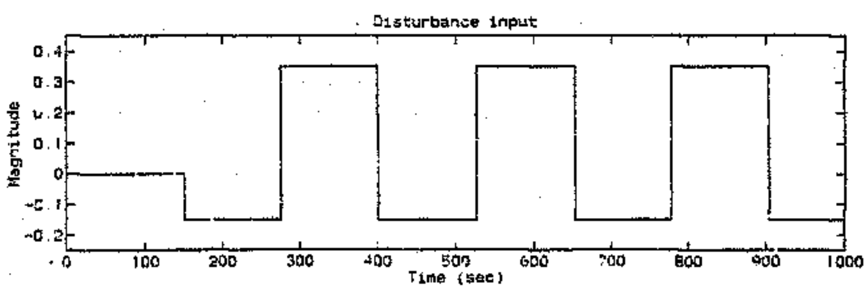

Figure 14.3: Disturbance Input (u_D)

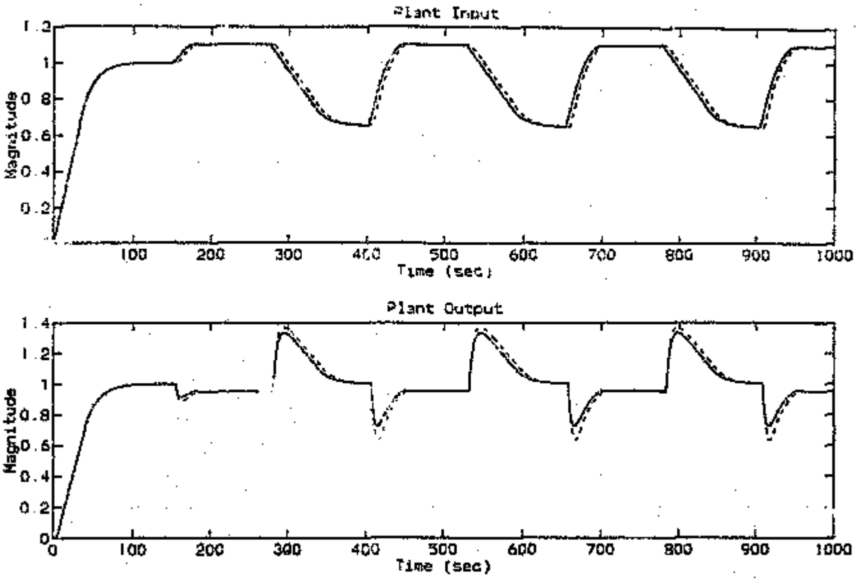

Figure 14.4: Simulation results. Feedback control only (dashed line). Feedback and feedforward (solid line).

14.3.3 Simulation results

The disturbance input signal, u_D, for the simulation is shown in Figure 14.3. The simulation results are shown in Figure 14.4.

The following conclusions are drawn from these results,

- The inclusion of the feedforward controller into the MSC algorithm provides improved disturbance rejection for disturbance responses which are accurately modelled and predictable.
- No constraint violations occur when feedforward control is included in the feedback system. Refer to Figure 14.4. Observe that the maximum plant input corresponds with the controllers constraint setting and that the rate constraints of the plant input are adhered to. Observe that the rate of increase is greater than the rate of decrease of the plant input signal, which corresponds with the controller settings.
- The controller has integral action with no visible integral windup (refer to simulation results). Integral windup can occur when the controller attempts to drive the output against a constraint.

14.4 Summary

A modular framework for Multi-Step Predictive Control (MSC) with feedforward control is presented in this chapter. Technical details of the feedforward module are given. Issues such as the feedforward predictor model, predictor equation for the feedforward module, interfacing of the module to the MSC feedback controller and tuning of the feedforward module are discussed. A simulation study of the proposed MSC algorithm applied to a typical process control dynamics problem is presented. The simulation results show that the inclusion of the feedforward controller into the MSC algorithm provides improved disturbance rejection for disturbance responses which are accurately modelled and predictable.

The signal flow diagram of the proposed feedforward controller is significant in that it provides insight into the interaction between the feedback and feedforward control mechanisms of Long Range Predictive Control. An important feature of the proposed model is the ability of the constraint mechanism to service both the feedback and feedforward controllers. This feature is important as it prevents constraint violations from occurring when feedforward control is included in the system.

Part III

Assessment of IMC and MSC Control

Chapter 15

Implementation

15.1 Description of the plant

The PT326 Process Trainer is a self-contained process supplied by Feedback Instruments Ltd (PT326). It has the basic characteristics of a large plant. A key feature of the process trainer is its long transfer lag, which makes this unit ideal for assessing advanced control algorithms. Refer to Appendix F for a picture of the PT326.

In this equipment, air drawn from atmosphere by a centrifugal blower is driven past a heater grid and through a length of tubing to atmosphere again. The plant consists of heating the air flowing in the tube to the desired temperature level (ambient to 60°C), and the purpose of the control equipment is to measure the air temperature, compare it with a value set by the operator and generate a control signal which determines the amount of electrical power supplied to a correcting element, in this case a heater mounted adjacent to the blower.

Table 15.1: Impact of varying throttle blower angle on plant dynamics

Throttle Blower Angle	Gain	Transfer lag	Transient response
Reduced	Increased	Increased	Slower
Increased	Decreased	Decreased	Faster

The operating condition of the PT326 can be changed by varying the shutter at the intake of the centrifugal blower. When the throttle blower angle is reduced the flowrate of air into the centrifugal blower decreases. The effect of this on the dynamic performance of the plant is indicated in Table 15.1.

The elements which form the system are shown in Figure 15.1.

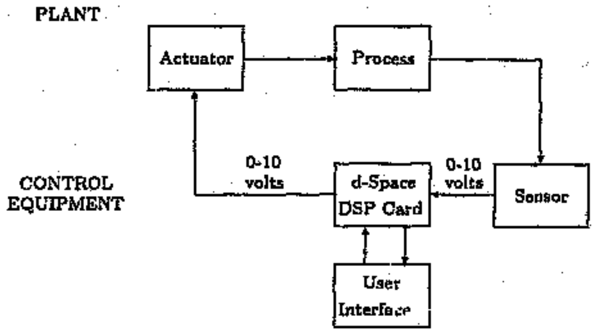

Figure 15.1: Elements comprising the feedback control system

15.2 Description of sensor

A bead thermistor fitted to the end of a probe can be inserted into the air stream at any one of three points along the tube, spaced 28mm, 140mm and 279mm from the heater. The 279mm position is used for all experiments. The thermistor probe forms one arm of a D.C. bridge which is in balance at 40°C. The bridge output voltage is applied to a d.c. amplifier and produces a voltage varying from 0 to +10 volts for air temperature change of 30°C to 60°C.

15.3 Description of control equipment

The control algorithm is executed on a digital signal processing (DS1102) card supplied by dSpace Ltd (DSpace 1997*a*). The DS1102 card contains a Texas Instrument TMS320C31 floating point DSP chip. The card has 4 analog to digital converters (two 16-bit and two 12-bit) and 4 digital to analog converts (each 12-bit).

The dSpace Real-Time Interface (RTI) (DSpace 1997*b*) connects the Mathwork's development software; Matlab, Simulink, and the Real-Time Workshop (RTW) with dSpace's real-time systems to form an integrated and ready-to-use development environment for real-time applications. It provides an automatic and seamless implementation of Simulink graphical models on dSpace real-time hardware systems for hardware-in-the-loop simulation and controller prototyping. Any kind of Simulink model for which code can be generated by means of the RTW can be implemented by the RTI, including continuous-time, discrete-time, and hybrid systems. Figure 15.2 describes the relationship of dSpace's RTI to the Mathwork's development software.

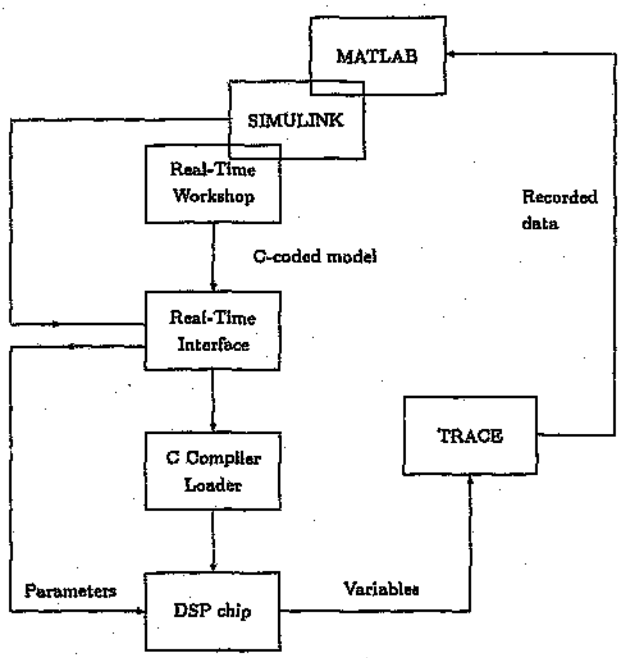

Figure 15.2: Development environment for prototyping the MSC controller

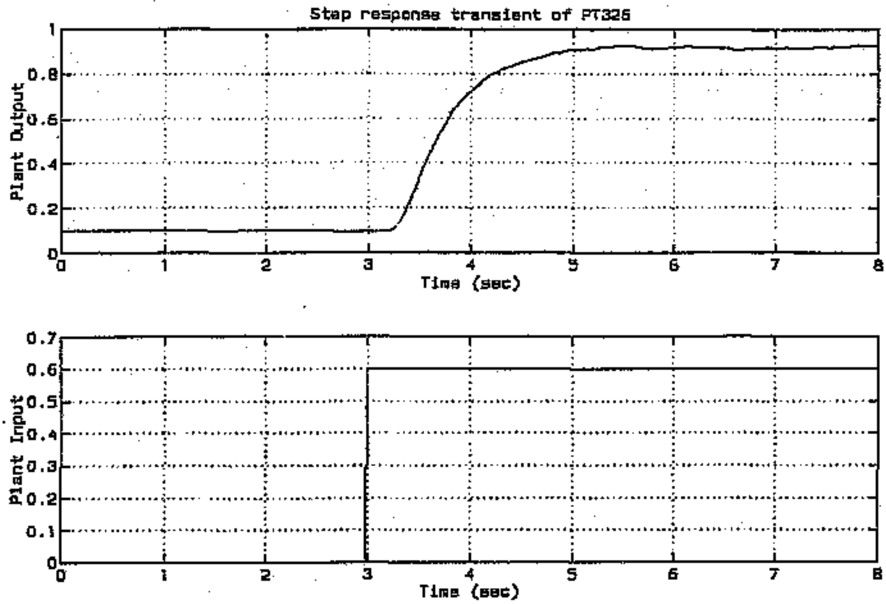

Figure 15.3: Dynamic response of PT326

15.4 Model identification

Based on the transient response characteristics of the plant and on the type of controller to be used, a suitable plant model which describes the dominant features of the dynamic response is selected. The dynamic response of the PT326 to a step change in the plant input signal is shown in Figure 15.3. From this plot it is observed that the dominant dynamics of the plant consist of a first order lag and a pure transport delay. A continuous time Laplace transform model which describes such a response is,

$$\hat{G}(s) = \frac{Ke^{-t_d s}}{\tau s + 1} \tag{15.1}$$

where K is the gain of the plant model, τ is the time constant of the transient, t_d is the transport delay and s is the Laplace transform variable.

The plant model, based on the model defined in Equation 15.1 is derived by finding the optimum set of parameters (K, τ and t_d) which describe the transient response of the plant. The solution to this problem is found by solving a least squares optimisation problem. Refer to Appendix C for details.

The transient response of the identified plant model, superimposed onto the measured transient response is shown in Figure 15.4. For this particular step test the

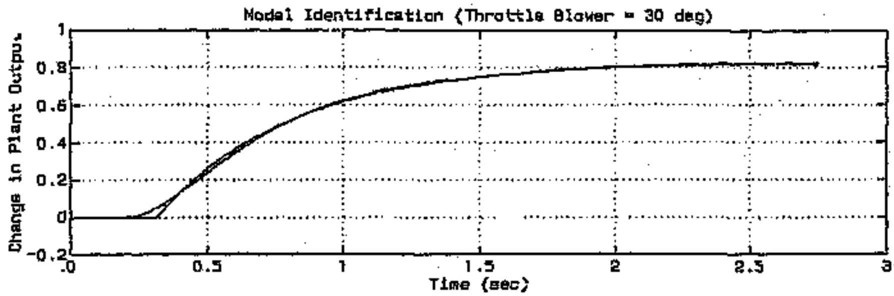

Figure 15.4: Model Identification (low order model)

plant model parameters are identified as,

$$K = 1.3617 \tag{15.2}$$

$$t_d = 0.3259 \text{ sec} \tag{15.3}$$

$$\tau = 0.4681 \text{ sec} \tag{15.4}$$

To design a robust controller that is expected to perform over a range of plant operating conditions it is necessary to model the plant dynamics over the expected operating range.

The plant operating conditions of the PT326 are conveniently changed by varying the throttle blower angle.

Based on the generic plant model defined in Equation 15.1 the following parameter variations are expected for a variation in throttle blower angle of 20° to 50°,

$$K = [0.9799 \;\; 1.5248] \tag{15.5}$$

$$t_d = [0.2440 \;\; 0.3562] \tag{15.6}$$

$$\tau = [0.4682 \;\; 0.54?3] \tag{15.7}$$

Refer to Appendix C for the results of the step response tests of the PT326 for different throttle blower settings.

An improvement of this model is possible by including a second order stage to the model defined in Equation 15.1. This second order stage models the high frequency dynamics of the plant. A new plant model is now defined as,

$$\hat{G}(s) = \left(\frac{K}{\tau s + 1}\right)\left(\frac{\omega_n^2}{s^2 + 2\zeta\omega_n + \omega_n^2}\right) e^{-t_d s} \tag{15.8}$$

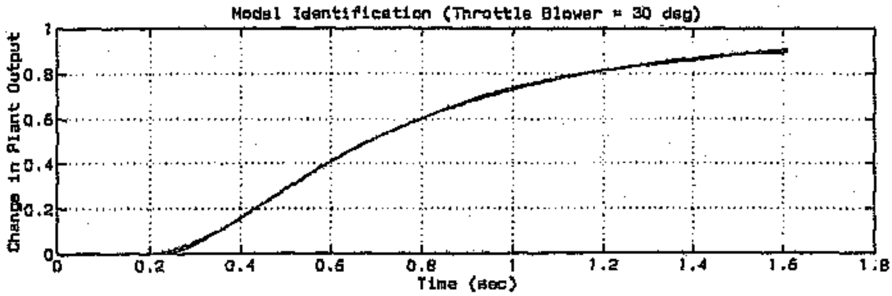

Figure 15.5: Model Identification (high order model)

The transient response of the identified plant model (Equation 15.8), superimposed onto the measured transient response is shown in Figure 15.5. For this particular step test the plant model parameters are identified as,

$$K = 1.3897 \tag{15.9}$$

$$t_d = 0.1989 \text{ sec} \tag{15.10}$$

$$\zeta = 1.1491 \tag{15.11}$$

$$\omega_n = 3.7973 \text{ rad/sec} \tag{15.12}$$

$$\tau = 0.25 \text{ sec} \tag{15.13}$$

Refer to Appendix C for the results of the step response tests of the PT326 for different throttle blower settings.

The plant model defined in Equation 15.8 is a high order model. This model is an ideal candidate for the predictor model in the IMC and MSC controllers. The IMC and MSC algorithms presented in this thesis are advanced control algorithms which provide good control when an accurate, high order model is used in the design of the controller.

15.5 Summary

This chapter presents the PT326 process supplied by Feedback Instruments Ltd. The significant features of the plant are identified, such as the long transfer lag and the ability to vary the plant dynamics by changing the throttle blower angle. A signal flow diagram of the feedback control system and a description of the dSpace hardware is presented. An investigation into the dynamic characteristics of the plant is carried out and two generic models of the plant are identified. The first is a low order model with a transport delay. This model is ideal for PID type controllers. The second is a high order model with a transport delay. Thi. model is ideal for the proposed IMC and MSC controllers.

Chapter 16

Demonstration of IMC Control

16.1 Need for active constraints

Classical type controllers are designed and implemented with the assumption that the plant behaves like a linear system. Through experience it has been shown that this approach to controller design leads to robust control if careful attention is paid to the design of the controller. However, problems arise when the plant's actuator is driven into saturation. Typical classical controllers (e.g. PID control) have no knowledge of actuator saturation. This effect is most visible in controllers that have integral action. When actuator saturation occurs the output of the integral component of the control algorithm increases in an attempt to null the set-point error. This control characteristic is known as integral windup and has serious detrimental effects on the performance of the feedback system.

The solution to this problem is addressed in Chapter 3 in which a special IMC framework is proposed that incorporates saturation elements into the feedback controller so that the controller maintains an awareness of the actuators operating range.

16.1.1 Example 1: Performance degradation resulting from integral windup

In order to demonstrate the performance degradation resulting from integral windup an experiment is performed using the PT326 process.

Experiment

The set-point signal is a series of square wave pulses that vary from 0 to 0.7 and the controller is a standard PID controller with transfer function,

$$\frac{U(s)}{E(s)} = K_c\left(1+\frac{1}{T_i s}+T_D s\right)\frac{1}{T_f s+1} \tag{16.1}$$

$$\tag{16.2}$$

The controller is designed according to the procedure presented in Appendix D. The nominal model (Equation 15.1) is based on the step response transient with the throttle blower set to 50°.

The controller is tuned using the following parameters,

$$K = 0.95 \tag{16.3}$$

$$t_d = 0.24 \text{ sec} \tag{16.4}$$

$$\tau = 0.46 \text{ sec} \tag{16.5}$$

$$\beta = 2 \tag{16.6}$$

The resulting PID parameters are,

$$K_c = 0.148 \tag{16.7}$$

$$T_i = 0.58 \tag{16.8}$$

$$T_D = 0.0952 \tag{16.9}$$

$$T_f = 0.971 \tag{16.10}$$

The controller is tested with the throttle blower angle set to 10°.

Results

The results of the experiment are shown in Figure 16.1.

When the throttle blower angle of the PT326 is small (10°) then an output offset exists. The PT326 has no cooling mechanism to null this offset. The result is that a set-point of 0 cannot be reached. The proposed PID controller attempts to drive the output to a set point of 0 by saturating the actuator with an input of less than zero. This results in integral windup.

The effect of the integral windup on the performance of the feedback system can be seen in Figure 16.1.

The integral windup causes poor set-point tracking as the controller must first unwind (recover from saturation) before it can respond to set-point changes. This unwinding effect is responsible for the additional delay and overshoot of the plant output when the set-point is changed from 0 to 0.7.

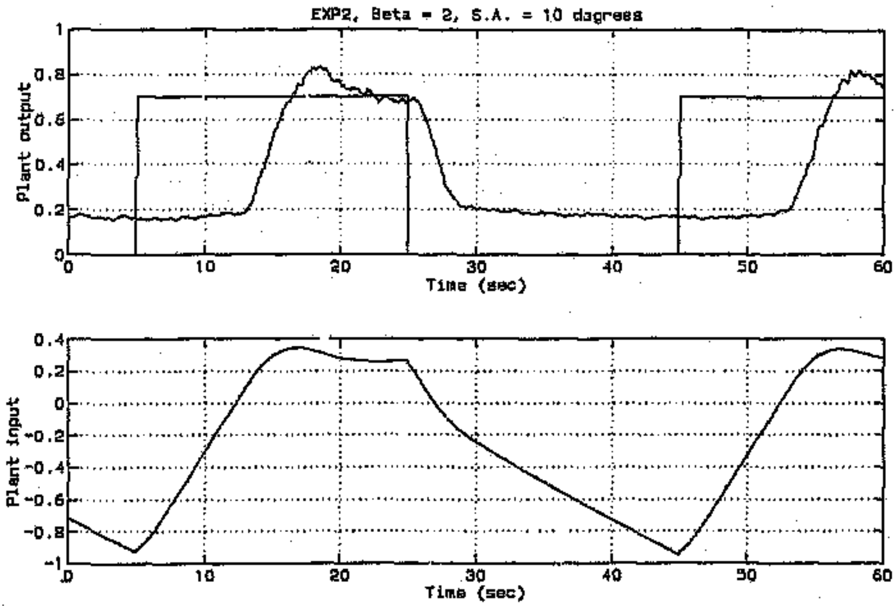

Figure 16.1: Excessive windup of controller caused by actuator saturation

If the controller maintains an awareness of the actuator's input range, which in this example is 0 to 1, then the output delay and overshoot would not occur.

16.1.2 Example 2: Incorrect constraint handling mechanism

The example presented in Section 16.1.1 demonstrates the need for the feedback controller to maintain an awareness of actuator saturation.

In some control problems a rate constraint is required on the plant input signal. An obvious method of including a rate constraint mechanism into the control algorithm is to place a constraint mechanism, such as the one proposed in Chapter 3 at the input of the plant. This ensures that the input signal to the plant is always in the allowable operating region. The example presented in this section shows that this method of handling absolute and rate actuator saturation is incorrect as suggested in Chapter 3.

Experiment

The experimental set-up is identical to the procedure explained in Section 16.1.1. However, in this example a constraint mechanism as shown in Figure 16.2 is placed at the plant's input with the following settings,

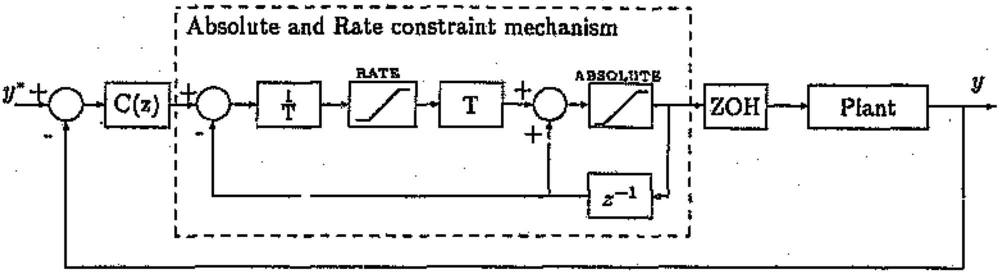

Figure 16.2: Incorrect method of rate and absolute constraint handling

Experiment A (Absolute plant input constraint)

$$u_{\min} = 0 \tag{16.11}$$

$$u_{\max} = 0.46 \tag{16.12}$$

$$\left[\frac{du}{dt}\right]_{\min} = -10 \tag{16.13}$$

$$\left[\frac{du}{dt}\right]_{\max} = 10 \tag{16.14}$$

Experiment B (Rate plant input constraint)

$$u_{\min} = 0 \tag{16.15}$$

$$u_{\max} = 1 \tag{16.16}$$

$$\left[\frac{du}{dt}\right]_{\min} = -10 \tag{16.17}$$

$$\left[\frac{du}{dt}\right]_{\max} = 0.1 \tag{16.18}$$

Throttle blower angle set to 20°.

Results

The results of the experiment are shown in Figure 16.3 and 16.4. These plots compare the proposed absolute and rate constraint mechanisms (Controller #1, Section 16.1.2) with the correct mechanism presented in Chapter 3 (Controller #2).

Controller #1 performs poorly. Integral windup occurs when the controller's output reaches the constraint limit. Potential problems may arise because while the controller is unwinding it cannot respond to disturbances or set-point changes. Controller #2 does not contain integral windup and will be in a better position to reject disturbances and respond to set-point changes.

The benefits of using the correct constraint mechanism is emphasised in the rate

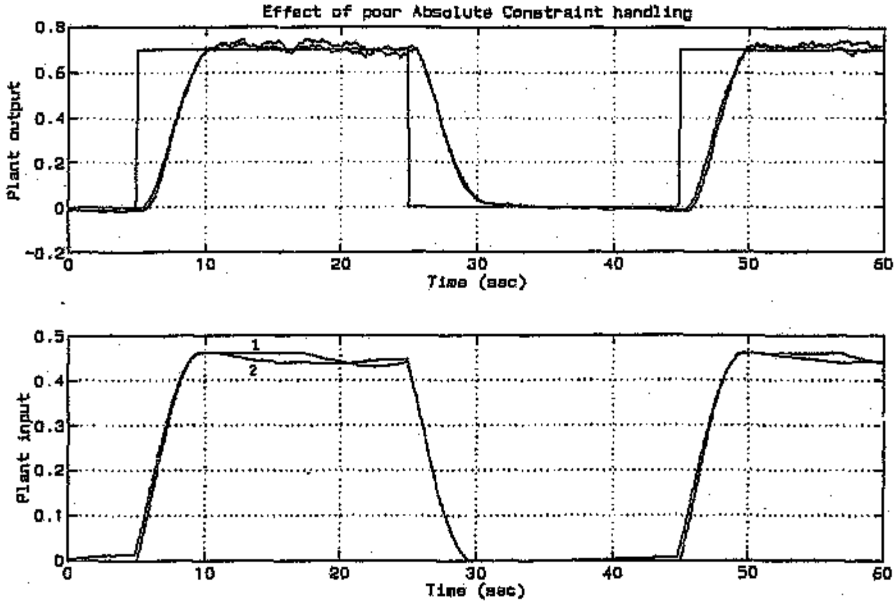

Figure 16.3: Experiment A: Comparison between incorrect (1) and correct (2) plant input absolute constraint mechanisms

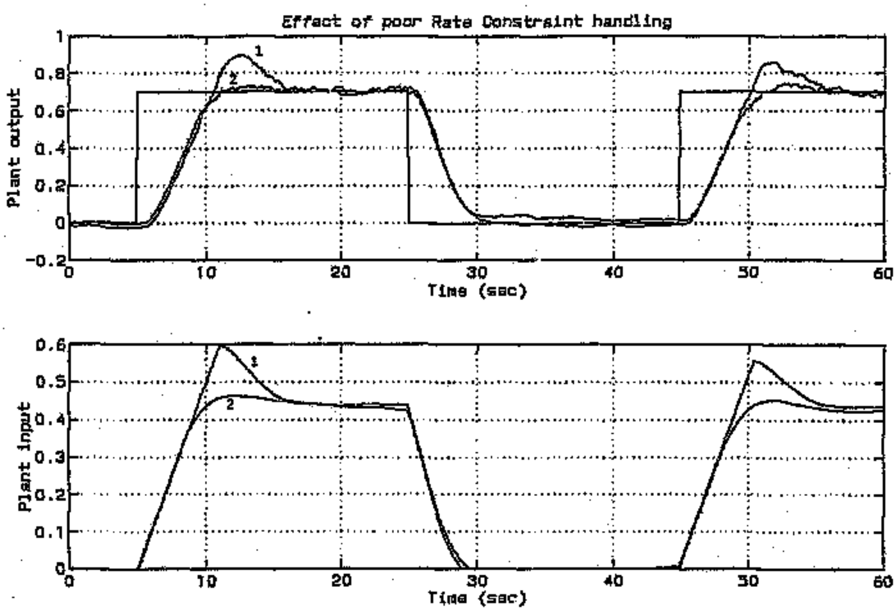

Figure 16.4: Experiment B: Comparison between incorrect (1) and correct (2) plant input rate constraint mechanisms

constraint example. Refer to Figure 16.4. When the incorrect mechanism is used (controller #1) the controller winds up, causing the plant output to overshoot. This does not occur when controller #2 is used (correct method).

16.2 Morari's IMC framework

Morari stated that if the feedback controller is implemented in the IMC configuration presented in Figure 10.2 then input constraints do not cause problems (Morari & Zafiriou 1989). The work presented in Part I of this thesis suggests otherwise.

This section presents an experiment which demonstrates the constraint handling ability of Morari's IMC configuration. The results of the experiment show that Morari's method of handling constraints is incorrect. Integral windup still occurs.

<u>Experiment</u>

The set-point signal is a series of square wave pulses that varies from 0 to 0.7 and the controller is an IMC controller as shown in Figure 2.1.

The estimated plant model, $\hat{G}(s)$, is based on the model,

$$\hat{G}(s) = \frac{Ke^{-t_d s}}{\tau s + 1} \tag{16.19}$$

The identified plant model (throttle blower angle = 50°) based on the step response tests presented in Appendix C are,

$$K = 0.95 \tag{16.20}$$

$$t_d = 0.24 \text{ sec} \tag{16.21}$$

$$\tau = 0.46 \text{ sec} \tag{16.22}$$

$$\tag{16.23}$$

The model $\hat{G}(s)$ is derived from Equation 16.19 where the delay is approximated using a first order Pade approximation.

$$\hat{G}(s) = \left[\frac{K}{\tau s + 1}\right]\left[\frac{-\frac{t_d}{2}s + 1}{\frac{t_d}{2}s + 1}\right] \tag{16.24}$$

The response filter is defined as,

$$F(s) = \frac{1}{(\beta s + 1)^2} \tag{16.25}$$

were $\beta = 2$.

The estimated plant model and response filter are selected so that the IMC controller is identical to the PID controllers used in Section 16.1.

The constraint mechanism used in this experiment is shown in Figure 16.2 and has the following settings,

Experiment A (Absolute plant input constraint)

$$u_{\text{min}} = 0 \tag{16.26}$$

$$u_{\text{max}} = 1 \tag{16.27}$$

$$\left[\frac{du}{dt}\right]_{\text{min}} = -10 \tag{16.28}$$

$$\left[\frac{du}{dt}\right]_{\text{max}} = 10 \tag{16.29}$$

Experiment B1 (Rate plant input constraint)

$$u_{\text{min}} = 0 \tag{16.30}$$

$$u_{\text{max}} = 1 \tag{16.31}$$

$$\left[\frac{du}{dt}\right]_{\text{min}} = -10 \tag{16.32}$$

$$\left[\frac{du}{dt}\right]_{\text{max}} = 0.3 \tag{16.33}$$

Experiment B2 (Rate plant input constraint)

$$u_{\text{min}} = 0 \tag{16.34}$$

$$u_{\text{max}} = 1 \tag{16.35}$$

$$\left[\frac{du}{dt}\right]_{\text{min}} = -10 \tag{16.36}$$

$$\left[\frac{du}{dt}\right]_{\text{max}} = 0.05 \tag{16.37}$$

Results

The results of the experiments which demonstrate Morari's constraint handling method are presented in Figure 16.5 and 16.6.

Morari's method still produces integral windup as indicated in Figure 16.5. When the set-point changes from 0 to 0.7 the controller should respond without a delay. Morari's IMC configuration produces a delay which is an indicator that the controller is unwinding.

Figure 16.6 presents results of Morari's IMC configuration when a rate constraint mechanism is applied. As the magnitude of the rate constraint is reduced the windup

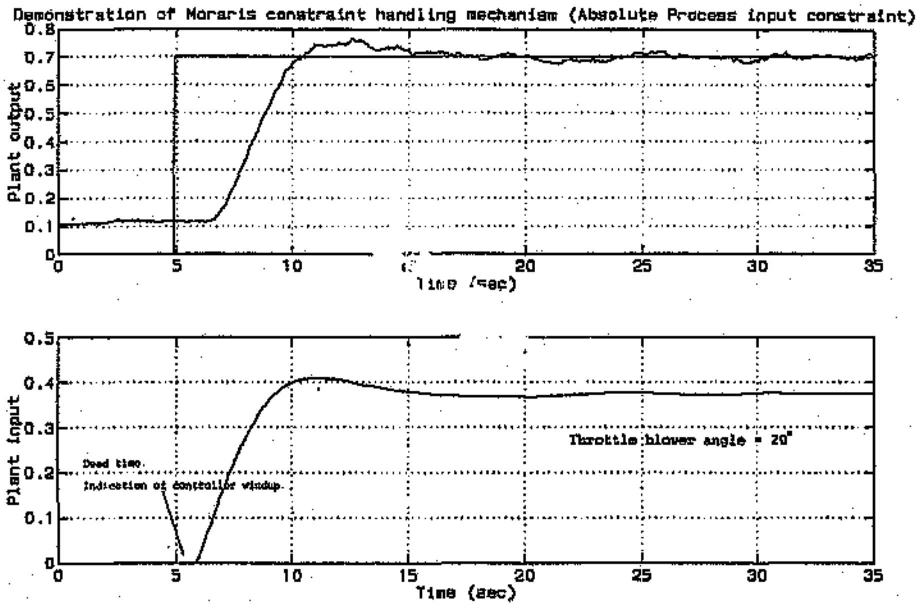

Figure 16.5: Experiment A: Demonstration of Morari's IMC framework with plant input absolute constraint mechanism

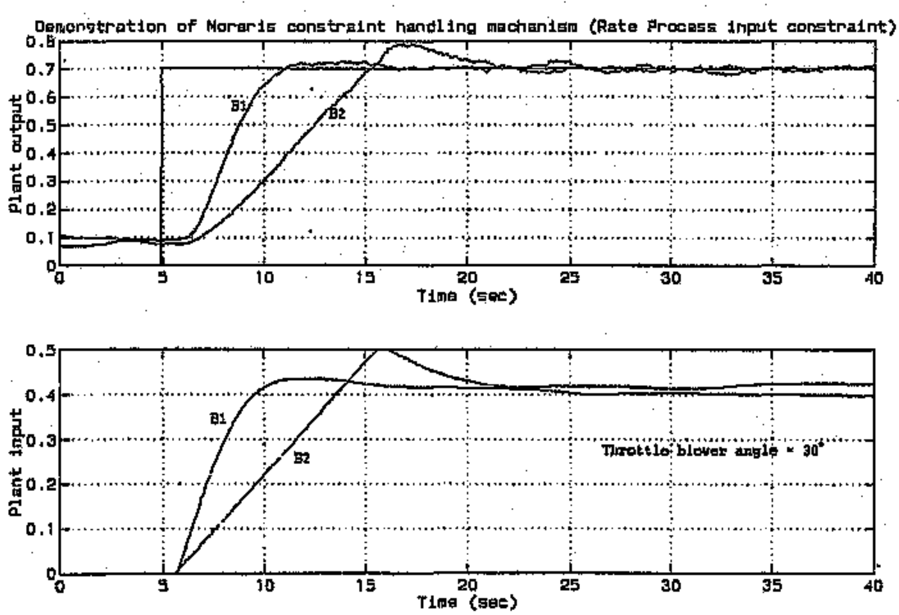

Figure 16.6: Experiment B: Demonstration of Morari's IMC framework with plant input rate constraint mechanism

of the controller becomes more apparent and the amount of overshoot caused by the integral windup becomes significant.

These results show that Morari's constraint handling mechanism is incorrect, as suggested in Part I of the thesis.

16.3 Proposed IMC framework

The argument presented in Section 16.1 stresses the need for the controller to maintain an awareness of actuator saturation. The obvious solution to constraint handling is to include a constraint mechanism such as the one proposed in Figure 16.2 at the input of the plant. The results of an experiment that demonstrates this constraint handling method, presented in Section 16.1.2, suggest that this technique is incorrect. Morari's solution to constraint handling is demonstrated in Section 16.2 and the results suggest that this method is also incorrect.

This section demonstrates the IMC control architecture proposed in Chapter 3.

Experiment
The experimental set-up is identical to the procedure explained in Section 16.2. However, in this example the IMC framework proposed in Chapter 3 is used.

Experiment A1 (Absolute and rate plant inputs constrained)

$$u_{\text{min}} = 0 \tag{16.38}$$

$$u_{\text{max}} = 0.5 \tag{16.39}$$

$$\left[\frac{du}{dt}\right]_{\text{min}} = -10 \tag{16.40}$$

$$\left[\frac{du}{dt}\right]_{\text{max}} = 0.6 \tag{16.41}$$

Experiment A2 (Absolute and rate plant inputs constrained)

$$u_{\text{min}} = 0 \tag{16.42}$$

$$u_{\text{max}} = 0.5 \tag{16.43}$$

$$\left[\frac{du}{dt}\right]_{\text{min}} = -10 \tag{16.44}$$

$$\left[\frac{du}{dt}\right]_{\text{max}} = 0.03 \tag{16.45}$$

Experiment B (Absolute and rate plant inputs constrained)

$$u_{\text{min}} = 0 \tag{16.46}$$

$$u_{\max} = 0.5 \tag{16.47}$$

$$\left[\frac{du}{dt}\right]_{\min} = -10 \tag{16.48}$$

$$\left[\frac{du}{dt}\right]_{\max} = 0.03 \tag{16.49}$$

<u>Results</u>

The results of the experiment which demonstrates the proposed IMC algorithm (Chapter 3) are presented in Figures 16.7 and 16.8.

The results show no evidence of integral windup and no evidence of overshoot when responding to a set-point step change.

The proper inclusion of an absolute and rate plant input constraint mechanism can enhance the quality of control that the feedback controller delivers. Refer to Figure 16.8. This plot clearly demonstrates the ability of the controller to control a plant that has a non-linear actuator, such as a pneumatic value which has different opening and closing characteristics. The controller is made aware of the actuator's nonlinearity by selecting the constraint bounds accordingly.

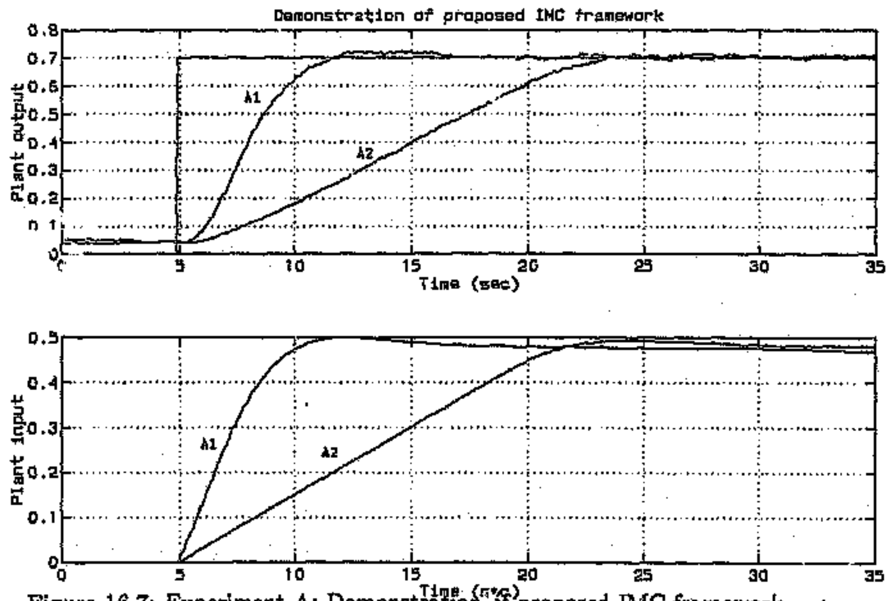

Figure 16.7: Experiment A: Demonstration of proposed IMC framework

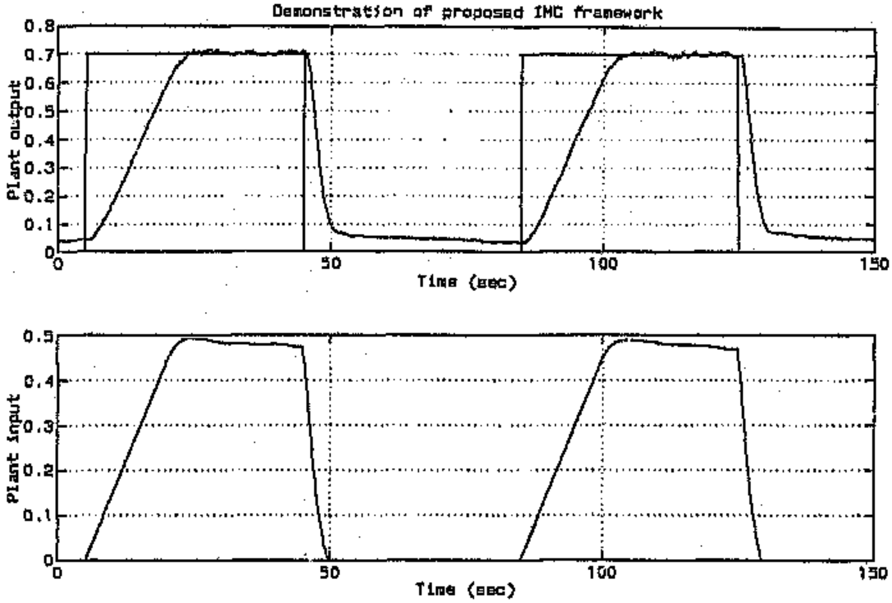

Figure 16.8: Experiment B: Demonstration of proposed IMC framework

16.4 Summary

This chapter assesses IMC control's plant input constraint handling mechanisms. Experiments are carried out on Feedback Instrument's PT326 process trainer.

An experiment is carried out that demonstrates the performance degradation resulting from integral windup caused by actuator saturation. This experiment justifies the need for the controller to maintain an awareness of actuator saturation. The obvious solution to plant input constraint handling is to include a constraint mechanism at the plant input. The results of an experiment that demonstrates this constraint handling approach suggest that it is highly ineffective.

A plant input constraint handling mechanism is proposed by Morari. Morari states that if the feedback controller is implemented in the IMC configuration and if both the plant input and the estimated plant model have identical plant input saturation constraints then actuator saturation does not cause a problem. A demonstration of Morari's proposed constraint handling method shows that Morari's method is incorrect. Morari's method shows evidence of controller windup when responding to a set-point step change. Significant overshoot is evident when a rate constraint mechanism is demonstrated using Morari's method.

The results of testing the proposed IMC controller (Chapter 3) are discussed. The experimental results show no evidence of integral windup and no evidence of overshoot when responding to a set-point step change. The conclusion, drawn from the experimental results, is that the proposed IMC controller is highly effective when handling plant input absolute and rate amplitude constraints.

Chapter 17

Demonstration of MSC Control

A modular framework of a Long Range Predictive Control algorithm called Multi-Step Predictive Control (MSC) is presented in Part II of this thesis. This framework is unique in that it incorporates absolute and rate plant input constraint mechanisms into the predictive control algorithm without the use of a quadratic program.

The important features of the MSC algorithm (Chapter 11) are summarised as follows: .

1. Fewer computations required when compared to the quadratic program approach to plant input constraint handling.
2. Controller has integral action, necessary for nulling constant offset disturbances appearing at the plant output.
3. Algorithm has an absolute and rate plant input constraint mechanism.
4. Anti-windup mechanism for preventing controller windup.
5. Use of a set-point reference trajectory.

This chapter demonstrates the MSC dynamic model developed for the MSC algorithm. The prototype MSC controller is programmed directly into the Mathworks' Simulink toolbox, which is converted into C-code and downloaded onto a DSP chip on dSpace's DS1102 card. The prototype MSC controller is applied to Feedback Instrument's PT326 process trainer.

The aim of the experiments are to:

1. Demonstrate the absolute plant input constraint mechanism of the MSC algorithm.

2. Demonstrate the interaction of the absolute and rate plant input constraint mechanisms.

3. Demonstrate the MSC algorithm controlling a plant that has a non-linear actuator, such as a pneumatic valve.

4. Demonstrate the impact the reference trajectory of the MSC algorithm has on the performance of the feedback controller.

5. Demonstrate the effect the length of control horizon has on the performance of the feedback controller.

17.1 Demonstration of MSC control's absolute plant input constraint mechanism

This section demonstrates the constraint handling ability of the MSC algorithm when actuator saturation occurs. The demonstration is presented in two parts. The first part presents the design of the MSC controller. The second part presents the experimental results.

Design of MSC controller for set-point control of PT326 process trainer

- The first step in the design of the predictive controller is to select an appropriate predictor model, $\hat{G}(s)$. For this experiment a high order model of the plant is selected. This model, which is presented in Equation 17.1,

$$\hat{G}(s) = \frac{19.2e^{-0.1843s}}{0.2601s^3 + 3.251s^2 + 12.35s + 14.22} \tag{17.1}$$

  is derived from the transient response of the plant when excited with a step change in the plant input. The step response test is carried out with the throttle blower angle set to 30°. Refer to Appendix C.2 for details of the modelling procedure.

- A suitable sampling period must be selected. Issues to consider when selecting the sampling period are:
  - Plant dynamics.
  - Prediction horizon lengths.
  - Anti-aliasing filter dynamics.

For this experiment the following parameters are selected,

$$T_{sp} = 0.05 \text{ sec} \tag{17.2}$$

$$\text{HP} = 40 \tag{17.3}$$

$$\text{CP} = 10 \tag{17.4}$$

- The predictive controller is tuned by setting β and τ_{ref}. For this experiment the reference trajectory is not used, therefore τ_{ref} is selected sufficiently small so that the effect of the reference trajectory is insignificant. The selected parameters are,

$$\lambda = 1 \tag{17.5}$$

$$\beta = 7 \tag{17.6}$$

$$\tau_{ref} = 0.01 \tag{17.7}$$

- The constraint settings of the MSC controller are selected based on the saturation characteristics of the actuator. For example if an actuator is expected to operate in the range 0 to 0.5 and can respond quickly to input changes then the MSC controller's constraint settings may be set as follows,

$$u_{min} = 0 \tag{17.8}$$

$$u_{max} = 0.47 \tag{17.9}$$

$$\Delta u_{min} = -1 \tag{17.10}$$

$$\Delta u_{max} = 1 \tag{17.11}$$

$$\tag{17.12}$$

The MSC controller settings for this experiment are summarised in Table 17.1.

Results of experiment

The throttle blower angle of the PT326 unit is set to 20°.

The result of the experiment which demonstrates the MSC controller's absolute constraint handling mechanism is presented in Figure 17.1.

The dynamic response of the system when responding to a set-point step change shows no evidence of overshoot or integral windup.

Table 17.1: MSC controller settings

Predictor Model	$\hat{G}(s) = \frac{19.2e^{-0.1843s}}{0.3601s^3+3.251s^2+12.35s+14.22}$
Sampling period	$T_{sp} = 0.05$ sec
Prediction Horizon	HP = 40
Control Horizon	CP = 10
Tuning parameters	$\lambda = 1$
	$\beta = 7$
Reference traj. time constant	$\tau_{ref} = 0.01$
Plant input constraints	$u_{min} = 0$
	$u_{max} = 0.47$
	$\Delta u_{min} = -1$
	$\Delta u_{max} = 1$

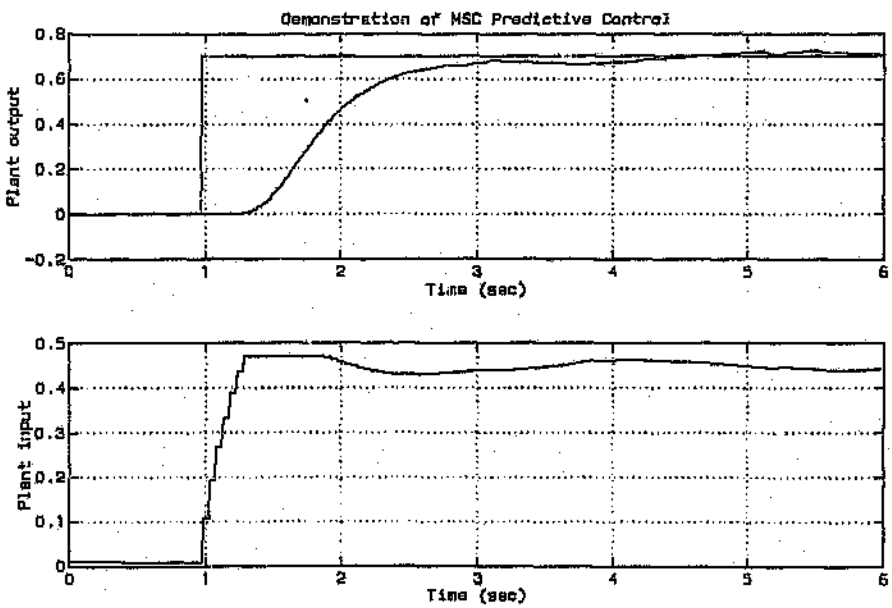

Figure 17.1: Demonstration of absolute plant input constraint handling of MSC controller

17.2 Demonstration of MSC control's absolute and rate plant input constraint mechanism

This section demonstrates MSC control when the absolute and rate constraint mechanisms interact. The design procedure of the MSC controller is presented in Section 17.1.

The incremental change of the plant input is set sufficiently low so as to effect the dynamic response of the plant input signal. The upper limit of the absolute plant input constraint setting is also set sufficiently low so as to cause the plant input signal to saturate. The combination of these constraint settings demonstrate the way the MSC controller's absolute and rate constraint mechanisms interact.

The MSC controller settings for this experiment are summarised in Table 17.2.

Table 17.2: MSC controller settings

Predictor Model	$\hat{G}(s) = \frac{19.2e^{-0.1843s}}{0.2601s^3+3.251s^2+12.35s+14.22}$
Sampling period	$T_{sp} = 0.05$ sec
Prediction Horizon	$\mathrm{HP} = 40$
Control Horizon	$\mathrm{CP} = 10$
Tuning parameters	$\lambda = 1$
	$\beta = 7$
Reference traj. time constant	$\tau_{ref} = 0.01$
Plant input constraints	$u_{min} = 0$
	$u_{max} = 0.47$
	$\Delta u_{min} = -0.01$
	$\Delta u_{max} = 0.01$

<u>Results of experiment</u>

The throttle blower angle of the PT326 unit is set to 20°.

The result of the experiment which demonstrates MSC controller when the absolute and rate constraint mechanisms interact is presented in Figure 17.2.

The dynamic response of the system when responding to a set-point step change shows no evidence of overshoot or integral windup. When comparing these results with the results of a similar experiment presented in Sections 16.4 and 16.6 it can

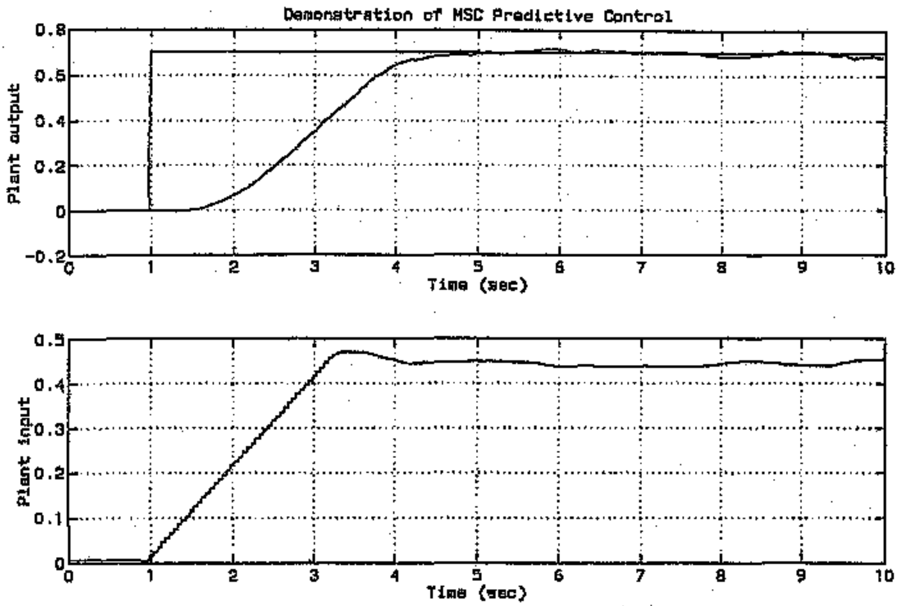

Figure 17.2: Demonstration of interaction of MSC controls absolute and rate constraint handling mechanisms

be concluded that the MSC controller performs well.

17.3 Demonstration of MSC control with a non-linear actuator

This section demonstrates MSC control with an actuator that has non-linear dynamics, such as a pneumatic valve which has different opening and closing characteristics. The controller is made aware of the actuator's nonlinearity by selecting the constraint bounds accordingly.

The MSC controller settings for this experiment are summarised in Table 17.3.

Results of experiment
The throttle blower angle of the PT326 unit is set to 30°.

The results of the experiment which demonstrates MSC control with a non-linear actuator are presented in Figure 17.3. The results show that the controller performs well. No overshoot and integral windup is evident. A plant with such an actuator is difficult to control using purely linear type controllers such as PID controllers

Table 17.3: MSC controller settings

Predictor Model	$\hat{G}(s) = \frac{19.2e^{-0.1843s}}{0.2601s^3+3.261s^2+12.35s+14.22}$
Sampling period	$T_{sp} = 0.05$ sec
Prediction Horizon	HP = 40
Control Horizon	CP = 10
Tuning parameters	$\lambda = 1$
	$\beta = 7$
Reference traj. time constant	$\tau_{ref} = 0.01$
Plant input constraints	$u_{min} = 0$
	$u_{max} = 1$
	$\Delta u_{min} = -0.01$
	$\Delta u_{max} = 0.003$

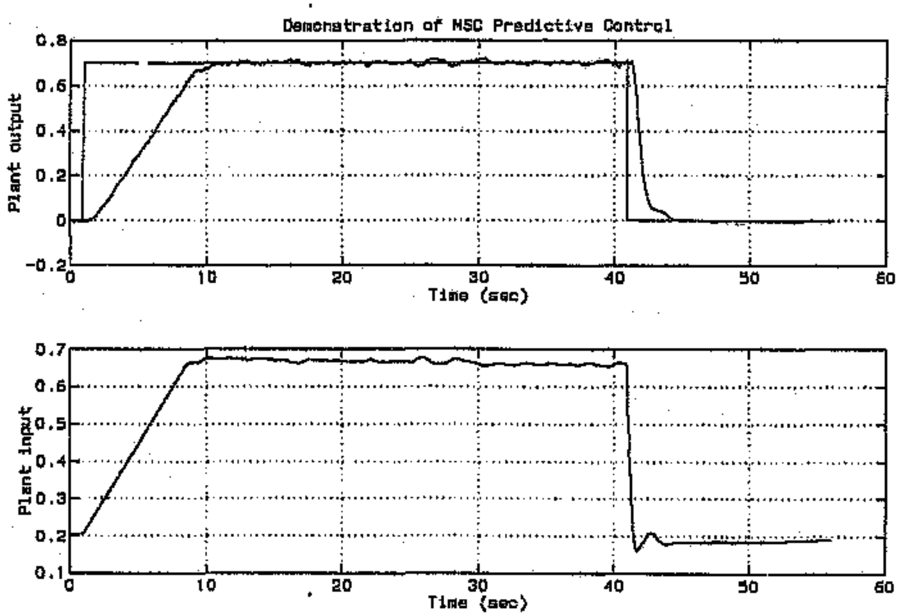

Figure 17.3: Demonstration of MSC controller controlling a plant that has a non-linear actuator

because the controller does not maintain an awareness of the actuator's non-linearity.

17.4 Demonstration of MSC control's reference trajectory mechanism

This section demonstrates the MSC controller's reference trajectory feature. Some predictive control algorithms, such as DMC, don't include a reference trajectory in their algorithms. The reason being that the predictive controller can be tuned for sufficient robustness by changing β. Including a reference trajectory does not have a significant effect on the robustness of the feedback system. However, the reference trajectory feature does introduce an extra degree of freedom in the design and implementation of the predictive controller.

This demonstration shows that the reference trajectory can enhance the quality of control.

Settings for two MSC controllers are presented in Table 17.4. Controller A2's reference trajectory time constant is significantly slower than controller A1.

Table 17.4: MSC controller settings

	A1	A2
Predictor Model	$\hat{G}(s) = \frac{19.2e^{-0.1843s}}{0.2601s^3+3.251s^2+12.35s+14.22}$	$\hat{G}(s) = \frac{19.2e^{-0.1843s}}{0.2601s^3+3.251s^2+12.35s+14.22}$
Sampling period	$T_{sp} = 0.05$ sec	$T_{sp} = 0.05$ sec
Prediction Horizon	$\mathrm{HP} = 40$	$\mathrm{HP} = 40$
Control Horizon	$\mathrm{CP} = 10$	$\mathrm{CP} = 10$
Tuning parameters	$\lambda = 1$	$\lambda = 1$
	$\beta = 7$	$\beta = 7$
Ref. traj. time constant	$\tau_{ref} = 0.01$	$\tau_{ref} = 1$
Plant input constraints	$u_{min} = 0$	$u_{min} = 0$
	$u_{max} = 1$	$u_{max} = 1$
	$\Delta u_{min} = -0.01$	$\Delta u_{min} = -0.01$
	$\Delta u_{max} = 0.003$	$\Delta u_{max} = 0.003$

Results of experiment

The throttle blower angle of the PT326 unit is set to 30°.

because the controller does not maintain an awareness of the actuator's non-linearity.

17.4 Demonstration of MSC control's reference trajectory mechanism

This section demonstrates the MSC controller's reference trajectory feature. Some predictive control algorithms, such as DMC, don't include a reference trajectory in their algorithms. The reason being that the predictive controller can be tuned for sufficient robustness by changing β. Including a reference trajectory does not have a significant effect on the robustness of the feedback system. However, the reference trajectory feature does introduce an extra degree of freedom in the design and implementation of the predictive controller.

This demonstration shows that the reference trajectory can enhance the quality of control.

Settings for two MSC controllers are presented in Table 17.4. Controller A2's reference trajectory time constant is significantly slower than controller A1.

Table 17.4: MSC controller settings

	A1	A2
Predictor Model	$\hat{G}(s) = \frac{19.2e^{-0.1843s}}{0.2601s^3+3.251s^2+12.35s+14.22}$	$\hat{G}(s) = \frac{19.2e^{-0.1843s}}{0.2601s^3+3.251s^2+12.35s+14.22}$
Sampling period	$T_{sp} = 0.05$ sec	$T_{sp} = 0.05$ sec
Prediction Horizon	$\mathrm{HP} = 40$	$\mathrm{HP} = 40$
Control Horizon	$\mathrm{CP} = 10$	$\mathrm{CP} = 10$
Tuning parameters	$\lambda = 1$	$\lambda = 1$
	$\beta = 7$	$\beta = 7$
Ref. traj. time constant	$\tau_{ref} = 0.01$	$\tau_{ref} = 1$
Plant input constraints	$u_{min} = 0$	$u_{min} = 0$
	$u_{max} = 1$	$u_{max} = 1$
	$\Delta u_{min} = -0.01$	$\Delta u_{min} = -0.01$
	$\Delta u_{max} = 0.003$	$\Delta u_{max} = 0.003$

Results of experiment

The throttle blower angle of the PT326 unit is set to 30°.

The results of the experiment which demonstrate MSC control's reference trajectory feature are presented in Figure 17.4. These results show that the use of the reference trajectory mechanism can be helpful in producing a smooth transient response. This confirms that the use of the reference trajectory enhances the quality of control.

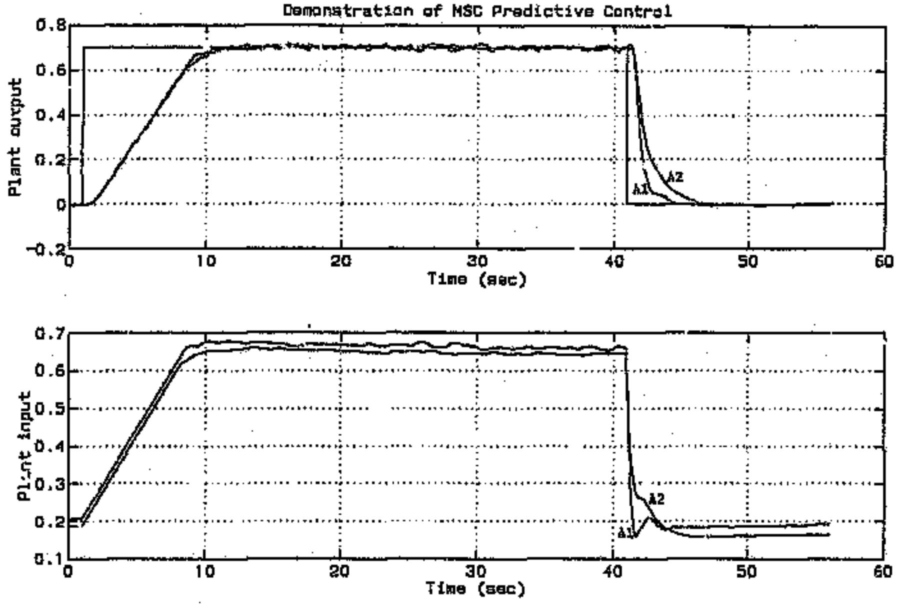

Figure 17.4: Demonstration of MSC control's reference trajectory feature

17.5 Demonstration of MSC control with different control horizon lengths

The length of the prediction horizons (HP and CP) have a significant effect on the number of computation that must be performed by the algorithm for each sampling period.

The prediction horizon (HP) is selected based on the plant dynamics and sampling period. The control horizon (CP) is usually a fraction of the prediction horizon. This demonstration investigates what effect varying CP has on the performance of the feedback system. A range of different MSC controllers are demonstrated, each with a different control horizon setting.

The MSC controller settings for this experiment are summarised in Table 17.5.

Table 17.5: MSC controller settings

Predictor Model	$G(s) = \frac{19.2e^{-0.1843s}}{0.2601s^3+3.251s^2+12.35s+14.22}$
Sampling period	$T_{sp} = 0.05$ sec
Prediction Horizon	HP = 40
Control Horizon	CP = 1,3,10,20
Tuning parameters	$\lambda = 1$
	$\beta = 10$
Reference traj. time constant	$\tau_{ref} = 10$
Plant input constraints	$u_{min} = 0$
	$u_{max} = 1$
	$\Delta u_{min} = -0.1$
	$\Delta u_{max} = 0.003$

Results of experiment

The throttle blower angle of the PT326 unit is set to 30°.

The results of the experiment which investigates what effect varying CP has on the performance of the MSC controller are presented in Figures 17.5 and 17.6. The results show that selecting a large control horizon yields a smooth transient response in the plant input signal. The effect on the plant output signal is not significant.

It is concluded that when making use of the reference trajectory feature of the MSC algorithm and a smooth plant input signal is desired, then CP must be selected sufficiently large.

17.6 Summary

The results of testing the proposed MSC controller are discussed in this chapter. The prototype MSC controller is programmed directly into the Mathworks' Simulink toolbox, which is converted into c-code and downloaded onto a DSP chip on dSpace's DS1102 card. The prototype MSC controller is applied to Feedback Instrument's PT326 process trainer.

The results of the MSC controller applied to the PT326 unit, provide a foundation based on measured plant responses, on which the MSC algorithm may be assessed. The PT326 process trainer has the basic characteristics typical of large industrial

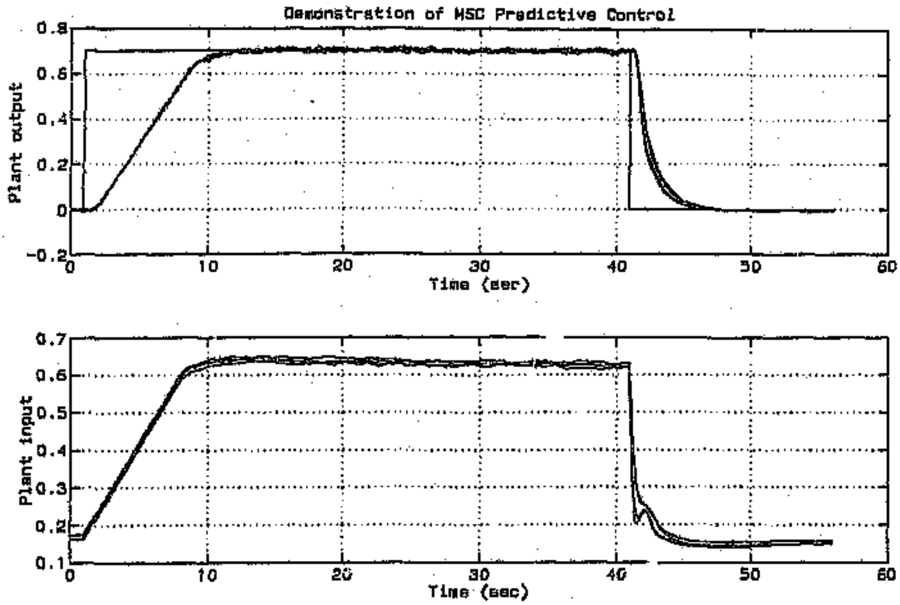

Figure 17.5: Demonstration of effect varying CP has on performance of MSC controller

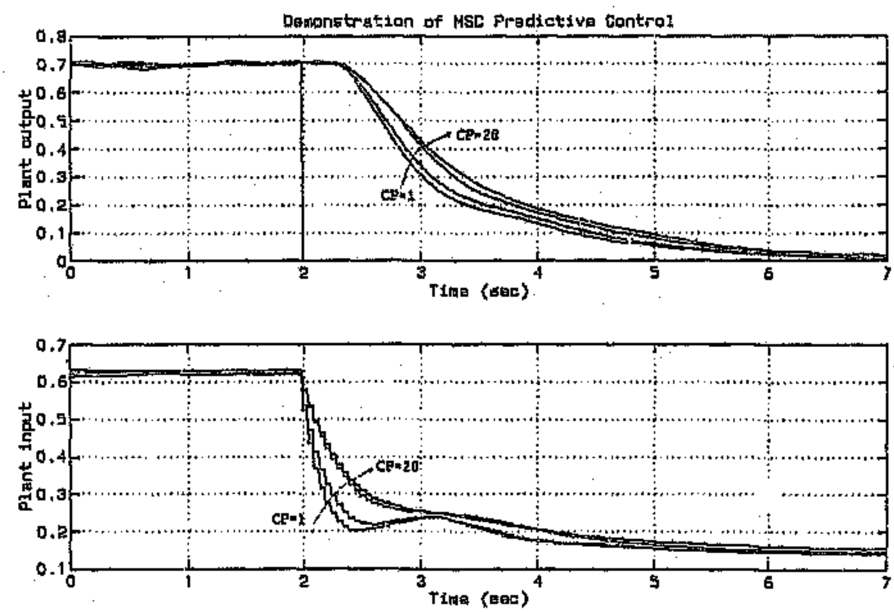

Figure 17.6: Demonstration of effect varying CP has on performance of MSC controller (zoomed)

plants, such as transfer lag, external disturbances and varying plant dynamics. This unit is therefore ideal for assessing the MSC algorithm's dead time compensation, constraint mechanisms, integral action and overall performance of the MSC controller.

The MSC algorithm is assessed by demonstrating varies key features of the algorithm and commenting on the results. The features that are investigated are summarised as follows:

- Demonstration of MSC's absolute and rate constraint mechanisms.
- Demonstration of the MSC algorithm controlling a plant which has a non-linear actuator, such as a pneumatic valve.
- Demonstration of MSC's reference trajectory feature.
- Investigation of what effect varying control horizon lengths have on the controller's performance.

The results of these demonstrations confirm that MSC control is a high performance control technique, well suited to controlling industrial plants that require dead time compensation, plant input constraints and integral action from the controller.

The demonstration of the algorithm's reference trajectory feature confirm that the reference trajectory adds an extra degree of freedom to the design and implementation of the controller, which enhances the quality of control.

Chapter 18

Comparison of PID, IMC and MSC Control

The PID control algorithm is a well known control algorithm capable of providing stable, 'straight line' control. Advanced control algorithms such as the IMC and MSC control algorithms presented in Parts I and II of this thesis are reputed to provide significantly better control performance than standard PID control.

This chapter compares the PID, IMC and MSC control algorithms. Each controller is evaluated by assessing the quality of control provided by the controller when applied to Feedback Instrument's PT326 industrial process trainer. The evaluation is based on the performance and robustness of the controller.

The study presented in this chapter is divided into two sections. The first section investigates the robustness of the proposed controllers. A complete control design for each of the proposed controllers is carried out in the frequency domain. Details of the designs are presented in Appendix E. These designs rely on step response modelling results presented in Appendices C.2 and C.3. The results of these designs are presented in the form of key frequency and transient response plots. Each controller is tested on the PT326 unit and its robustness is investigated by changing the throttle blower angle of the PT326 and recording the corresponding transient response of the system when a set-point step change occurs. These transient responses are graphed and form the basis on which the robustness characteristics of the controllers are compared.

The second section of this chapter investigates the transient performance of the controllers. The plant is remodelled with the throttle blower angle set to 30°. The controllers are redesigned and transient responses for each of the controllers are measured when,

- a step change in the set-point occurs.
- a step change in throttle blower angle occurs (disturbance rejection)

These transient responses are graphed and form the basis on which the performance characteristics of the controllers are compared.

A summary of the results is presented in Section 18.3.

18.1 Robustness

The feedback controller is expected to provide stable, robust control that removes offset disturbances that appear at the plant output.

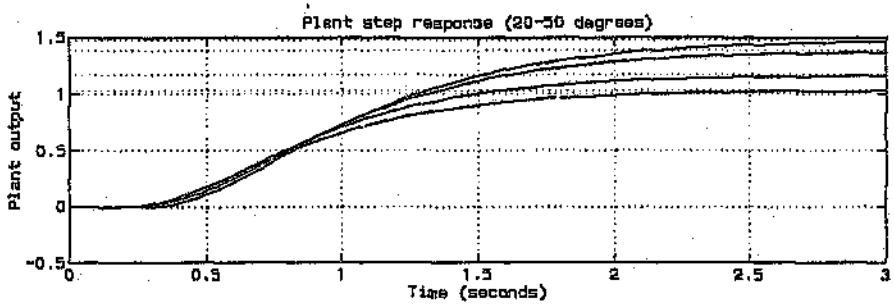

Figure 18.1: Step response of plant

Measured step response plots of the plant when the throttle angle blower varies from 20° to 50° is shown in Figure 18.1. This plot gives an indication of the uncertainty that the controller is expected to minimise. The control design is subject to the following design constraints.

Design Constraints

The following constraints are placed on the design,

- Due to noise constraints the controller's bandwidth should not exceed 0.8 rad/sec.
- The PT326's throttle blower angle varies between 20° and 50°. The controller must provide robust control over the specified operating range of the plant, with not more than 10 % overshoot when responding to a set-point step change.

- Plant input constraints.

$$0 \leq u \leq 1 \tag{18.1}$$

18.1.1 Design phase

PID control

The transfer function for the PID controller is,

$$\frac{U(s)}{E(s)} = K_c\left(1+\frac{1}{T_i s}+T_D s\right)\frac{1}{T_f s+1} \tag{18.2}$$

The tuning parameters of the PID controller are,

Table 18.1: PID controller tuning parameters

$K_c = 0.275$	$T_i = 0.655$	$T_D = 0.1222$	$T_f = 0.363$

A detailed explanation of the PID controller design is presented in Appendix E.3.

IMC control

The IMC controller is based on the identified plant model (throttle angle blower = 30°),

$$G(s) = \frac{19.2e^{-0.1843s}}{0.2601s^3+3.251s^2+12.35s+14.22} \tag{18.3}$$

and closed loop response filter,

$$F(s) = \frac{1}{(\beta s+1)^n} \tag{18.4}$$

The plant model used in the IMC controller, $\hat{G}(s)$, is based on the model defined in Equation 18.3 with the delay approximated using a third order Pade approximation.

A suitable IMC controller is obtained by setting,

$$n = 6 \tag{18.5}$$

$$\beta = 0.25 \tag{18.6}$$

A detailed explanation of the IMC controller design is presented in Appendix E.4.

MSC control

The MSC controller settings are summarised in Table 18.2. Refer to Appendix E.4 for a detailed explanation of the design.

Table 18.2: MSC controller settings

Predictor Model	$\hat{G}(s) = \frac{[illegible]e^{-0.1843s}}{0.2601s^3+3.251s^2+12.35s+14.22}$
Sampling period	$T_{sp} = 0.05$ sec
Prediction Horizon	HP = 40
Control Horizon	CP = 10
Tuning parameters	$\lambda = 1$
	$\beta = 10$
Reference traj. time constant	$\tau_{ref} = 0.01$
Plant input constraints	$u_{min} = 0$
	$u_{max} = 1$
	$\Delta u_{min} = -100$
	$\Delta u_{max} = 100$

18.1.2 Implementation phase

The PID, IMC and MSC controllers presented in Section 18.1.1 were tested on the PT326 p[illegible] nd the results of transient response tests are presented in Figures 18.2, 18.3 a[illegible].

The plant is effected by external disturbances. The temperature of the ambient air at the air intake changes. This causes offsets at the plant output. Integral action is required to remove these offsets from the plant output.

The following characteristics of the controllers are observed,

- Clearly the proposed controllers do have integral action. No steady state errors occur at any of the plant outputs (except when the controller's output saturates).
- Although the IMC and MSC controllers are based on a specific predictor model, which is accurate when the throttle blower angle is set to 30°, the controllers provide robust control over a range of settings.
- The performance of the IMC and MSC controllers is influenced by the accuracy of the predictor model. Example: When the throttle angle blower is set to 50° the transient performance of the controller is reduced. This is because the gain of the plant is significantly less than the predictor model's gain.
- The IMC and MSC controllers are high order controllers. The effect of the dead

time compensation can be seen in the IMC and MSC's plant input signal. The plant input signal increases rapidly when responding to a set-point change. However, because the controller maintain an awareness of the plant's dead time, the controller responds in such a way that no overshoot is observed in the plant output.

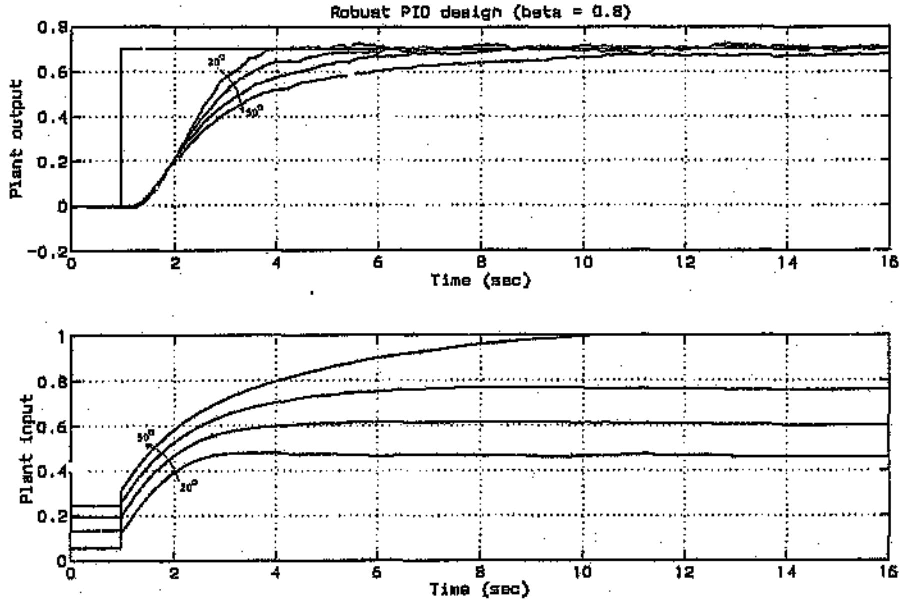

Figure 18.2: Results of implementation of PID controller

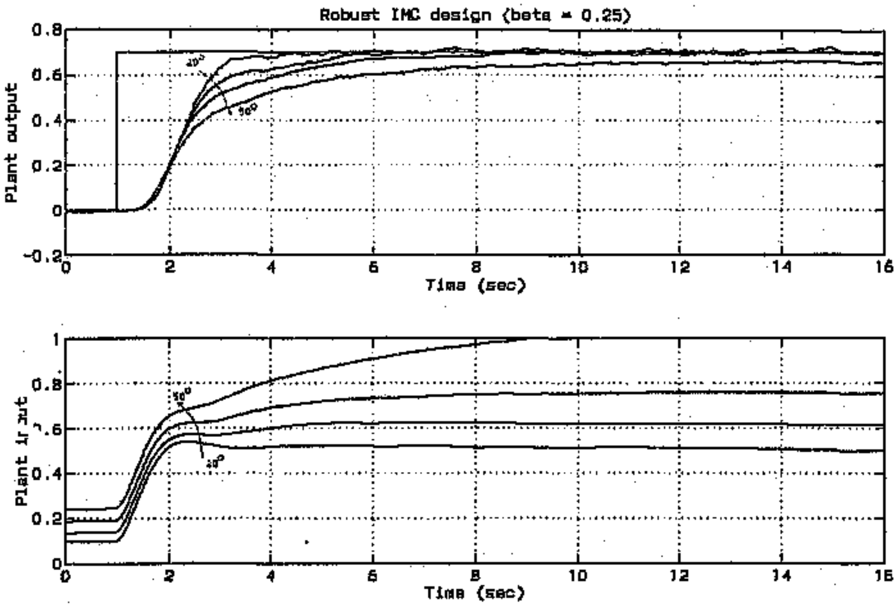

Figure 18.3: Results of implementation of IMC controller

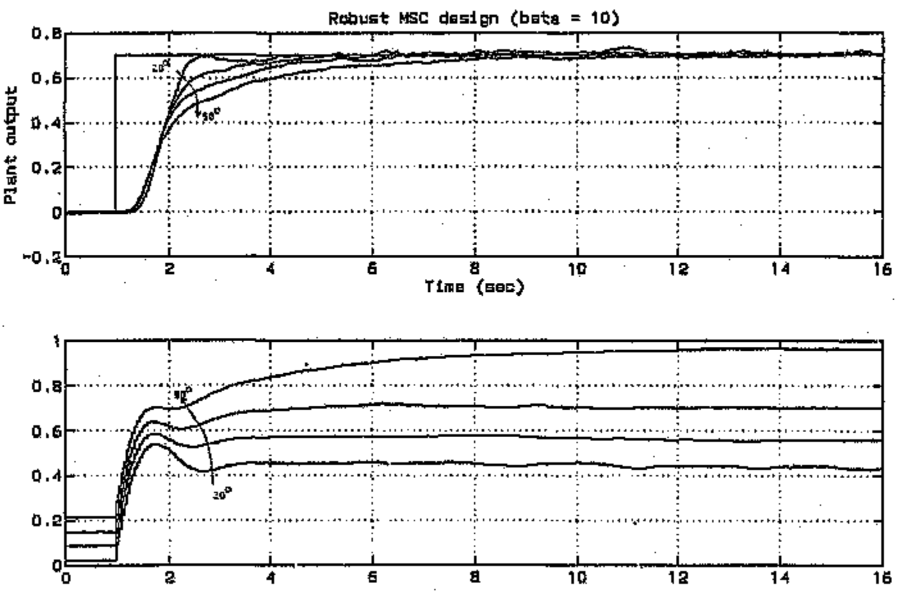

Figure 18.4: Results of implementation of MSC controller

18.2 Transient response

This section investigates the transient performance of the controllers. The plant is remodelled with the throttle blower angle set to 30°. The controllers are redesigned and transient responses for each of the controllers are measured when a step change in the set-point occurs and a step change in throttle blower angle occurs (disturbance rejection).

The controller settings are summarised as follows.

PID controller
The PID controller is redesigned using the following low order model,

$$G(s) = \frac{1.3833e^{-0.6030s}}{0.3081s+1} \tag{18.7}$$

and setting (refer to Appendix D),

$$\beta = 0.8 \tag{18.8}$$

results in the PID settings,

$K_c = 0.218$	$T_I = 0.560$	$T_D = 0.138$	$T_f = 0.346$

IMC and MSC controller
The IMC and MSC controllers are redesign using the same settings as used in Section 18.1.1. A new predictor model is defined based on the remodelling test. The model is,

$$\hat{G}(s) = \frac{19.2e^{-0.1843s}}{0.2601s^3 + 3.251s^2 + 12.35s + 14.22} \tag{18.9}$$

18.2.1 Set-point transient response

Figure 18.5 presents the results of the set-point transient responses when the proposed PID, IMC and MSC controllers are implemented. Clearly the MSC controller performs best, followed by the IMC controller. These results are to be expected since the MSC controller is a high order controller with an advanced, high performance algorithm, capable of being tuned with a few, easy to select tuning parameters. The IMC controller is capable of matching the MSC's performance if careful attention is paid to the selection of the closed loop response filter.

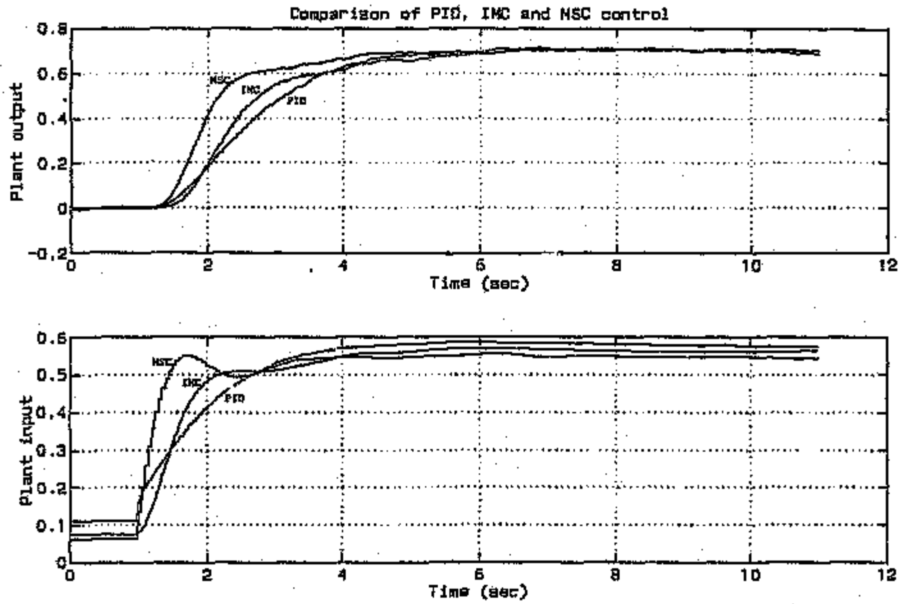

Figure 18.5: Comparison between PID, IMC and MSC's set point transient response

18.2.2 Disturbance rejection transient response

Figure 18.6 presents the results of the disturbance rejection transient responses when the proposed PID, IMC and MSC controllers are used to control the plant.

Disturbance: The plant is in a steady state and the throttle blower angle is set to 40°. A step change in the plant output is introduced by rapidly changing the throttle blower angle setting from 40° to 30°.

Clearly the MSC controller performs best, followed by the IMC controller. The settling time of the PID controller is significantly longer than the IMC and MSC controller, which is to be expected.

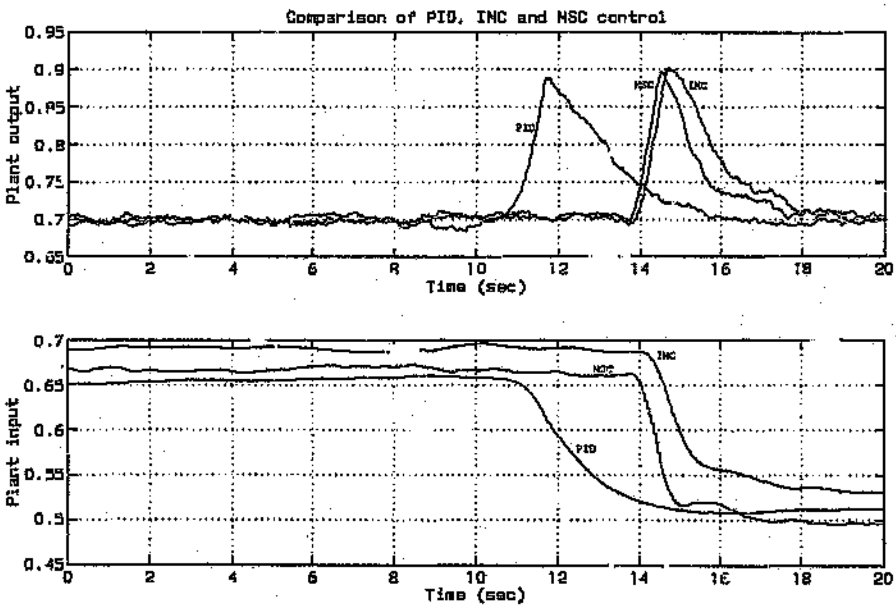

Figure 18.6: Comparison between PID, IMC and MSC's disturbance rejection transient response

Table 18.3: Comparison of PID, IMC & MSC Control

	Controller Order	*Integral Action*	*Constraint Handling*	*Dead time Compensation*
PID	Low.	Yes.	None.	No.
IMC	High.	Yes.	Absolute plus rate plant input constraints.	Yes.
MSC	High.	Yes.	Absolute plus rate plant input constraints. Additional constraints, such as plant output constraints, may be included by replacing K_{msc} with a quadratic program with inequality constraints.	Yes.

	Tuning Complexity	*Performance*	*Availability*
PID	Complex.	Adequate. Not good when plant has long dead time.	Widely available.
IMC	Easier than PID, but not trivial.	Good. But must pay careful attention to the design of the controller if high performance is required.	Difficult. Special hardware and software required. IMC configuration may be executed on standard control software development platforms such as the Mathwork's Simulink.
MSC	Significantly easier than PID, IMC. Based on dynamic model of plant. Few, easy to select tuning parameters.	Very good.. Easy to tune and gives high performance control.	Difficult. Special hardware and software required. However, using the modular framework presented in Part II the MSC algorithm may be executed on standard control software development platforms such as the Mathwork's Simulink.

18.3 Summary

This chapter compares PID, IMC and MSC control by carrying out investigations into the robustness and transient performance of the controllers. The results of the study confirm that MSC control is a high performance control algorithm which significantly improves on the quality of control offered by PID controllers. These results are significant as they demonstrate the benefits of using advanced control.

The chapter is separated into two sections. The first section investigates the robustness of the controllers. This is done by designing robust PID, IMC and MSC controllers which conform to design specifications. Issues such as plant uncertainty, constraints on controller bandwidth due to sensor noise and constraints on the transient response of the feedback system are considered in the design. These controllers are demonstrated on Feedback Instrument's PT326 industrial process trainer. The plant dynamics are changed by varying the throttle blower angle between 20° and 50°. The transient response thumb print for each controller is recorded and graphed. The results show that the controllers have integral action (no steady state errors at plant output). Although the IMC and MSC controllers are based on an accurate plant model (30°), the controllers provide robust control for a range of plant operating conditions. However, the accuracy of the model does influence the performance of the controllers.

The second section investigates the transient performance of the controllers. The PT326 is remodelled with the throttle blower angle set to 30°. The controllers are re-designed and tested on the PT326. The transient performance of the controllers are compared when a set-point change and a disturbance at the plant output occurs. The results show that the MSC controller performs best, followed by the IMC controller. The PID's settling time is significantly longer than the IMC and MSC controller's. The IMC and MSC's dead time compensation is also evident in the transient response.

The chapter is concluded with a table which compares PID, IMC and MSC control.

Part IV

Conclusion

Chapter 19

Conclusions

19.1 General

Current research into model based control seems to be moving towards incorporating non-linear models into Model Predictive Control (MPC) techniques. However, recent research by Goodwin suggests that the work on MPC using linear system models is still incomplete. Goodwin's results and the block diagram modelling approach used to identify and solve the problem of actuator saturation has prompted a similar investigation, carried out in this thesis, into other methods for MPC. The aim of this thesis is to investigate MPC control and to develop signal processing models for improving the understanding and interpretation of MPC algorithms. Although the work is limited to the single-input-output case, it builds a foundation on which the multivariable algorithms may be developed and analysed.

The work is presented in three parts. Part I continues Goodwin's work on constrained Internal Model Control (IMC). Part II develops and investigates a Long Range Predictive Control (LRPC) algorithm called Multi-Step Predictive Control (MSC). Part III assesses the IMC and MSC algorithms proposed in Parts I and II. This is done by carrying out experiments on Feedback Instrument's PT326 industrial process trainer. The control algorithms were implemented on dSpace's DS1102 digital signal processing card, which has all the signal processing features required to implement advanced control algorithms.

The work on Internal Model Control, presented in Part I includes a modified version of Goodwin's IMC model that extends the controller to the strictly proper case, a constraint handling mechanism that handles absolute as well as rate actuator amplitude constraints and a new approach for designing and implementing feedforward control. The proposed architecture, based on an IMC configuration, enables the same constraint handling mechanism to service both the feedback and feedforward controllers. A design equation is proposed for designing the feedforward controller. This equation is significant as it is a function of the feedback and feedforward controller's response filters. Rules for ensuring integral action when using the proposed feedforward framework are presented. All the features presented in Part I are demonstrated and proven via simulation studies.

Part II of the thesis is concerned with developing and investigating a LRPC algorithm called Multi-Step Predictive Control (MSC). A signal flow diagram of the MSC algorithm is developed using discrete building blocks. Investigations based on this model confirm that LRPC algorithms, such as the MSC algorithm, are consistent with Goodwin's constraint handling architecture. This confirms many reports of successful applications of constrained LRPC. Chapter 12 forges links between classical and predictive control by deriving equations for the transfer functions of the loop transmission and closed loop response of the feedback system.

A control design method is proposed in Chapter 13 for designing robust MSC controllers. The method is demonstrated by solving a typical predictive control design problem for a plant model with specified uncertainty. The design is analysed via computer simulation.

A feedforward control module is presented in Chapter 14 which extends the proposed MSC modular model to include feedforward control. Similarities with the feedforward IMC model presented in Part I are highlighted. A mechanism for de-tuning the feedforward controller is included in the design. Both the feedforward and feedback controllers are serviced by the same constraint handling mechanism. The proposed framework is useful for interpreting the interaction between LRPC's feedback and feedforward control mechanisms.

Part III of the thesis is concerned with demonstrating the proposed IMC and MSC algorithms. Experiments are carried out on Feedback Instrument's PT326 industrial process trainer. The experimental results confirm many issues put forward in Parts I and II.

The initial sections of Chapter 15 discuss the results of experiments that demonstrate the need for correct constraint handling methods. Four experiments are presented. The first experiment demonstrates the performance degradation resulting from integral windup caused by actuator saturation when no constraint handling mechanism is included in the controller. The second experiment is similar. However, in this case a constraint mechanism is placed at the input of the plant. The experimental results show that this method, which is commonly used in industry, promotes integral windup which significantly degrades the feedback system's performance. The third experiment tests Morari's IMC constraint handling method. The experimental results show evidence of integral windup, which confirms Goodwin's suspicions that Morari's method is incorrect. The forth experiment demonstrates the absolute and rate actuator constraint mechanisms of the IMC controller proposed in Part I. No evidence of integral windup is observed, which confirms that the proposed IMC framework for implementing absolute and rate actuator constraints is correct.

Chapter 16 presents several experiments which demonstrate the MSC modular framework presented in Part II, Chapter 11. Results of experiments demonstrating the algorithm's absolute and rate constraint mechanisms show no evidence of integral windup or overshoot caused by incorrect constraint handling. These results confirm the conclusions drawn in Chapter 10 which link LRPC with Goodwin's IMC architecture. Other issues, such as the reference trajectory and the selection of the control horizon are also investigated.

Chapter 17 presents experiments which compare the robustness and transient performance of PID, IMC and MSC controllers. The first set of experiments investigate the robustness of the controllers when the PT326's throttle angle blower is varied between 20^o and 50^o. The experimental results of the MSC controller compare favourably with the predicted results of the frequency domain design of the controller. This comparison verifies the accuracy of the equations presented in Chapter 12 which link classical and predictive control. Evidence of the IMC and MSC controller's dead time compensation and integral action are also observed in the experimental results. The second set of experiments compare the set-point and disturbance rejection transient responses of the controllers. The results confirm reports in the control literature that MPC controllers can out-perform PID controllers.

19.2 Assessment

The aim of this thesis is to investigate Model Predictive Control (MPC) and to develop new methods for interpreting and implementing Long Range Predictive Control (LRPC). These objectives are accomplished by investigating and developing signal processing models for implementing MPC. Although the models presented in this thesis are limited to single-input-output systems, the potential for extending the models to the multivariable case does exist. However, much work remains to be done in extending the framework of the proposed IMC and MSC models to the

MIMO case.

Two types of Model Predictive Control techniques are investigated in this thesis - Internal Model Control and Long Range Predictive Control.

Internal Model Control (IMC)

An IMC framework is presented in this thesis which makes provision for absolute and rate process input constraints. Demonstrations of the proposed IMC architecture verify the method's effectiveness in handling constraints. The significance of the proposed method is that it presents a technique for handling absolute as well as rate process input amplitude constraints at the design stage of the controller.

A new approach to implementing feedforward control is presented. This method is based on an IMC configuration. It is unique in that it has a constraint mechanism that handles absolute and rate process input constraints which services both the feedback and feedforward controllers. Design equations and rules for ensuring integral action when using the feedforward controller are also presented.

Long Range Predictive Control (LRPC)

A modular model of a LRPC algorithm called Multi-Step Predictive Control (MSC) is developed in this thesis. Although LRPC algorithms are typically used for multivariable control, the work presented in this thesis suggests that when considering SISO loops, a LRPC algorithm can significantly improve the quality of control when compared to standard PID control. The proposed MSC algorithm has the following features,

- The ability to incorporate a plant model directly into the control algorithm.
- Integral action.
- Dead-time compensation.
- Ease of tuning for robustness.
- Constraint mechanism that handles absolute and rate process input constraints.
- A reference trajectory (optional) for on-line tuning,
- Feedforward control. The model of the disturbance is incorporated directly into the feedforward module. The module has a mechanism for tuning the feedforward controller.

Demonstrations of the MSC algorithm confirm that the MSC controller's performance is an improvement on standard PID control.

The significance of the proposed MSC model is summarised as follows,

- The signal processing and structure of the MSC algorithm, based on the proposed model, is now completely transparent.
- It is possible to implement the MSC model directly on standard control software development platforms such as the Mathwork's Simulink, enabling rapid prototyping of Long Range Predictive Controllers.
- The model is useful for investigating the properties of LRPC. A comparative study concludes that the MSC algorithm and Goodwin's IMC[1] algorithm have similar constraint handling properties. This link confirms many reports of successful applications of constrained LRPC.
- Based on the results of the investigation, a new constraint handling mechanism for the MSC algorithm which handles absolute and rate process input constraints is proposed. This approach requires less computations than the traditional constrained quadratic programming approach.
- A separate feedforward control module is developed which extends the MSC model to include feedforward control. The interaction of the feedback and feedforward components in LRPC algorithms is now transparent in the MSC model.
- Based on the proposed dynamic model of the MSC algorithm, equations linking classical and predictive control are derived. The equations are,
  - the transfer function for the equivalent classical controller,
  - the transfer function for the loop transmission and
  - the transfer function for the closed loop response.

  Using these equations, it is now possible to analyse prospective MSC controllers using classical control concepts.

[1] Goodwin shows that a special architecture is required if process constraints are to be handled correctly.

19.3 Suggestions for Future Work

Suggestions for future work include,

- Experimental evaluation of the MSC model's feedforward control module.
- Experimental evaluation of the MSC model when output constraints are included in the algorithm (K_{MSC} is replaced with a quadratic program).
- Extension of the MSC model to handle multi-variable control.
- Investigation into the effectiveness of the proposed absolute and rate process input constraint mechanism (Chapter 11) when MIMO control is considered.
- Experimental evaluation of the MIMO MSC model.
- Investigate analytical tools which translate the MIMO MSC controller into an equivalent MIMO classical controller.
- Develop a design methodology for designing robust MIMO MSC controllers.

Part V

Appendices

Appendix A

Appendix for IMC Control

A.1 Derivation of K(s)

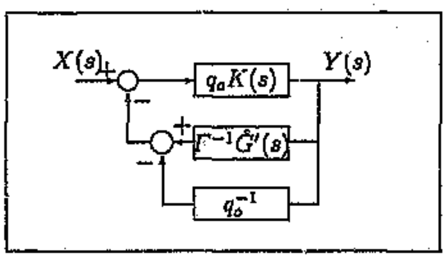

Figure A.1: Block diagram of $Q'(s)$

Consider the feedback configuration shown in Figure A.1. The transfer function for this configuration is,

$$\frac{Y(s)}{X(s)} = \frac{q_o K(s)}{1 + q_o K(s)[F^{-1}(s)\hat{G}'(s) - q_o^{-1}]} \tag{A.1}$$

Let

$$\frac{Y(s)}{X(s)} = F(s)(\hat{G}')^{-1}(s)K'(s) \tag{A.2}$$

Equating Equations A.1 and A.2 and solving for $K(s)$ yields,

$$K(s) = \frac{F(s)(\hat{G}')^{-1}(s)K'(s)}{q_o - K'(s)[q_o - F(s)(\hat{G}')^{-1}(s)]} \tag{A.3}$$

A.2 Stability of K(s)

Let

$$Q'(s) = Q(s)K'(s) = F(s)(\hat{G}')^{-1}(s)K'(s) \tag{A.4}$$

Then Equation A.3 can be rewritten as,

$$K(s) = \frac{Q'(s)}{q_o[1 - K'(s)] + Q'(s)} \tag{A.5}$$

Dividing numerator and denominator by $q_o[1 - K'(s)]$ results in,

$$K(s) = \frac{\frac{Q'(s)}{q_o[1-K'(s)]}}{1 + \frac{Q'(s)}{q_o[1-K'(s)]}} \tag{A.6}$$

This equation can be modelled with a feedback configuration shown in Figure A.2.

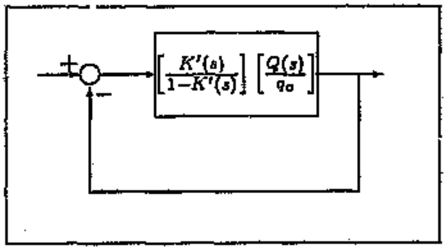

Figure A.2: Feedback model of $K'(s)$

A.2.1 Root locus method for selecting $K'(s)$

Typically $K'(s)$ is a first or second order transfer function. A typical second order transfer function is,

$$K'(s) = \frac{\omega_n^2}{s^2 + 2\zeta\omega_n s + \omega_n^2} \tag{A.7}$$

with $\zeta = 0.6$.

A suitable ω_n must be selected for the intended filter with the constraint that $K(s)$ must be stable. The Root Locus (based on parameter ω_n) of the feedback model shown in Figure A.2 show which ω_n's give stable $K(s)$'s.

A.3 Derivation of feedforward controller

Consider the signal flow diagram of the equivalent IMC filter (Q) shown in Figure A.3. The loop gain of this module is,

$$L_Q = q_o F^{-1} \hat{G}' K - K \tag{A.8}$$

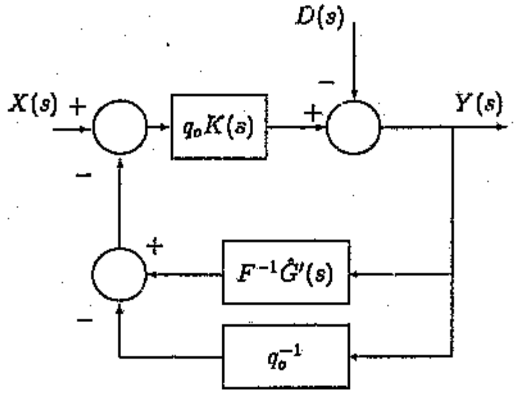

Figure A.3: Signal flow diagram of Q, ignoring constraint mechanism

Equation A.8 can be approximated with,

$$L_Q \approx q_o F^{-1} \hat{G}' - 1 \tag{A.9}$$

by making the assumption that $K \approx 1$ for frequencies $\omega < \omega_Q$. Where ω_Q is the bandwidth of the IMC filter $Q = F(\hat{G}')^{-1}$

Therefore $L_Q + 1$ is approximated using,

$$L_Q + 1 \approx q_o F^{-1} \hat{G}' \tag{A.10}$$

The signal flow diagram of the system shown in Figure 4.1 is re-arranged using block diagram manipulation resulting in the block diagram shown in Figure A.4. The constraint mechanism has been ignored in this manipulation. The feedforward filter Q_f is defined using this block diagram.

$$\begin{aligned} Q_f &= F_f (L_Q + 1)(\hat{G}')^{-1} \\ &= F_f (q_o F^{-1} \hat{G}')(\hat{G}')^{-1} \\ &= q_o F_f F^{-1} \end{aligned} \tag{A.11}$$

The transfer function of the block diagram shown in Figure A.4 is,

$$[y^* - y]\left[\frac{QG}{1 - Q\hat{G}}\right] + G_d d - \frac{G}{1 - Q\hat{G}}\left[\frac{Q_f}{L_Q + 1} - Q\hat{G}_d\right] d = y \tag{A.12}$$

$$\left[\frac{QG}{1 - Q\hat{G}}\right] y^* + G_d d - \frac{G}{1 - Q\hat{G}}\left[\frac{Q_f}{L_Q + 1} - Q\hat{G}_d\right] d = \left[\frac{QG}{1 - Q\hat{G}} + 1\right] y \tag{A.13}$$

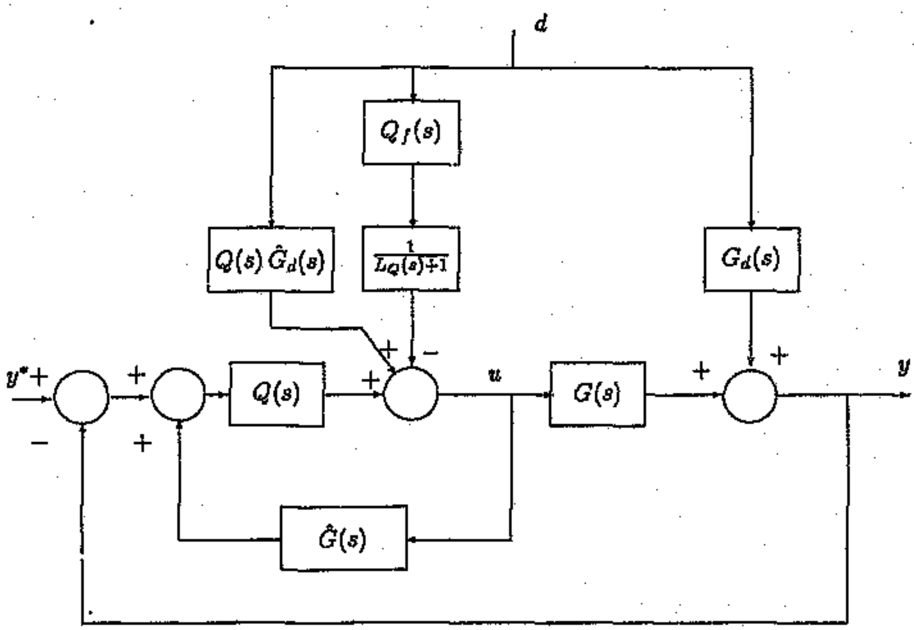

Figure A.4: Signal flow diagram of system

$$y = \left[\frac{\frac{QG}{1-Q\hat{G}}}{\frac{QG}{1-Q\hat{G}}+1}\right] y^* + \left[\frac{G_d - \frac{G}{1-Q\hat{G}}\left[\frac{Q_f}{L_Q+1} - Q\,\hat{G}_d\right]}{\frac{QG}{1-Q\hat{G}}+1}\right] d \tag{A.14}$$

The transfer function of the disturbance response is,

$$\frac{y}{d} = \frac{G_d - \frac{G}{1-Q\hat{G}}\left[\frac{Q_f}{L_Q+1} - Q\,\hat{G}_d\right]}{\frac{QG}{1-Q\hat{G}}+1} \tag{A.15}$$

which can be simplified to,

$$\frac{y}{d} = \frac{G_d(1-Q\,\hat{G}) - G(\frac{Q_f}{L_Q+1} - Q\,\hat{G}_d)}{1+Q(G-\hat{G})} \tag{A.16}$$

To null an offset caused by a disturbance, the numerator of the disturbance response defined in Equation A.16 must equal zero at $\omega = 0$ rad/sec. This is accomplished by setting,

$$1 - Q\hat{G} = 0 \tag{A.17}$$

$$Q\hat{G} = 1 \tag{A.18}$$

and

$$\frac{Q_f}{L_Q+1} - Q\hat{G}_d = 0 \tag{A.19}$$

Equation A.19 is re-arranged to

$$Q_f = (L_Q+1)Q\hat{G}_d \tag{A.20}$$

Substituting Q_f (Equation A.11) and L_Q+1 (Equation A.10) into Equation A.20 results in,

$$q_o F_f F^{-1} = q_o F^{-1}\hat{G}' Q\hat{G}_d \tag{A.21}$$

After simplifying Equation A.21,

$$F_f = \hat{G}' Q\hat{G}_d \tag{A.22}$$

There, let

$$\hat{G}' Q = 1 \tag{A.23}$$

and

$$F_f = \hat{G}_d \tag{A.24}$$

Therefore, to null a constant offset disturbance, Equations A.18, A.23 and A.24 must hold at $\omega = 0$ rad/sec.

Appendix B

Appendix for MSC Control

B.1 Derivation of j step ahead predictor

Consider the discrete time transfer function of the compensated predictor model described in Section 5.2.

$$A'(q^{-1})\hat{y}(t) = B'(q^{-1})u'(t) \tag{B.1}$$

Where $A'(q^{-1})$ and $B'(q^{-1})$ are

$$B'(q^{-1}) = 0 + b'_1q^{-1} + b'_2q^{-2} + ... + b'_{\mathrm{nb'}}q^{-\mathrm{nb'}} \tag{B.2}$$

$$A'(q^{-1}) = 1 + a'_1q^{-1} + a'_2q^{-2} + ... + a'_{\mathrm{na'}}q^{-\mathrm{na'}} \tag{B.3}$$

Equation B.1 is expanded to,

$$\left[1 + a'_1q^{-1} + a'_2q^{-2} + ... + a'_{\mathrm{na'}}q^{-\mathrm{na'}}\right]\hat{y}(t) = \left[0 + b'_1q^{-1} + b'_2q^{-2} + ... + b_{\mathrm{nb'}}q^{-\mathrm{nb'}}\right]u'(t) \tag{B.4}$$

$y(t)$ is solved for and written in matrix notation as,

$$\hat{y}(t) = [-a'_1 \ -a'_2 \ ... \ -a'_{\mathrm{na'}}]\begin{bmatrix} \hat{y}(t-1) \\ \hat{y}(t-2) \\ \vdots \\ \hat{y}(t-\mathrm{na'}) \end{bmatrix} + [b'_1 \ b'_2 \ ... \ b_{\mathrm{nb'}}]\begin{bmatrix} u'(t-1) \\ u'(t-2) \\ \vdots \\ u'(t-\mathrm{nb'}) \end{bmatrix} \tag{B.5}$$

B.1.1 Prediction $\hat{y}(t+1)$

Using shift operator notation, the prediction $y(t+1)$ is written,

$$\hat{y}(t+1) = q\hat{y}(t) \tag{B.6}$$

and substituting equation B.5 into B.6 results in,

$$\hat{y}(t+1) = [-a'_1 \ -a'_2 \ \ldots \ -a'_{\mathrm{na}'}] \begin{bmatrix} \hat{y}(t) \\ \hat{y}(t-1) \\ \vdots \\ \hat{y}(t-(\mathrm{na}'-1)) \end{bmatrix} + [b'_1 \ b'_2 \ \ldots \ b_{\mathrm{nb}'}] \begin{bmatrix} u'(t) \\ u'(t-1) \\ \vdots \\ u'(t-(\mathrm{nb}'-1)) \end{bmatrix} \tag{B.7}$$

Equation B.7 can be written as,

$$\hat{y}(t+1) = [-a'_1 \ -a'_2 \ \ldots \ -a'_{\mathrm{na}'}] \begin{bmatrix} \hat{y}(t) \\ \hat{y}(t-1) \\ \vdots \\ \hat{y}(t-(\mathrm{na}'-1)) \end{bmatrix} + [0 \ \ldots \ 0 \ b'_1 \ b'_2 \ \ldots \ b_{\mathrm{nb}'}] \begin{bmatrix} u'(t+\mathrm{CP}-1) \\ \vdots \\ u'(t+1) \\ u'(t) \\ u'(t-1) \\ \vdots \\ u'(t-(\mathrm{nb}'-1)) \end{bmatrix} \tag{B.8}$$

Let

$$q_1 = [-a'_1 \ -a'_2 \ \ldots \ -a'_{\mathrm{na}'}] \tag{B.9}$$

$$x_1 = [0 \ \ldots \ 0 \ b'_1 \ b'_2 \ \ldots \ b_{\mathrm{nb}'}] \tag{B.10}$$

then,

$$\hat{y}(t+1) = q_1 \begin{bmatrix} \hat{y}(t) \\ \hat{y}(t-1) \\ \vdots \\ \hat{y}(t-(\mathrm{na}'-1)) \end{bmatrix}$$

$$+x_1 \begin{bmatrix} u'(t+\mathrm{CP}-1) \\ \vdots \\ u'(t+1) \\ u'(t) \\ u'(t-1) \\ \vdots \\ u'(t-(\mathrm{nb}'-1)) \end{bmatrix} \tag{B.11}$$

B.1.2 Prediction $\hat{y}(t+2)$

Using shift operator notation, the prediction $y(t+2)$ is written,

$$\hat{y}(t+2) = q\hat{y}(t+1) \tag{B.12}$$

and substituting equation B.8 into B.12 results in,

$$\begin{aligned} \hat{y}(t+2) &= [-a'_1 \; -a'_2 \; ... \; -a'_{\mathrm{na}'}] \begin{bmatrix} \hat{y}(t+1) \\ \hat{y}(t) \\ \vdots \\ \hat{y}(t-(\mathrm{na}'-1)+1) \end{bmatrix} \\ &\quad + [0 \; ... \; 0 \; b'_1 \; b'_2 \; ... \; b_{\mathrm{nb}'}] \begin{bmatrix} u'(t+\mathrm{CP}) \\ \vdots \\ u'(t+2) \\ u'(t+1) \\ u'(t) \\ \vdots \\ u'(t-(\mathrm{nb}'-1)+1) \end{bmatrix} \end{aligned} \tag{B.13}$$

Equation B.13 is re-arranged to give,

$$\begin{aligned} \hat{y}(t+2) &= -a'_1\hat{y}(t+1) \\ &\quad + [-a'_2 \; -a'_3 \; ... \; -a'_{\mathrm{na}'}0] \begin{bmatrix} \hat{y}(t) \\ \hat{y}(t-1) \\ \vdots \\ \hat{y}(t-(\mathrm{na}'-2)) \\ \hat{y}(t-(\mathrm{na}'-1)) \end{bmatrix} \\ &\quad +0u(t+\mathrm{CP}) \end{aligned}$$

$$+\begin{bmatrix} 0 & \dots & 0 & b'_1 & b'_2 & \dots & b_{\mathrm{nb}'} & 0 \end{bmatrix} \begin{bmatrix} u'(t+\mathrm{CP}-1) \\ \vdots \\ u'(t+1) \\ u'(t) \\ u'(t-1) \\ \vdots \\ u'(t-(\mathrm{nb}'-2)) \\ u'(t-(\mathrm{nb}'-1)) \end{bmatrix} \quad \text{(B.14)}$$

Using matrices (S_1 and S_2) which perform the required time-shifting operation, the solution to $y(t+2)$ is,

$$\begin{aligned} \hat{y}(t+2) &= [(q_1 S_3)q_1 + q_1 S_1] Y_{\mathrm{past}} \\ &\quad + [(q_1 S_3)x_1 + x_1 S_2] \begin{bmatrix} U_{\mathrm{pred}} \\ U_{\mathrm{past}} \end{bmatrix} \end{aligned} \quad \text{(B.15)}$$

The matrices S_1, S_2 and S_3 are defined,

$$S_1 = \begin{bmatrix} 0 \dots 0 \\ I_1 \;\; \vdots \\ \quad 0 \end{bmatrix} S_2 = \begin{bmatrix} 0 \dots 0 \\ I_2 \;\; \vdots \\ \quad 0 \end{bmatrix} \quad \text{(B.16)}$$

$$S_3 = [1 \;\; 0 \;\; \dots \;\; 0]^T \quad \text{(B.17)}$$

I_1 is an identity matrix with dimensions (na$'-1$) x (na$'-1$). I_2 is an identity matrix with dimensions (CP+nb$'-1$) x (CP+nb$'-1$). S_3 is defined so that $q_1 S_3 = -a'_1$.

B.1.3 Prediction $\hat{y}(t+j)$

Based on the result of section A.2, the j step ahead prediction is,

$$\hat{y}(t+j) = q_j Y_{\mathrm{past}} + x_j \begin{bmatrix} U_{\mathrm{pred}} \\ U_{\mathrm{past}} \end{bmatrix} \quad \text{(B.18)}$$

where,

$$q_j = (q_{j-1} S_3) q_1 + q_{j-1} S_1 \quad \text{(B.19)}$$

$$x_j = (q_{j-1} S_3) x_1 + x_{j-1} S_2 \quad \text{(B.20)}$$

B.2 Derivation of discrete time model

The continuous time model of the reference trajectory is,

$$R(s) = \frac{1}{\tau_{\mathrm{ref}} s + 1} \tag{B.21}$$

The discrete time model (with zero order hold on input) is (Franklin et al. 1986),

$$\begin{aligned} R(z) &= (1 - z^{-1}) Z \left[\frac{R(s)}{s} \right] && \text{(B.22)} \\ &= (1 - z^{-1}) Z \left[\frac{1}{s(\tau_{\mathrm{ref}} s + 1)} \right] && \text{(B.23)} \\ &= \frac{1 - \beta}{z - \beta} && \text{(B.24)} \end{aligned}$$

where, $\beta = e^{-T_s/\tau}$

The discrete time transfer function, using shift operator notation is written,

$$[q - \beta]\, y_{\mathrm{ref}}(t) = [1 - \beta]\, y^*(t) \tag{B.25}$$

Expanding equation B.25.

$$y_{\mathrm{ref}}(t+1) = \beta\, y_{\mathrm{ref}}(t) + [1 - \beta]\, y^*(t) \tag{B.26}$$

Let $a = (1 - \beta)\, y^*$, then

$$y_{\mathrm{ref}}(t+1) = \beta\, y_{\mathrm{ref}}(t) + a \tag{B.27}$$

B.3 Derivation of j step-ahead reference

Recursive substitution of equation B.27 and simplification of the resulting equation yields the j step-ahead reference equation.

From equation B.27.

$$\begin{aligned} y_{\mathrm{ref}}(t+1) &= \beta\, y_{\mathrm{ref}}(t) + a \\ &= \beta\, y_o(t) + a && \text{(B.28)} \\ y_{\mathrm{ref}}(t+2) &= q\, y(t+1) \\ &= \beta\, y_{\mathrm{ref}}(t+1) + a \\ &= \beta\, [\beta\, y_o(t) + a] + a \\ &= \beta^2\, y_o(t) + a\, [1 + \beta] && \text{(B.29)} \\ y_{\mathrm{ref}}(t+3) &= q\, y(t+2) \end{aligned}$$

$$
\begin{aligned}
&= \beta\,[\beta^2\, y_o(t) + \beta\, a + a] + a \\
&= \beta^3\, y_o(t) + a\,[1 + \beta + \beta^2] && \text{(B.30)}\\
y_{\text{ref}}(t+4) &= q\,y(t+3) \\
&= \beta\,[\beta^3\, y_o(t) + \beta^2\, a + \beta\, a + a] + a \\
&= \beta^4\, y_o(t) + a\,[1 + \beta + \beta^2 + \beta^3] && \text{(B.31)}
\end{aligned}
$$

Note: The series $1+\beta+\beta^2+\beta^3+...+\beta^{j-1}$ is a geometric series which has a solution.

$$S_{j-1} = 1 + \beta + \beta^2 + \beta^3 + ... + \beta^{j-1} = \frac{1-\beta^j}{1-\beta} \tag{B.32}$$

Therefore, in general,

$$
\begin{aligned}
y(t+j) &= \beta^j\, y_o(t) + a\left[\frac{1-\beta^j}{1-\beta}\right] \\
&= \beta^j\, y_o(t) + (1-\beta)\, y^* \left[\frac{1-\beta^j}{1-\beta}\right] \\
&= \beta^j\, y_o(t) + (1-\beta^j)\, y^* && \text{(B.33)}
\end{aligned}
$$

B.4 Derivation of equivalent LRPC filter

The discrete time equation relating input to output is shown in Equation 7.7,

$$y(t) = \beta\, y(t-1) + a\, x(t) \tag{B.34}$$

Using shift operator notation, $y(t+1)$ can be written,

$$
\begin{aligned}
y(t+1) &= q\,y(t) \\
&= \beta\, y(t) + a\, x(t+1) && \text{(B.35)}
\end{aligned}
$$

Let $y(t) = x(t+1)$ (initial condition), then

$$
\begin{aligned}
y(t+1) &= \beta\, x(t+1) + a\, x(t+1) && \text{(B.36)}\\
y(t+2) &= q\,y(t+1) \\
&= \beta\, y(t+1) + a\, x(t+2) \\
&= \beta[\beta\, x(t+1) + a\, x(t+1)] \\
&\quad + a\, x(t+2) \\
&= \beta^2\, x(t+1) + a\,\beta\, x(t+1) \\
&\quad + a\, x(t+2) && \text{(B.37)}\\
y(t+3) &= q\,y(t+2)
\end{aligned}
$$

$$
\begin{aligned}
&= \beta\, y(t+2) + a\, x(t+3) \\
&= \beta[\beta^2 x(t+1) + a\,\beta\, x(t+1) \qquad\qquad (B.38)\\
&\quad + a\, x(t+2)] + a\, x(t+3) \\
&= \beta^3 x(t+1) + a\,\beta^2 x(t+1) \\
&\quad + a\,\beta\, x(t+2) + a\, x(t+3) \qquad\qquad (B.39)
\end{aligned}
$$

$$
\begin{aligned}
y(t+4) &= q\, y(t+3) \\
&= \beta\, y(t+3) + a\, x(t+4) \\
&= \beta^4 x(t+1) + a\,\beta^3 x(t+1) \\
&\quad + a\,\beta^2 x(t+2) + a\,\beta\, x(t+3) \\
&\quad + a\, x(t+4) \qquad\qquad (B.40)
\end{aligned}
$$

The above equations can be written in matrix form,

$$Y = [K_{14A} + a\, K_{14B}]\, X \qquad (B.41)$$

where,

$$K_{14A} = \begin{bmatrix} \beta & 0 & \dots & 0 \\ \beta^2 & 0 & \dots & 0 \\ \beta^3 & 0 & \dots & 0 \\ \beta^4 & 0 & \dots & 0 \\ \vdots & & & \\ \beta^{\mathrm{HP}} & 0 & \dots & 0 \end{bmatrix} \qquad (B.42)$$

and

$$K_{14B} = \begin{bmatrix} 1 & 0 & 0 & 0 & \dots & 0 \\ \beta & 1 & 0 & 0 & \dots & 0 \\ \beta^2 & \beta & 1 & 0 & \dots & 0 \\ \beta^3 & \beta^2 & \beta & 1 & \dots & 0 \\ \vdots & & & & & \\ \beta^{\mathrm{HP}-1} & \beta^{\mathrm{HP}-2} & \beta^{\mathrm{HP}-3} & \beta^{\mathrm{HP}-4} & \dots & 1 \end{bmatrix} \qquad (B.43)$$

Equation B.41 is reduced to,

$$Y = K_{14} X \qquad (B.44)$$

where,

$$K_{14} = K_{14A} + a\, K_{14B} \qquad (B.45)$$

B.5 Derivation of transfer function of the loop transmission

The signal flow diagram for the calculation of the transfer function of the loop transmission is presented in Figure 12.1.

$$\hat{Y}_1 = QS_1\hat{G}n_O + RS_2C_5R_{RFB}n_O \quad (B.46)$$

$$E = K_7[Gn_I - \hat{G}n_O] \quad (B.47)$$

$$Y_{ref} = K_8Gn_I + K_9y^* \quad (B.48)$$

Assuming $y^* = 0$,

$$Y_{ref} = K_8Gn_I \quad (B.49)$$

$$\begin{aligned} n_O &= T_DK_1K_{MSC}[Y_{ref} - \hat{Y}_1 - E] \quad (B.50)\\ &= T_DK_1K_{MSC}[K_8Gn_I - QS_1\hat{G}n_O \\ &\qquad -RS_2C_5R_{RFB}n_O - K_7Gn_I \\ &\qquad +K_7\hat{G}n_O] \quad (B.51)\\ &= T_DK_1K_{MSC}[K_8G - K_7G]n_I \\ &\qquad +T_DK_1K_{MSC}[K_7\hat{G} - QS_1\hat{G} \\ &\qquad -RS_2C_5R_{RFB}]n_O \end{aligned}$$

$$[1 - T_DK_1K_{MSC}[K_7\hat{G} - QS_1\hat{G} - RS_2C_5R_{RFB}]]n_O = T_DK_1K_{MSC}[K_8G - K_7G]n_I \quad (B.52)$$

$$\frac{n_O}{n_I} = \frac{T_DK_1K_{MSC}[K_8G - K_7G]}{1 - T_DK_1K_{MSC}[K_7\hat{G} - QS_1\hat{G} - RS_2C_5R_{RFB}]} \quad (B.53)$$

Now,

$$L(z) = -\frac{n_O}{n_I} \quad (B.54)$$

therefore,

$$L(z) = \frac{T_DK_1K_{MSC}[K_7 - K_8]G}{1 - T_DK_1K_{MSC}[K_7\hat{G} - QS_1\hat{G} - RS_2C_5R_{RFB}]} \quad (B.55)$$

B.6 Derivation of the closed loop transfer function

The signal flow diagram for the calculation of the closed loop transfer function is presented in Figure 12.2.

$$\hat{Y}_1 = QS_1\hat{G}u + RS_2C_5R_{RFB}u \quad (B.56)$$

$$E = K_7[Gu - \hat{G}u] \quad (B.57)$$

$$Y_{\text{ref}} = K_8 G u + K_9 y^* \tag{B.58}$$

$$\begin{aligned}
u &= T_D K_1 K_{\text{MSC}}[Y_{\text{ref}} - \hat{Y}_1 - E] \qquad \text{(B.59)}\\
&= T_D K_1 K_{\text{MSC}}[K_8 G u + K_9 y^* - Q S_1 \hat{G} u \\
&\qquad - R S_2 C_5 R_{\text{RFB}} u - K_7 G u + K_7 \hat{G} u] \\
&= T_D K_1 K_{\text{MSC}}[K_8 G - Q S_1 \hat{G} - R S_2 C_5 R_{\text{RFB}} \\
&\qquad - K_7 G + K_7 \hat{G}] u + T_D K_1 K_{\text{MSC}} K_9 y^*
\end{aligned}$$

$$[1 - T_D K_1 K_{\text{MSC}}[K_8 G - Q S_1 \hat{G} - R S_2 C_5 R_{\text{RFB}} - K_7 G + K_7 \hat{G}]] u = T_D K_1 K_{\text{MSC}} K_9 y^* \tag{B.60}$$

$$\begin{aligned}
\frac{u}{y^*} &= \frac{T_D K_1 K_{\text{MSC}} K_9}{1 - T_D K_1 K_{\text{MSC}}[K_8 G - Q S_1 \hat{G} - R S_2 C_5 R_{\text{RFB}} - K_7 G + K_7 \hat{G}]} \\
&= \frac{T_D K_1 K_{\text{MSC}} K_9}{1 - T_D K_1 K_{\text{MSC}}[(K_8 - K_7) G + (K_7 - Q S_1) \hat{G} - R S_2 C_5 R_{\text{RFB}}]}
\end{aligned}$$

Now

$$T(z) = \frac{y(z)}{y^*(z)} = G(z) \frac{u(z)}{y^*(z)} \tag{B.61}$$

therefore,

$$T(z) = \frac{G T_D K_1 K_{\text{MSC}} K_9}{1 - T_D K_1 K_{\text{MSC}}[(K_8 - K_7) G + (K_7 - Q S_1) \hat{G} - R S_2 C_5 R_{\text{RFB}}]} \tag{B.62}$$

B.7 Results of final design iteration

The frequency points selected for the MSC Robust Control design are shown in the vector of Equation B.63. The graphs of the final design iteration are shown in Table 13.1.

$$\begin{aligned}
w = [&0.0109\ \ 0.0208\ \ 0.0236\ \ 0.0314\ \ 0.0338\ \ 0.0397 \\
&0.0442\ \ 0.0557\ \ 0.0567\ \ 0.0632\ \ 0.064[illegible]\ \ 0.0756 \\
&0.1439\ \ 0.3162\ \ 0.4136\ \ 0.4523\ \ 0.4947\ \ 0.5127 \\
&0.5410\ \ 0.5708\ \ 0.6023\ \ 0.6242\ \ 0.6826\ \ 0.6950 \\
&0.7465\ \ 0.8019\ \ 0.8312\ \ 0.9090\ \ 0.9941\ \ 1.0678 \\
&1.0971\ \ 1.1168\ \ 1.1267\ \ 1.1329\ \ 1.1471\ \ 1.1533 \\
&1.3021\ \ 1.4736\ \ 2.3051\ \ 2.3891\ \ 3.4790\ \ 5.2506 \\
&5.9513]
\end{aligned} \tag{B.63}$$

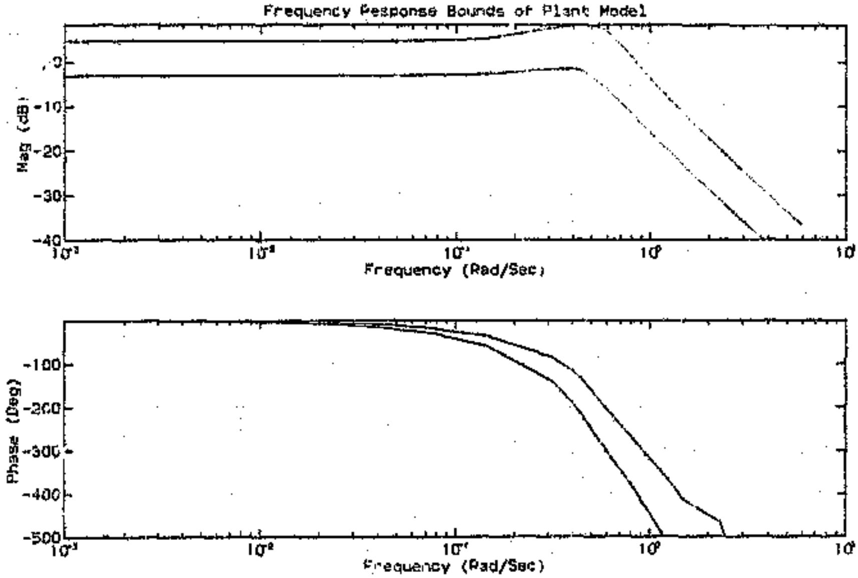

Figure B.1: Frequency Response Plot of Plant Model Bounds

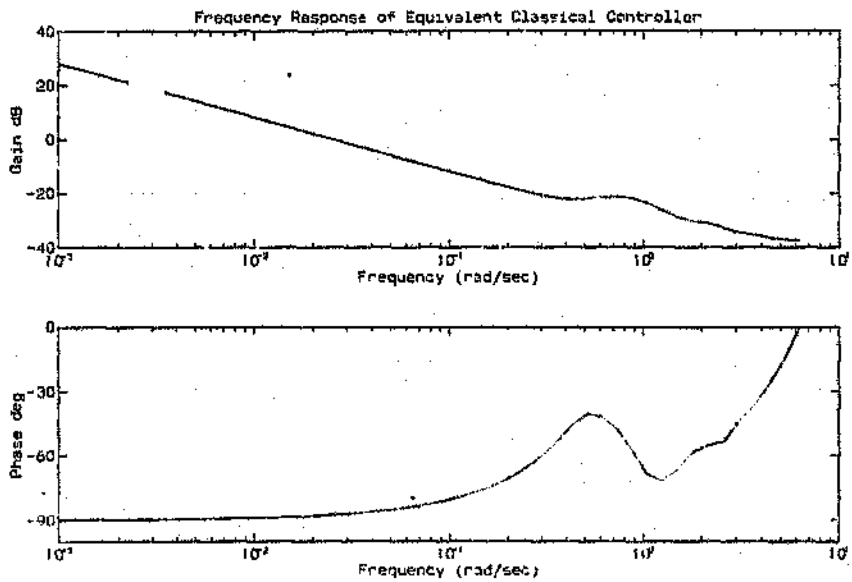

Figure B.2: Frequency Response of Equivalent Classical Controller

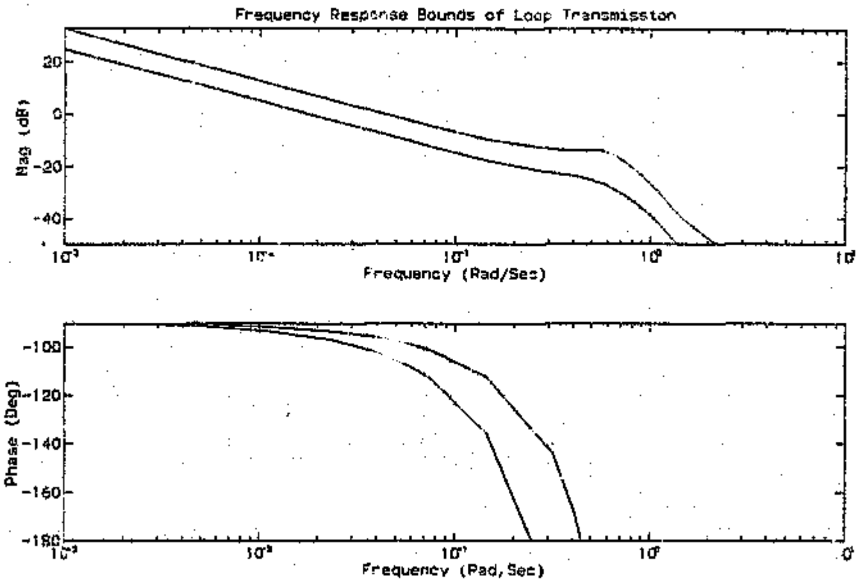

Figure B.3: Frequency Response of Loop Transmission

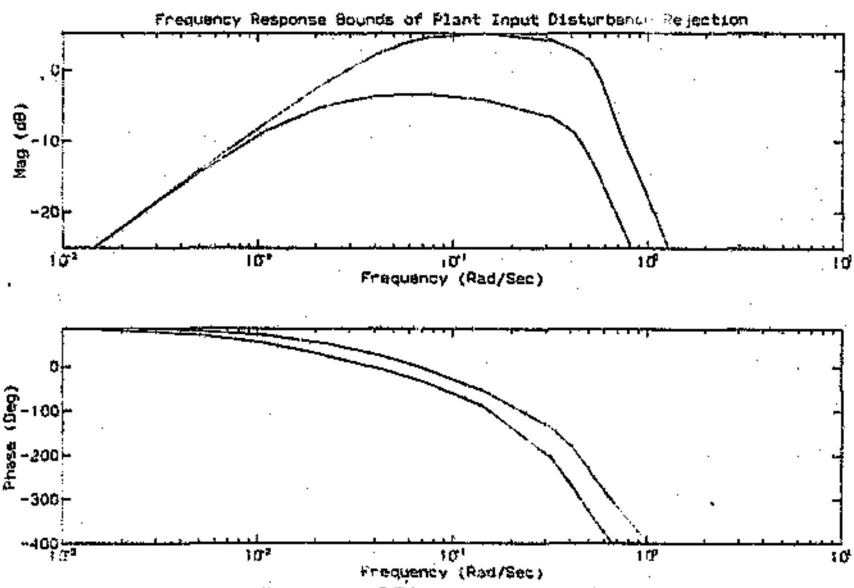

Figure B.4: Frequency Response of Plant Input Disturbance Rejection

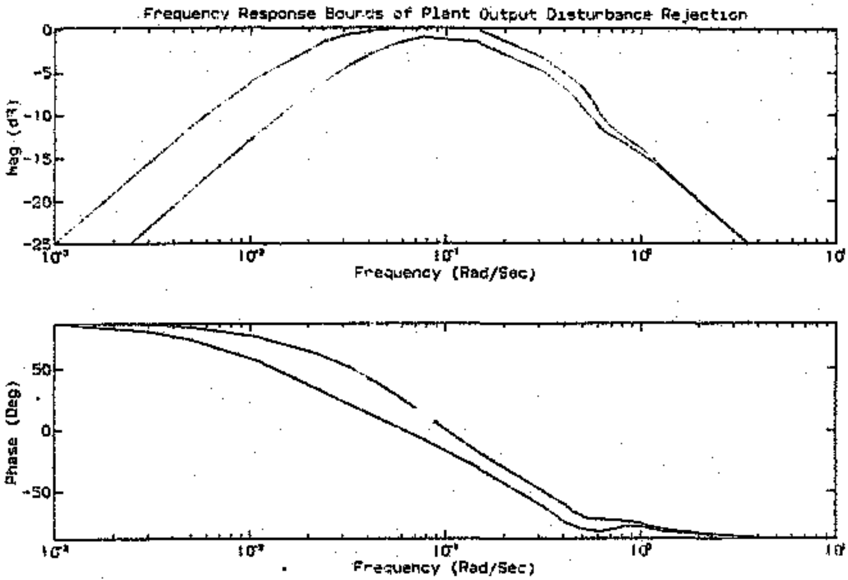

Figure B.5: Frequency Response of Plant Output Disturbance Rejection

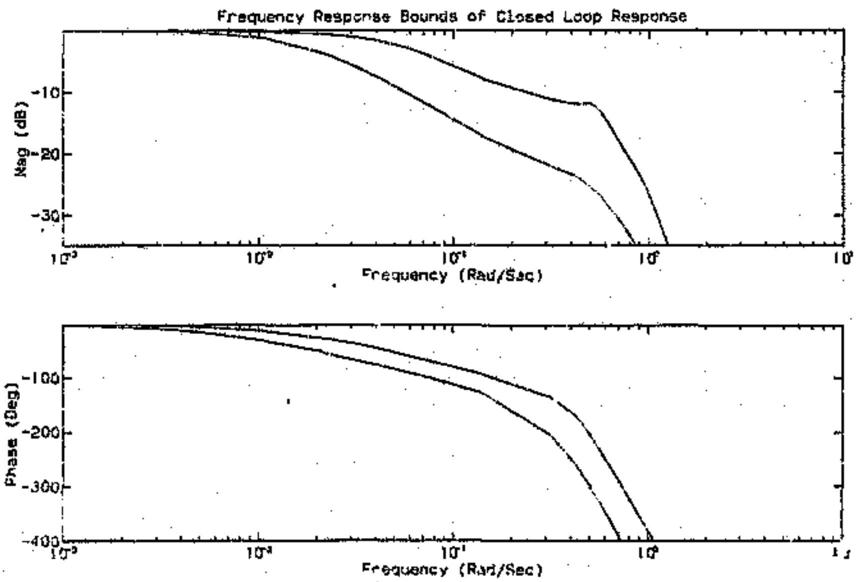

Figure B.6: Frequency Response of Closed Loop Bounds

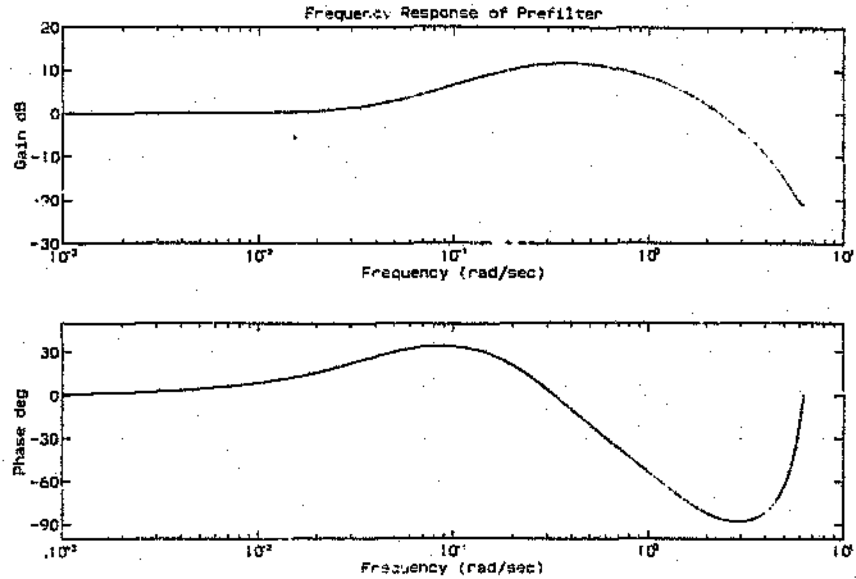

Figure B.7: Frequency Response of Prefilter

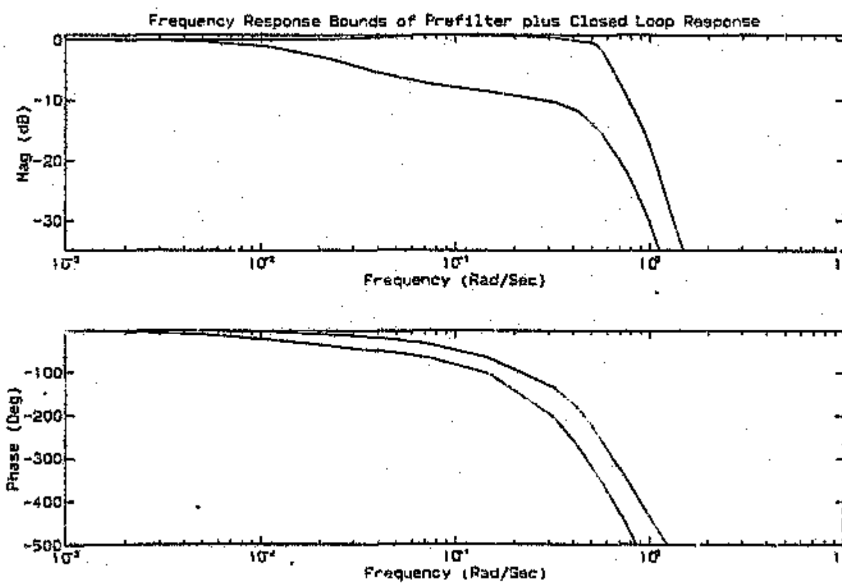

Figure B.8: Frequency Response of Prefilter plus Closed Loop

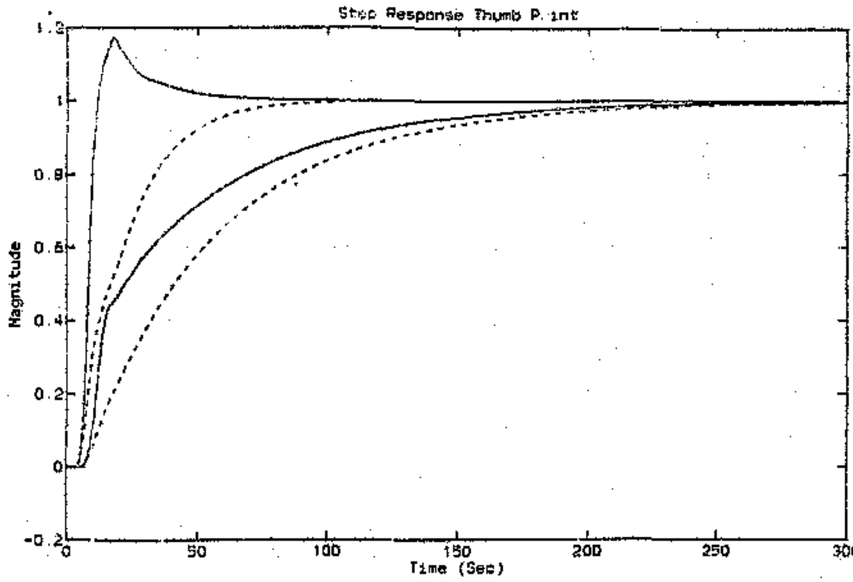

Figure B.9: Plant output thumb print caused by a unit step change in the set-point

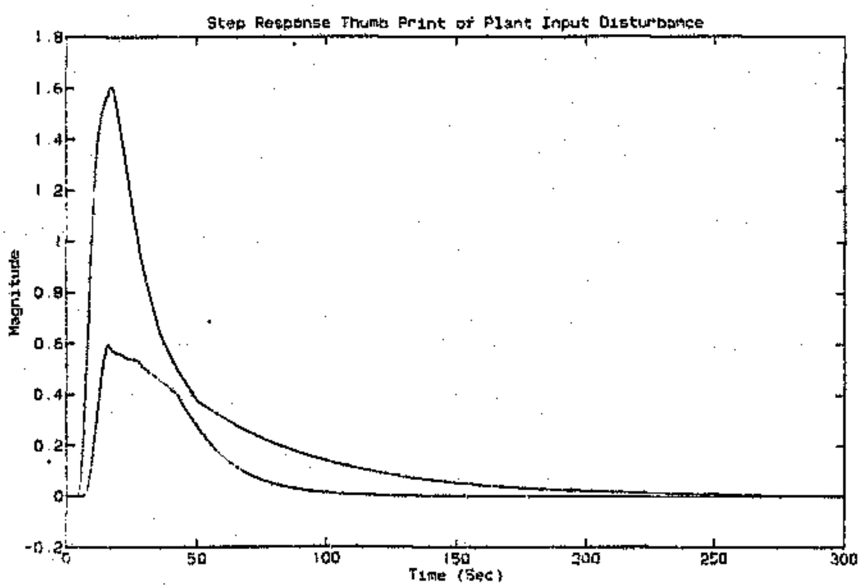

Figure B.10: Plant output thumb print caused by a unit step change in the plant input disturbance (d_1)

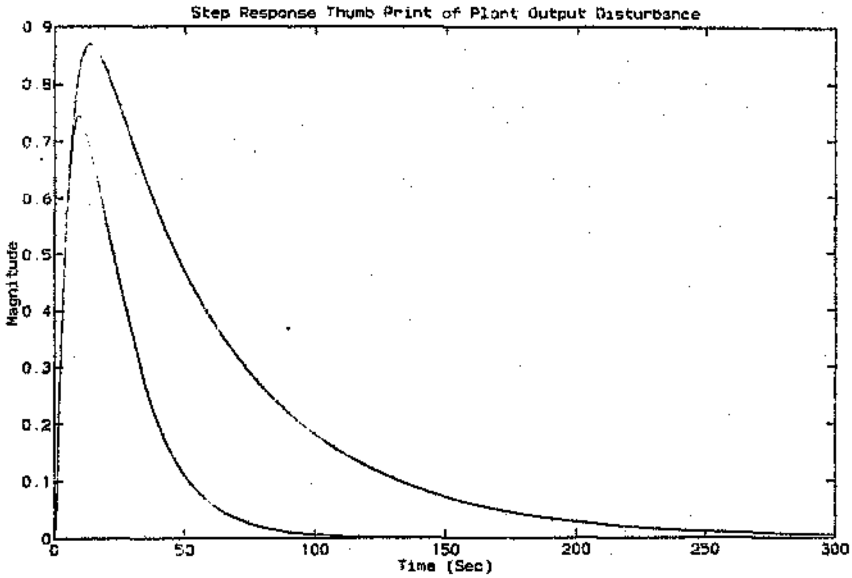

Figure B.11: Plant output thumb print caused by a unit step change in the plant output disturbance (d_2)

B.8 Using the DC-gain of the predictor model to tune the MSC controller

A simplified signal flow diagram of a feedback system using an MSC controller (ignoring the reference trajectory mechanism) is shown in Figure B.12. Q_{MSC} is the equivalent MSC filter, G is the real plant model and $\hat{G}$ is the predictor model. The

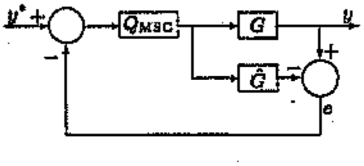

Figure B.12: Signal flow diagram of simplified MSC feedback system

transfer function of the equivalent classical controller is,

$$C = \frac{Q_{MSC}}{1 - Q_{MSC}\hat{G}} \tag{B.64}$$

One of the properties of the MSC algorithm is integral action. Therefore, at DC the gain of the equivalent classical controller is infinite. Therefore,

$$1 - Q_{MSC}\hat{G} = 0 \tag{B.65}$$

It can be seen from Equation B.65 that if the DC gain of the predictor model ($\hat{G}$) is decreased, then the gain of the MSC filter Q_{MSC} must increase, causing the bandwidth of the MSC controller to increase.

Appendix C

Model Identification of Feedback Instrument's PT326 Process Trainer

C.1 Physical plant model

This section identifies the dominant dynamics of Feedback Instrument's PT326 process trainer. This is done by analysing the physics of the plant.

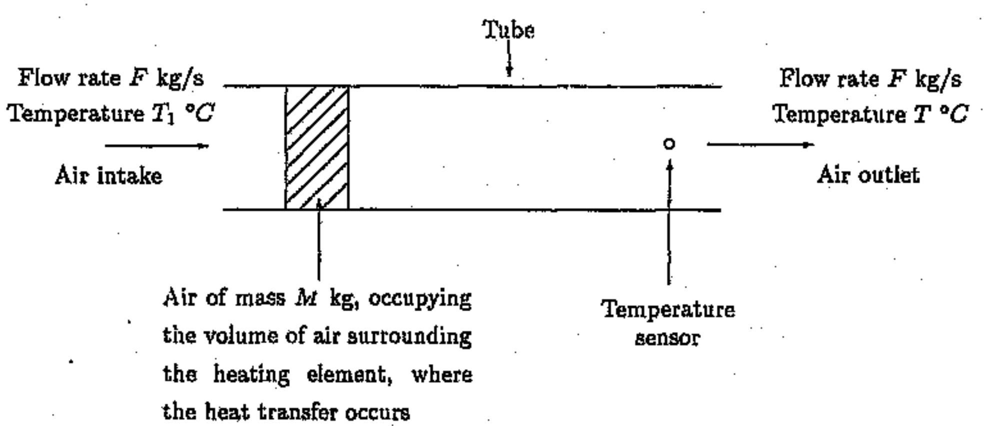

Figure C.1: Model of energy balance

Assume that heat transfer takes place in a fixed volume in the immediate vicinity of the heater element which contains mass M of air. Air enters this volume at a mass flow rate F kg/s and temperature T_1 and leaves with a flow rate F and temperature T, which is the same as the temperature throughout the volume if it is well mixed. The specific heat capacity of the air is c.

Assume that the plant is operating steadily at an initial equilibrium point. If we take all variables to represent increments about this equilibrium point, the law of conservation of energy (which states that the energy accumulated in time interval Δt is equal to the inflow of energy minus the outflow of energy) gives

$$Mc\Delta T = (FcT_1 + Q - FcT)\Delta t \qquad \text{(C.1)}$$

where Q is heater power in Watts. In the limit as $\Delta t \to 0$, this gives

$$\frac{M}{F}\frac{dT}{dt} + T = T_1 + \frac{Q}{Fc} \qquad \text{(C.2)}$$

The corresponding transfer function from Q to T is

$$\frac{T(s)}{Q(s)} = \frac{1}{Fc(\tau s + 1)} \qquad \text{(C.3)}$$

The time domain solution for a step input is therefore a first-order response with time constant $\tau = M/F$.

After leaving the heater, the air experiences a *pure delay* of t_d seconds before it arrives at the sensor.

The resulting transfer function of the plant is of the form,

$$\frac{Y(s)}{U(s)} = \frac{Ke^{-t_d s}}{\tau s + 1} \qquad \text{(C.4)}$$

where K is the steady state gain of the plant.

C.2 Results of step response modelling of PT326 (Model1)

Based on the analysis presented in Section C.1, a suitable transfer function of the plant is,

$$\hat{G}(s) = \frac{Ke^{-t_d s}}{\tau s + 1} \qquad \text{(C.5)}$$

The model identification results are presnted in Table C.1.

C.3 Results of step response modelling of PT326 (Model2)

The model identified in Section C.2 is based on the dominant dynamics of the plant. It is proposed that a second order section be added to this model to account for the high frequency dynamics of the plant. Compare the responses in Figures 15.4 and 15.5.

Table C.1: Results of model identification (Model1)

Throttle blower angle	Input step size (volts)	K	t_d	τ
10°	6	1.8157	0.4414	0.5551
	5	1.7624	0.4030	0.6034
	3	1.8242	0.4655	0.6495
	3	1.8060	0.4748	[illegible]
20°	8	1.4767	0.3497	0.5153
	8	1.4757	0.3451	0.5613
	6	1.5789	0.3600	0.5291
	3	1.5679	0.3698	0.5785
30°	8	1.3169	0.3039	0.4974
	8	1.3174	0.3100	0.4807
	6	1.3820	0.3101	0.5076
	6	1.3842	0.3079	0.5104
	3	1.3476	0.3611	0.4596
	[illegible]	1.3756	0.3494	0.5028
40°	[illegible]	1.1763	0.2677	0.5102
	8	1.1658	0.2797	0.4651
	10	1.0396	0.2806	0.4670
	3	1.1869	0.2848	0.4559
50°	8	1.0408	0.2452	0.4671
	10	0.9190	0.2427	0.4693
60°	8	0.9248	0.2301	0.4550
	10	0.8373	0.2230	0.4630
80°	10	0.7124	0.1872	0.4524
	10	0.6979	0.1974	0.4487
100°	10	0.6082	0.1837	0.4090
120°	10	0.5569	0.2101	0.3626
140°	10	0.5218	0.1564	0.4107
160°	10	0.4711	0.2003	0.3144

The proposed dynamic model of the plant is defined in Equation C.6

$$\hat{G}(s) = \left(\frac{K}{\tau s + 1}\right)\left(\frac{\omega_n^2}{s^2 + 2\zeta\omega_n + \omega_n^2}\right) e^{-t_d s} \tag{C.6}$$

The model identification results are presnted in Table C.2.

Table C.2: Results of model identification (Model2)

Throttle blower angle	Input step size (volts)	K	t_d	ζ	ω_n	τ
10°	6	1.8014	0.3000	1.0580	3.2128	0.2500
	5	1.7616	0.2998	1.2379	3.4943	0.2504
20°	8	1.4761	0.2469	1.1616	3.8961	0.2507
	8	1.4812	0.2458	1.2537	3.8507	0.2500
	6	1.5876	0.2456	1.2437	3.9096	0.2617
	3	1.5685	0.2463	1.2998	3.7871	0.2500
30°	8	1.3207	0.1853	1.1587	3.9072	0.2557
	8	1.3169	0.1854	1.1458	3.9098	0.2533
	6	1.3806	0.1861	1.1855	3.8753	0.2500
	6	1.3319	0.1868	1.1711	3.8329	0.2894
	3	1.3506	0.1781	1.0757	3.3292	0.2517
40°	8	1.1758	0.1658	1.1967	4.0853	0.2578
	8	1.1664	0.1655	1.1591	4.1151	0.2500
	10	1.0400	0.1656	1.1457	4.0682	0.2847
	3	1.1884	0.1668	1.1513	4.1069	0.2500
50°	8	1.0300	0.1482	1.1662	4.3115	0.2521
	10	0.9047	0.1486	1.1243	4.2754	0.2573
60°	8	0.9145	0.1257	1.1167	4.2842	0.2586
	10	0.8356	0.1257	1.1497	4.2818	0.2620
80°	10	0.7103	0.1050	1.1128	4.4053	0.2586
	10	0.6996	0.1100	1.1527	4.5100	0.2553
100°	10	0.6009	0.1045	1.1673	4.9727	0.2500
120°	10	0.5456	0.1037	1.1155	5.1812	0.2500
140°	10	0.5069	0.0999	1.1659	5.48[illegible]	0.2606
160°	10	0.4707	0.0897	1.1257	5.4806	0.2545

Appendix D

PID controller design equations

This chapter presents a procedure for tuning a PID controller for the control of Feedback Instrument's PT326 industrial plant trainer.

The procedure for designing the PID controller is summarised as follows.

- Assume a specific plant model.

$$\tilde{G}(s) = \frac{Ke^{-t_d s}}{\tau s + 1} \tag{D.1}$$

- Design an IMC controller based on an approximation of the plant model defined in Equation D.1 (1st order Pade approximation) and a closed loop response filter defined in Equation D.2.

$$F(s) = \frac{1}{(\beta s + 1)^2} \tag{D.2}$$

- Calculate the transfer function of the IMC's equivalent classical controller and compare it with the transfer function of the PID controller.

- Calculate equations for tuning the PID controller based on the plant model and the response filter's tuning factor, β.

D.1 Derivation of design calculations

The approximation of the plant model define in Equation D.1 using a first order Pade approximation results in the transfer function,

$$\tilde{G}(s) = \left[\frac{K}{\tau s + 1}\right]\left[\frac{-\frac{t_d}{2}s + 1}{\frac{t_d}{2}s + 1}\right] \tag{D.3}$$

The IMC filter Q(s) is defined as,

$$Q(s) = F(s)\hat{G}^{-1}(s) \tag{D.4}$$

where

$$F(s) = \frac{1}{(\beta s + 1)^2} \tag{D.5}$$

and

$$\hat{G}^{-1}(s) = \frac{(\tau s + 1)(\frac{t_d}{2}s + 1)}{K(-\frac{t_d}{2}s + 1)} \tag{D.6}$$

The IMC filter, Q(s), can only be implemented with stable poles. Therefore the inverse plant model must be modified by removing all unstable poles. The approximate inverse plant model is therefore,

$$\hat{G}^{-1}(s) = \frac{(\tau s + 1)(\frac{t_d}{2}s + 1)}{K} \tag{D.7}$$

The IMC filter is therefore,

$$\begin{aligned} Q(s) &= \frac{(\tau s + 1)(\frac{t_d}{2}s + 1)}{K(\beta s + 1)^2} && \text{(D.8)} \\ &= \frac{1}{K}\left[\frac{(\tau s + 1)(\frac{t_d}{2}s + 1)}{(\beta s + 1)^2}\right] && \text{(D.9)} \end{aligned}$$

The equivalent classical controller is calculated from the identity,

$$\begin{aligned} C(s) &= \frac{Q(s)}{1 - Q(s)\hat{G}(s)} && \text{(D.10)} \\ &= \frac{1}{K}\left[\frac{\frac{\tau t_d}{2}s^2 + (\tau + \frac{t_d}{2})s + 1}{\beta^2 s^2 + (2\beta + \frac{t_d}{2})s}\right] && \text{(D.11)} \\ &= \frac{\frac{1}{K}}{2\beta + \frac{t_d}{2}}\left[\frac{\frac{\tau t_d}{2}s^2 + (\tau + \frac{t_d}{2})s + 1}{\left(\frac{\beta^2}{2\beta + \frac{t_d}{2}}\right)s^2 + s}\right] && \text{(D.12)} \end{aligned}$$

The transfer function for the PID controller is,

$$\begin{aligned} \frac{U(s)}{E(s)} &= K_c\left(1 + \frac{1}{T_i s} + T_D s\right)\frac{1}{T_f s + 1} && \text{(D.13)} \\ &= \frac{K_c}{T_i}\left[\frac{T_i T_D s^2 + T_i s + 1}{s(T_f s + 1)}\right] && \text{(D.14)} \end{aligned}$$

Equation Equations D.12 and D.14 and solving for the PID parameters results in the following design equations,

$$K_c = \frac{\tau + \frac{t_d}{2}}{K(2\beta + \frac{t_d}{2})} \tag{D.15}$$

$$T_i = \tau + \frac{t_d}{2} \tag{D.16}$$

$$T_D = \frac{\tau t_d}{2\tau + t_d} \tag{D.17}$$

$$T_f = \frac{\beta^2}{2\beta + \frac{t_d}{2}} \tag{D.18}$$

Appendix E

Robust PID, IMC and MSC controller design

This appendix presents designs for PID, IMC and MSC controllers, for implementation on Feedback Instrument's PT326 process unit. The PT326 process dynamics are changed by varying the throttle angle blower between 20° and 50°. The controllers must provide stable, robust control.

E.1 Process dynamics

The PT326's dynamics can be described using the Laplace transform model,

$$\hat{G}(s) = \left(\frac{K}{\tau s+1}\right)\left(\frac{\omega_n^2}{s^2+2\zeta\omega_n+\omega_n^2}\right)e^{-t_d s} \tag{E.1}$$

Refer to Chapter 15.4 for details.

The results of step response modelling tests, presented in Appendix C.3, are used to select sets of plant model parameter (Table E.1) which adaquetly describe the process dynamics when the throttle angle blower is varied between 20° and 50°. Using these model parameters a step response plot is generated in Figure E.1.

E.2 Design specifications

The feedback controller is expected to provide stable, robust control that removes offset disturbances that appear at the plant output.

Appendix E

Robust PID, IMC and MSC controller design

This appendix presents designs for PID, IMC and MSC controllers, for implementation on Feedback Instrument's PT326 process unit. The PT326 process dynamics are changed by varying the throttle angle blower between 20° and 50°. The controllers must provide stable, robust control.

E.1 Process dynamics

The PT326's dynamics can be described using the Laplace transform model,

$$\hat{G}(s) = \left(\frac{K}{\tau s + 1}\right)\left(\frac{\omega_n^2}{s^2 + 2\zeta\omega_n + \omega_n^2}\right)e^{-t_d s} \tag{E.1}$$

Refer to Chapter 15.4 for details.

The results of step response modelling tests, presented in Appendix C.3, are used to select sets of plant model parameter (Table E.1) which adaquetly describe the process dynamics when the throttle angle blower is varied between 20° and 50°. Using these model parameters a step response plot is generated in Figure E.1.

E.2 Design specifications

The feedback controller is expected to provide stable, robust control that removes offset disturbances that appear at the plant output.

Table E.1: Selected plant model parameters

Angle	K	t_d	ζ	ω_n	τ
20°	1.4812	0.2458	1.2537	3.8507	0.2500
30°	1.3819	0.1868	1.1711	3.8329	0.2894
40°	1.1664	0.1655	1.1591	4.1151	0.2500
50°	1.0300	0.1482	1.1662	4.3115	0.2521

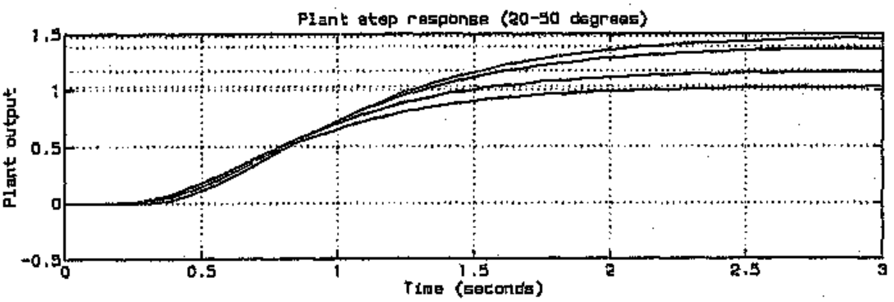

Figure E.1: Step response model of plant

Design Constraints

The following constraints are placed on the design.

- Due to noise constraints the controller's bandwidth should not exceed 0.8 Rad/Sec.
- The PT326's throttle blower angle varies between 20° and 50°. The controller must provide robust control over the specified operating range of the process, with not more than 10 % overshoot when responding to a set-point step change.
- Process input constraints.

$$0 \leq u \leq 1 \tag{E.2}$$

E.3 PID control

A procedure for designing a PID controller is presented in Appendix D. This method relies on the following dynamic model of the process,

$$\hat{G}(s) = \frac{K}{\tau s+1} e^{-t_d s} \tag{E.3}$$

$$K = 1.3540 \tag{E.4}$$

$$t_d = 0.3237 \tag{E.5}$$

$$\tau = 0.4931 \tag{E.6}$$

which is a low order dynamic model of the PT326 with the throttle blower angle set to 30°. Refer to Appendix C.2 for details of the step response modelling test.

A suitable PID controller is obtained using the method in Appendix D. By settings

$$\beta = 0.8 \tag{E.7}$$

and using the model presented in Equation E.3 a suitable PID controller is obtained which has transfer function,

$$\frac{U(s)}{E(s)} = K_c\left(1 + \frac{1}{T_i s} + T_D s\right)\frac{1}{T_f s + 1} \tag{E.8}$$

and tuning parameters,

$K_c = 0.275$	$T_i = 0.655$	$T_D = 0.1222$	$T_f = 0.363$

The Bode plot of the PID controller is shown in Figure E.2. The frequency response of the loop transmission is calculated using the proposed plant model parameters presented in Table E.1. The Bode plot of the loop transmission is shown in Figure E.3 and the Bode plot of the closed loop frequency response is shown in Figure E.4.

The step response thumb print is presented in Figure E.5.

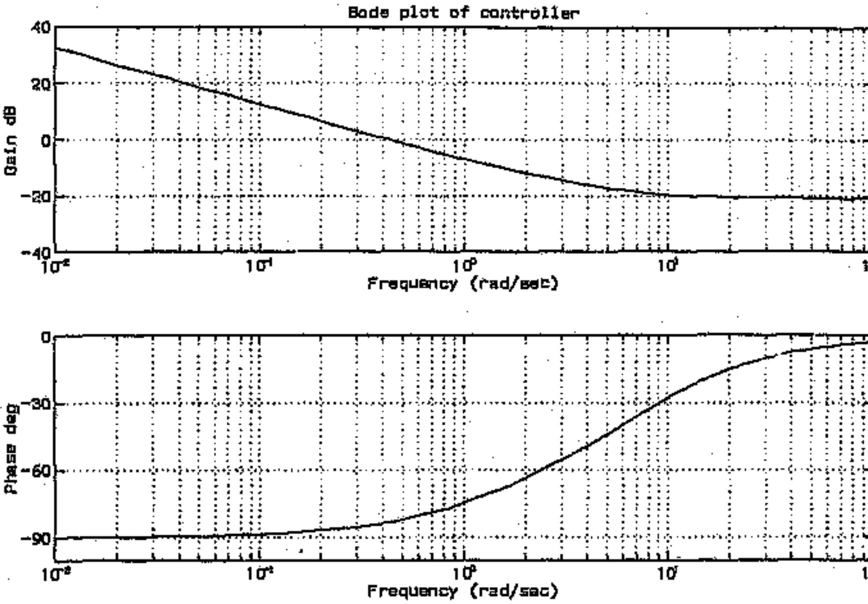

Figure E.2: Bode plot of controller (PID)

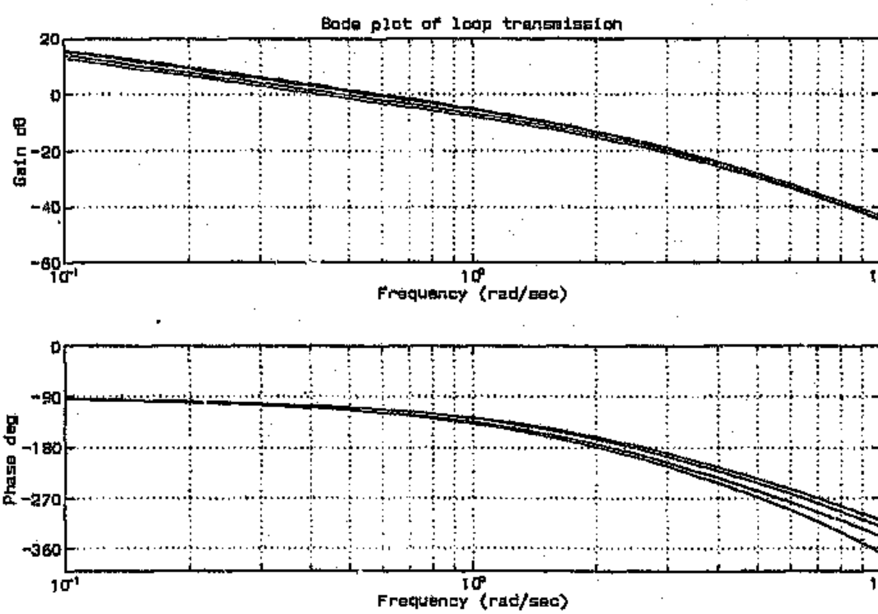

Figure E.3: Bode plot of Loop Transmission (PID)

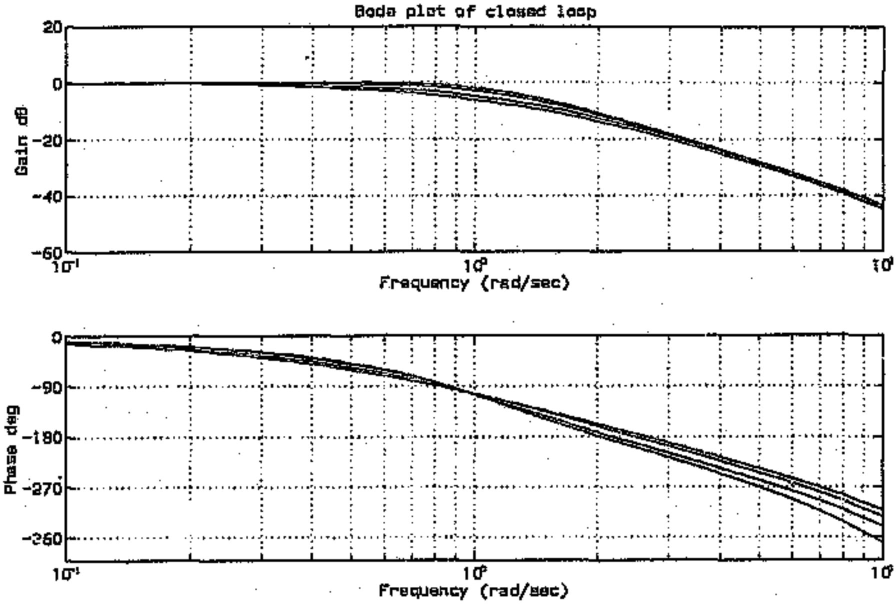

Figure E.4: Bode plot of Closed Loop transfer function (PID)

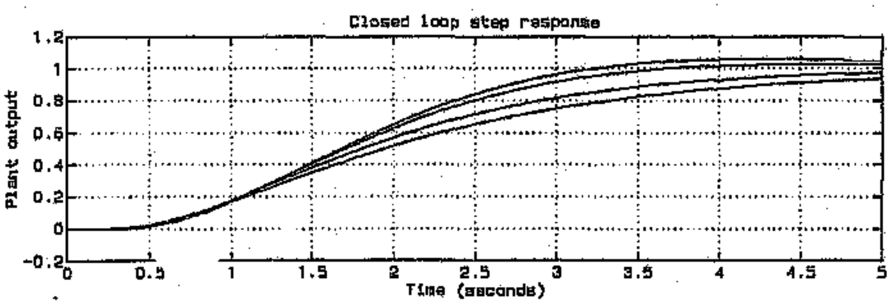

Figure E.5: Closed loop step response (PID)

E.4 IMC control

A suitable IMC controller is design using the closed loop response filter,

$$F(s) = \frac{1}{(\beta s + 1)^n} \tag{E.9}$$

and plant model,

$$G(s) = \left(\frac{K}{\tau s + 1}\right)\left(\frac{\omega_n^2}{s^2 + 2\zeta\omega_n + \omega_n^2}\right)e^{-t_d * s} \tag{E.10}$$

" ne basic IMC configuration is shown in Figure E.4

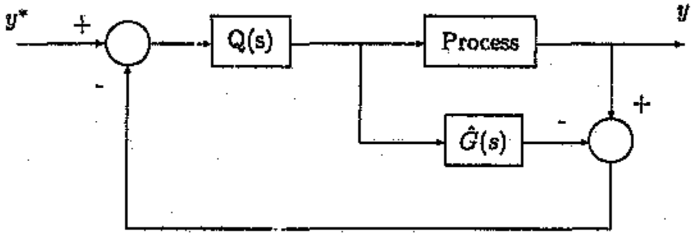

Figu E.6: Basic IMC configuration

An estimated plant model ($\hat{G}(s)$) is selected based on the plant model defined in Equation E.10. The transport delay is approximated with a third order Pade approximation, where the r'th order Pade approximation is defined as,

$$D_r(s) = \left[\frac{1 - s\frac{t_d}{2r}}{1 + s\frac{t_d}{2r}}\right]^r \tag{E.11}$$

The estimate plant model $\hat{G}(s)$ is now defined as,

$$\hat{G}(s) = \left(\frac{K}{\tau s + 1}\right)\left(\frac{\omega_n^2}{s^2 + 2\zeta\omega_n + \omega_n^2}\right)\left(\frac{1 - s\frac{t_d}{6}}{1 + s\frac{t_d}{6}}\right)^3 \tag{E.12}$$

The specification of the IMC filter (Q(s)) is defined using the equation,

$$Q(s) = F(s)(\hat{G}')^{-1}(s) \tag{E.13}$$

where F(s) is the closed loop response filter (Equation E.9) and $\hat{G}'$ is a model of the plant with the non-minimum phase zeros removed. $\hat{G}'$ is defined as,

$$\hat{G}'(s) = \left(\frac{K}{\tau s + 1}\right)\left(\frac{\omega_n^2}{s^2 + 2\zeta\omega_n + \omega_n^2}\right)\frac{1}{(1 + s\frac{t_d}{6})^3} \tag{E.14}$$

Using Equation E.13 the IMC filter is now defined as,

$$Q(s) = \frac{1}{(\beta s+1)^n}\left[\frac{(\tau s+1)(s^2+2\zeta\omega_n s+\omega_n^2)(\frac{td}{6}s+1)^3}{K\omega_n^2}\right] \tag{E.15}$$

A suitable IMC controller is designed by setting,

$$\beta = 0.25 \tag{E.16}$$

and

$$n = 6 \tag{E.17}$$

The Bode plots of the controller, the loop transmission and closed loop transfer function are shown in Figures E.7, E.8 and E.9. The step response thumb print of the controller is presented in Figure E.10.

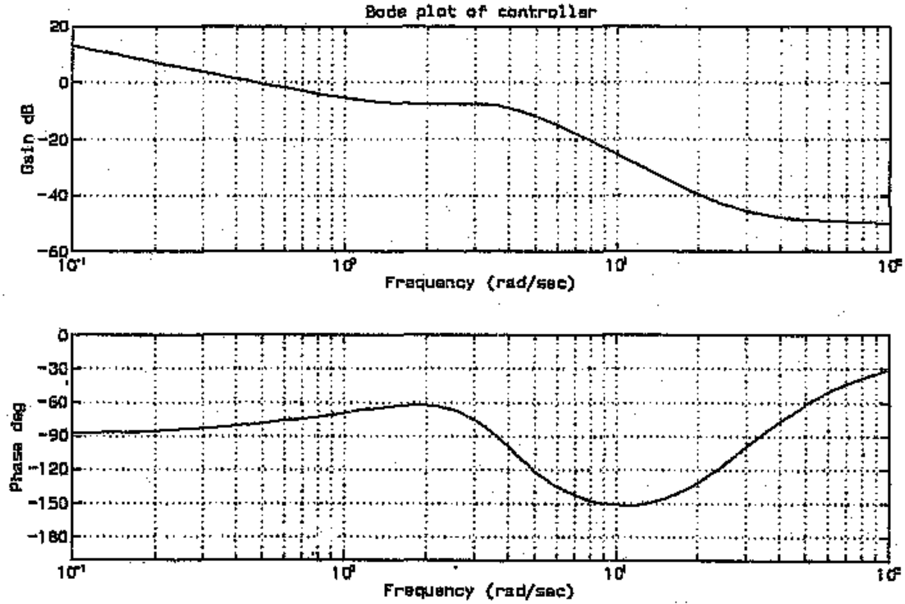

Figure E.7: Bode plot of controller (IMC)

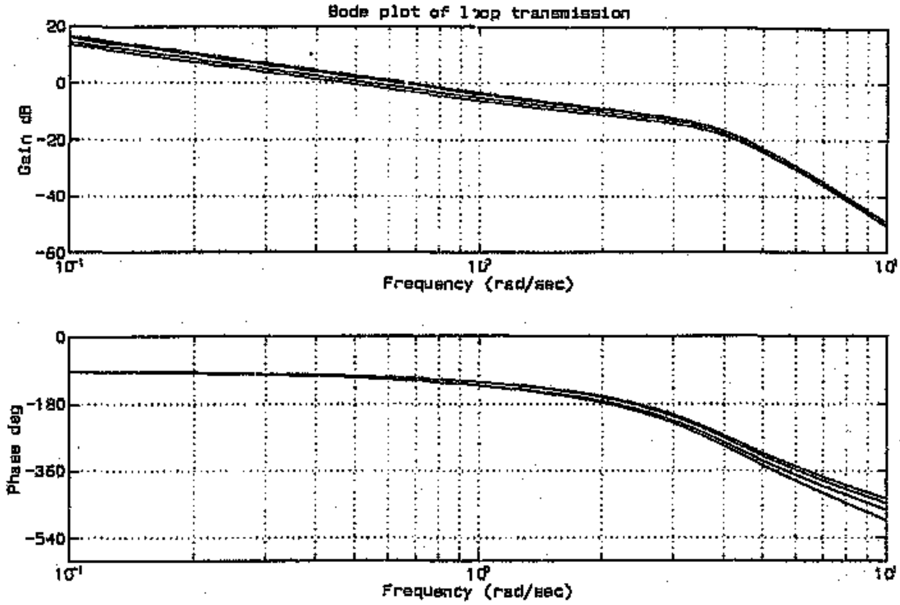

Figure E.8: Bode plot of Loop Transmission (IMC)

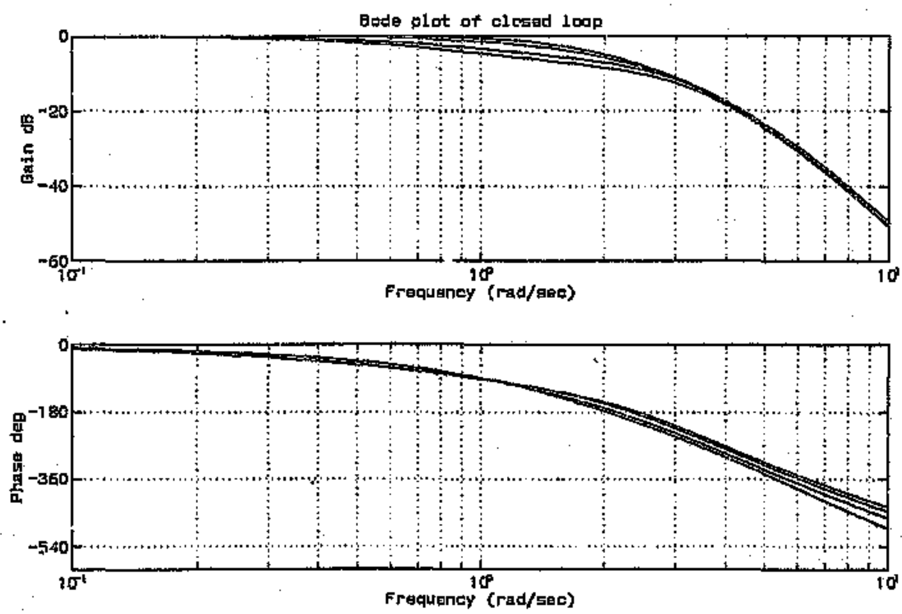

Figure E.9: Bode plot of Closed Loop transfer function (IMC)

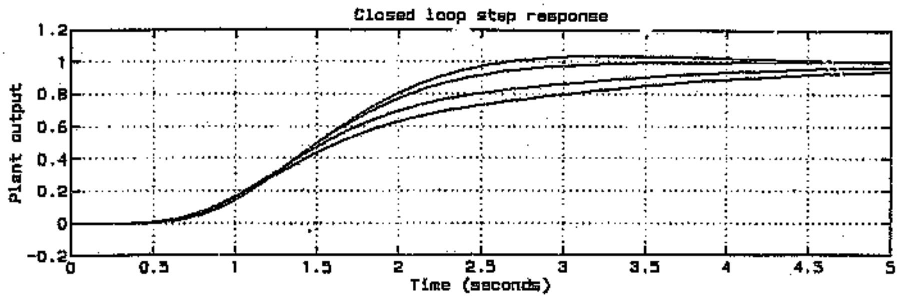

Figure E.10: Closed loop step response (IMC)

E.5 MSC control

A procedure for designing an MSC controller is outlined in Section 17.1.

A suitable MSC controller which meets the design specifications defined in Section E.2 has the controller settings defined in Table E.5

The Bode plots of the controller, the loop transmission and closed loop transfer function are shown in Figures E.11, E.12 and E.13. The step response thumb print of the controller is presented in Figure E.14.

Table E.2: MSC controller settings

Predictor Model	$\hat{G}(s) = \frac{19.2e^{-0.1843s}}{0.2601s^3+3.251s^2+12.36s+14.22}$
Sampling period	$T_{sp} = 0.05$ Sec
Prediction Horizon	HP = 40
Control Horizon	CP = 10
Tuning parameters	$\lambda = 1$
	$\beta = 10$
Reference traj. time constant	$\tau_{ref} = 0.0$[illegible]
Process input constraints	$u_{min} = 0$
	$u_{max} = 1$
	$\Delta u_{min} = -100$
	$\Delta u_{max} = 100$

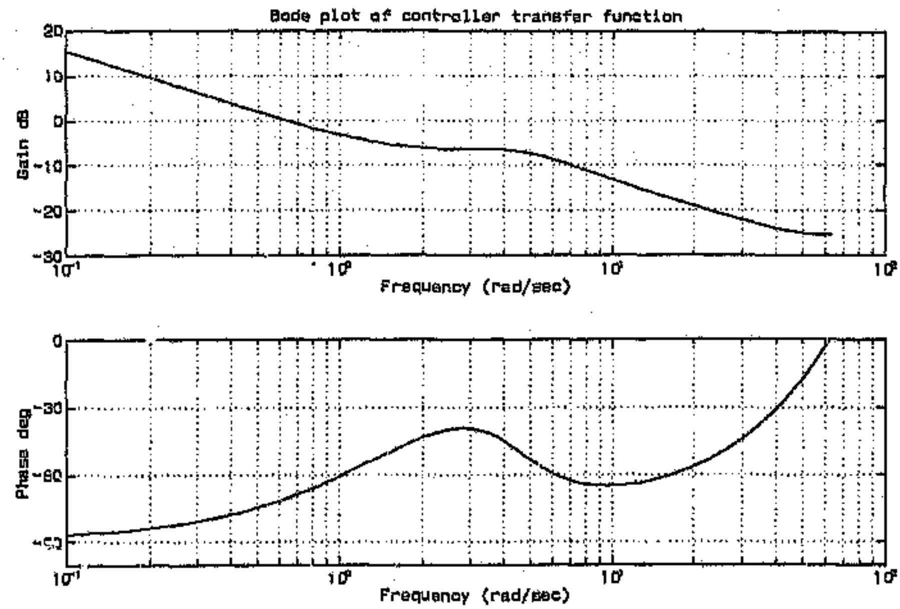

Figure E.11: Bode plot of controller (MSC)

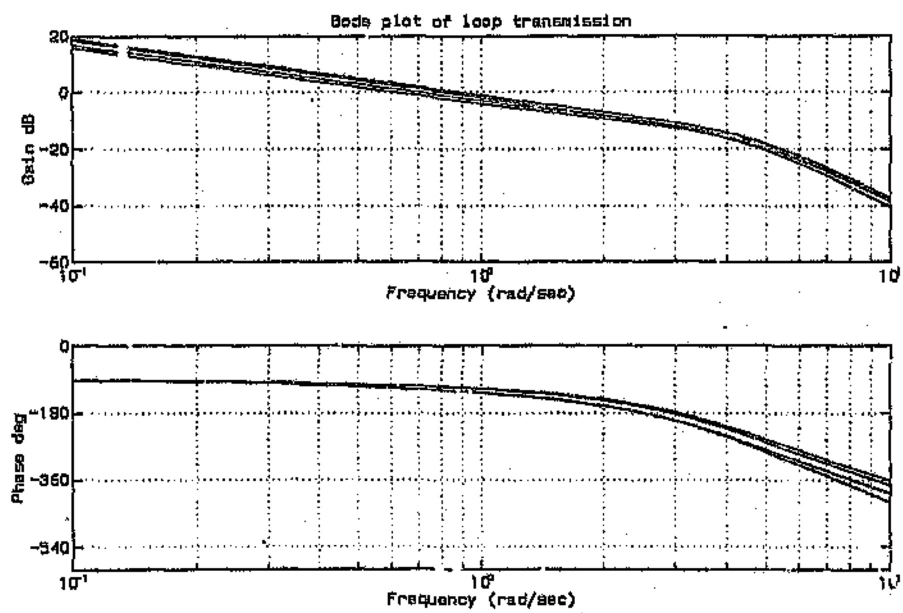

Figure E.12: Bode plot of Loop Transmission (MSC)

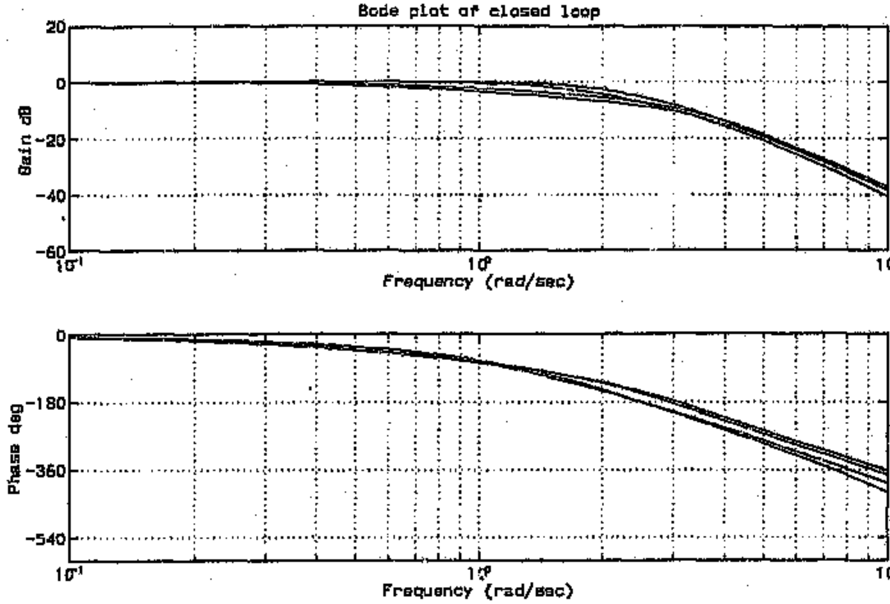

Figure E.13: Bode plot of Closed Loop transfer function (MSC)

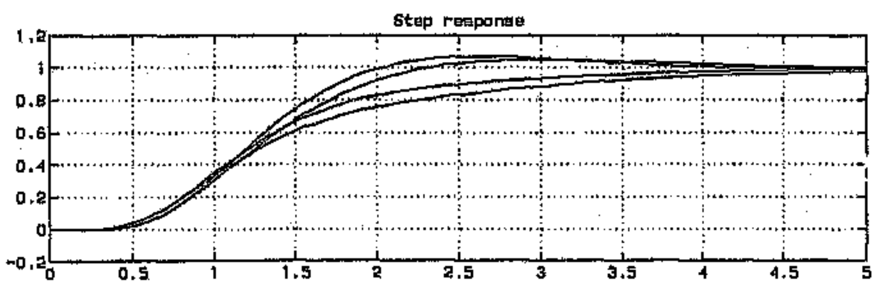

Figure E.14: Closed loop step response (MSC)

Appendix F

Feedback Instrument's PT326 Process Trainer

The layout of the PT326's front panel is shown in Figure F (Photo courtesy of Feedback Instruments Ltd).

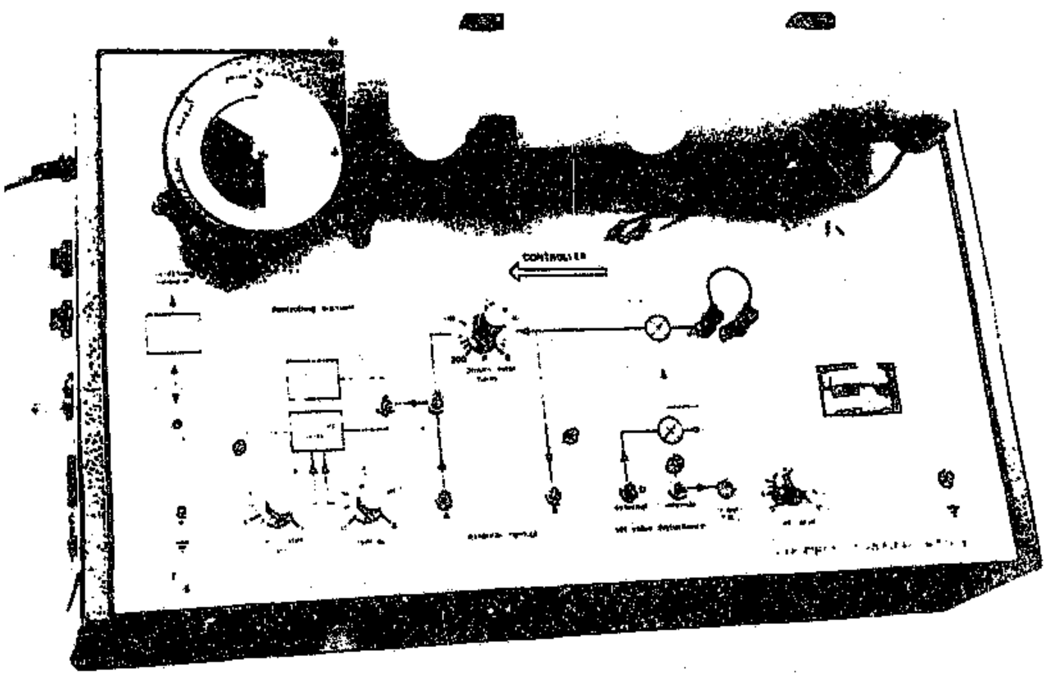

Figure F.1: Feedback Instrument's PT326 Process Trainer

Bibliography

Arkun, Y. (1978), 'Design of steady-state optimizing control structures for chemical processes.', *PhD Thesis, University of Minnesota.*

Athans, M. & Falb, P. (1966), *Optimal Control*, New York Mcgraw-hill.

Bhat, N. & McAvoy, T.J. (1990), 'Use of neural nets for dynamic modeling and control of chemical process systems', *Computers Chem. Engng* 14(4/5), 573–583.

Bolton, R.L.J. (1994), Development and evaluation of a new predictive control algorithm for the control of multivariable systems., Master's thesis, University of the Witwatersrand, Johannesburg.

Bolton, R.L.J. & MacLeod, I.M. (1995), 'A simulation study of multi-step predictive control applied to a mill feeder system', *The 8th IFAC International Symposium on Automation in Mining, Mineral and Metal Processing.*

Bolton, R.L.J. & MacLeod, I.M. (1997*a*), 'Constrained feedforward control for internal model control', *IEE Proc. Control Theory and Applications.* Submitted for review.

Bolton, R.L.J. & MacLeod, I.M. (1997*b*), 'Evaluation of a constraint mechanism for multi-step predictive control', *Control Engineering Practice.* Submitted for review.

Bolton, R.L.J. & MacLeod, I.M. (1997*c*), 'Evaluation of internal model control with absolute and rate constraints on process inputs', *Int. J. Control.* Submitted for review.

Bolton, R.L.J. & MacLeod, I.M. (1997*d*), 'A first order filter building block for long-range predictive control', *Systems and Control Letters.* Submitted for review.

Bolton, R.L.J. & MacLeod, I.M. (1997*e*), 'Formulation of an algorithm for multi-step predictive control', *Int. J. Control.* Submitted for review.

Bolton, R.L.J. & MacLeod, I.M. (1997*f*), 'Investigation into structure of long-range predictive control', *IEE Proc. Control Theory and Applications.* Submitted for review.

Bolton, R.L.J. & MacLeod, I.M. (1997*g*), 'Links between long-range predictive control and classical control', *IEEE Trans. Automatic Control.* Submitted for review.

Bolton, R.L.J. & MacLeod, I.M. (1997*h*), 'A method for designing robust multi-step predictive controllers', *IEEE Trans. Automatic Control.* Submitted for review.

Bolton, R.L.J. & MacLeod, I.M. (1997*i*), 'A modular approach to long-range predictive control', *Int. J. Control.* Submitted for review.

Bolton, R.L.J. & MacLeod, I.M. (1997*j*), 'Multi-step predictive control with feedforward control', *Int. J. Control.* Submitted for review.

Bolton, R.L.J. & MacLeod, I.M. (1997*k*), 'The predictor equation for multi-step predictive control', *Systems and Control Letters.* Submitted for review.

Bolton, R.L.J. & MacLeod, I.M. (1997*l*), 'Reference trajectory generation for a modular approach to long-range predictive control', *Systems and Control Letters.* Submitted for review.

Bolton, R.L.J. & MacLeod, I.M. (1997*m*), 'A strictly proper internal model controller with process input constraints', *Trans. S.A. Institute of Electrical Engineers.* Submitted for review.

Brengel, D.D. & Seider, W.D. (1989), 'Multistep nonlinear predictive controller', *Ind. Eng. Chem. Res.*

Chu, C. (1985), 'H_∞ optimization and robust multivariable control', *PhD Thes, University of Minnesota.*

Clarke, D.W. & Mohtadi, C. (1989), 'Properties of generalized predictive control', *Automatica* **25**, 859–875.

Clarke, D.W., Mohtadi, C. & Tuffs, P.S. (1987*a*), 'Generalized predictive control - part i. the basic algorithm', *Automatica* **23**(2), 137–148.

Clarke, D.W., Mohtadi, C. & Tuffs, P.S. (1987*b*), 'Generalized predictive control - part ii extensions and interpretations', *Automatica* **23**, 149–160.

Cutler, C.R. (1983), 'Dynamic matrix control: An optimal multivariable control algorithm with constraints', *Ph.D. Thesis, University of Houston, Houston, T.X.*

Cutler, C.R. & Ramaker, B.L. (1979), 'Dynamic matrix control - a computer control algorithm', *86th AIChE National Meeting*.

DSpace (1997*a*), *Floating-Point Controller Board (DS1102)*, dSpace Ltd (Digital Signal Processing and Control Engineering GmbH), Technologiepark 25, D 33100 Paderborn, Germany.

DSpace (1997*b*), *Real-Time Interface to Simulink (RTI 31)*, dSpace Ltd (Digital Signal Processing and Control Engineering GmbH), Technologiepark 25, D 33100 Paderborn, Germany.

Franklin, G.F., Powell, J.D. & Emami-Naeini, A. (1986), *Feedback Control of Dynamic Systems*, Addison Wesley.

Garcia, C.E. & Morari, M. (1982), 'Internal model control - 1. a unifying review and some new results', *Ind. Engng Chem. Process Des. Dev.* **21**, 308–323.

Garcia, C.E. & Morshedi, A. (1986), 'Quadratic programming solution of dynamic matrix control (QDMC)', *Shell Development Company, Houston, Texas.*

Garcia, C.E., Prett, D.M. & Morari, M. (1989), 'Model predictive control: Theory and practice a survey', *Automatica* **25**(3), 335–348.

Goodwin, G.C. & Sin, K.S. (1984), *Adaptive Filtering Prediction and Control*, Prentice-Hall, Englewood Cliffs.

Goodwin, G.C., Graebe, S.F. & Levine, W.S. (1993), 'Internal model control of linear systems with saturating actuators.', *Proc. of the 2nd European Control Conference.*

Greco, C., Menga, G., Mosca, E. & Zappa, G. (1984), Performance improvements of self-tuning controllers by multistep horizons : The MUSMAR approach, Technical report, Automatica (Vol 20, No 5, pp 681-699).

Hernandez, E. & Arkun, Y. (1990), 'Neural network modeling and an extended DMC algorithm to control nonlinear systems', *Proc. Amer. Control Conf.*

Horowitz, I.M. (1963), *Synthesis of Feedback Systems*, Academic Press, New York.

Horowitz, I.M. (1979), 'Quantitative synthesis of uncertain multiple input-output feedback systems', *International Journal of Control* **30**, 81–106.

Horowitz, I.M. (1982), 'Quantitative feedback theory.', *Proceedings of the Institution of Electrical Engineers* **129**, 215–26.

Horowitz, I.M. & Sidi, M. (1980), 'Practical design of multivari. ..le feedback systems with large plant uncertainty.', *International Jo...nal of Systems Science* 11, 851–75.

Kunzi, H.P. & Wilhelm, K. (1962), *Non-linear Programming*, Blaisdell Publishing Company.

Lee, M. & Park, S. (' . 2), 'A new scheme combining neural feedforward control with model-predictive control', *AIChE* 38(2), 193–200.

Maciejowski, J.. :)89), *Multivariable Feedback Design*, Addison-Wesley.

Morari, M. & Zafiriou, E. (1989), *Robust Process Control*, Prentice Hall.

Newton, G.C. (1952), 'Compensation of feedback control systems subject to saturation', *J. Franklin Inst.* 254, 281–286 and 391–413.

Parisini, T. & Zoppoli, R. (1994), 'Neural networks for feedback feedforward nonlinear control systems', *IEEE Transactions on Neural Networks.*

Patwardhan, A. ... tings, J.B. & Edgar, T.F. (1990), 'Nonlinear model predictive control', *C? ...g. Comm.*

Peterka, V. (1984), 'Predictor-based self-tuning control', *Automatica* 20, 39–50.

Prett, D.M. & Gillette, R.D. (1979), 'Optimization and constrained multivariable control of a catalytic cracking unit.', *AIChE National Mtg, Houston, Texas.*

PT326, *Process Trainer PT326*, manual 326 rev 0282 edn, Feedback Instruments Ltd.

Richalet, J., Rault, A., Testud, J.L. & Papon, J. (1978), 'Model predictive heuristic control : Applications to industrial processes', *Automatica* 14, 413–428.

Ricker, N.L. (1985), 'Use of quadratic programming for constrained internal model control', *American Chemical Society.*

Rouhani, R. & Mehra, R.K. (1982), 'Model algorithmic control (MAC); basic theoretical properties', *Automatica* 18(4), 401–414.

Seron, M.M., Goodwin, G.C. & Graebe, S.F. (1995), 'Control system design issues for unstable linear systems with saturated inputs', *IEE Proc. Control Theory and Applications.*

Smith, C.L. (1972), *Digital Computer Process Control*, Intext, Scranton, Pennsylvania.

VanCauwenberghe, A.R. & DeKeyser, R.M.C. (June 1985), Self-adaptive long-range predictive control, Tp10-3:30, Proceedings of American Control Conference.

Ydstie, B.E. & Liu, L.K. (1984), Single and multi-variable control with extended prediction horizons, Fa4-11:45, Proceedings of American Control Conference.

Ydstie, B.E., Kershenbaum, L.S. & Sargent, R.W.H. (Nov 1985), Theory and application of an extended horizon self-tuning controller, Technical report, AIChE Journal (Vol. 31, No. 11).

Author: Bolton, Roland Leslie John.
Name of thesis: A modular approach to model predictive control linking classical and predictive control concepts.

PUBLISHER:
University of the Witwatersrand, Johannesburg
©2015

LEGALNOTICES:

Copyright Notice: All materials on the University of the Witwatersrand, Johannesburg Library website are protected by South African copyright law and may not be distributed, transmitted, displayed or otherwise published in any format, without the prior written permission of the copyright owner.

Disclaimer and Terms of Use: Provided that you maintain all copyright and other notices contained therein, you may download material (one machine readable copy and one print copy per page)for your personal and/or educational non-commercial use only.

The University of the Witwatersrand, Johannesburg, is not responsible for any errors or omissions and excludes any and all liability for any errors in or omissions from the information on the Library website.